EEG Complexity as an ASD Biomarker: a Data-Driven Study for the Identification of Electrophysiological Correlates of ASD

MSc by Research in Psychiatry

Oana Gurau

Somerville College

University of Oxford

Department of Psychiatry

Section of Child and Adolescent Psychiatry

Supervisor: Prof Charles Newton

Collaborator: Dr William Bosl

EEG Complexity as an ASD Biomarker: a Data-Driven Study for the Identification of Electrophysiological Correlates of ASD

Oana Gurau, MSc by Research in Psychiatry, Somerville College

Trinity 2017

Abstract

Autism Spectrum Disorders (ASD) are a group of lifelong neurodevelopmental disorders, described by three core deficits which are thought to be consequences of atypical cortical activity. Abnormal neural connectivity underlying ASD could be inferred from dynamical system characteristics of the brain measured from electroencephalography (EEG) time series. Simple EEG measurement have the potential to provide important clinical biomarkers for early identification, risk assessment and monitoring the progression of ASD, while spanning the spectrum's heterogeneity of severity. The explicit goal of this project was to use Multiscale Entropy (sample entropy) measures and Recurrence Quantitative Analysis (RQA) on EEG to identify quantifiable neural correlates of behaviours associated with an ASD diagnosis. The hypotheses were tested on two cohorts: the Kenyan cohort with data collected in Kilifi, Kenya from both neurotypical children as well as children diagnosed with ASD and the NDAR cohort from the National Database for Autism Research (NDAR), also containing data from both groups. The results showed that complexity measured using sample entropy is useful in distinguishing the two groups, both at a whole brain level in the alpha, beta and gamma bands, and at a single electrode level, mainly in the theta band in the frontal, occipital and parietal electrodes and in the high gamma band in the frontal and prefrontal areas. RQA variables analysis showed that determinism can delineate ASD in the theta, gamma and high gamma bands in all electrode locations, in the delta band in the left frontal and temporal areas and in the alpha band in the left hemisphere in the occipital, parietal, temporal and central electrodes; laminarity is useful in delineating ASD in the frontal, temporal and parietal regions in the theta band and the occipital, parietal and temporal regions in the delta band; l_entropy played a role in ASD delineation in the central, temporal and occipital areas in the theta frequency; lastly, l_max accurately distinguished the two groups, mainly in the frontal and central areas in the theta band and in the parietal region in the alpha frequency. These findings represent pilot evidence of potential high utility of this method, which can have great impact on clinical practice, in the early screening and diagnosis stages of ASD.

Table of contents

1. Introduction

1.1. Autism Spectrum Disorders

Autism Spectrum Disorders (ASD) are a group of lifelong neurodevelopmental disorders, which traditionally includes the following subtypes: Autistic Disorder, Asperger Syndrome, Childhood Disintegrative Disorder and Pervasive Developmental Disorder-Not Otherwise Specified (PDD-NOS) (American Psychiatric Association 1994). In the most recent classification in the Diagnostic and Statistical Manual of Mental Disorders, Fifth Edition (DSM-V), however, all these subtypes are incorporated under ‘‘Autism Spectrum Disorder’’(American Psychiatric Association 2013).

In 1943, Leo Kanner published the first clinical description of ASD. In his description, he emphasized an underlying ‘innate inability to form the usual biologically provided affective contact with people’ (Kanner 1943). The following year, Hans Asperger identified several clinical cases that he diagnosed using the term ‘autistic psychopathy’. He observed that ‘the disturbance results in severe and characteristic difficulties in social integration’ (Asperger 1944). Later, Lorna Wing and Judith Gould identified a triad of core features that characterise ASD patients: impaired social interaction and verbal and non-verbal communication, a restricted repertoire of interests and a range of repetitive and unusual behaviours (Wing and Gould 1979).

It was not until 1980 that the American Psychiatric Association coined the term pervasive developmental disorders (PDD), which encompassed several ASD subtypes. Historically, ASD was also referred to as early infantile autism, childhood autism, Kanner's autism, high-functioning autism, atypical autism, pervasive developmental disorder not otherwise specified, childhood disintegrative disorder, and Asperger's disorder. The current international diagnostic guidelines are ICD-10 and DSM V. Both define ASD according to specific developmental

history profiles and present behavioural traits, very similar across the two sets of guidelines. In the most recent edition of the DSM guidelines, the three core characteristics of ASD were collapsed into two and now DSM V includes the following diagnostic criteria: A. persistent qualitative impairments in social communication and social interaction across multiple circumstances; B. a range of repetitive, limited and non-adaptive behaviours, activities or interests; C. evidence of developmental delay or abnormality in the early developmental stages; D. the symptom severity has significant negative impact on social, professional or other aspects of everyday life of the patient; E. the identified symptoms are not better explained by intellectual disability or global developmental delay (American Psychiatric Association 2013). Moreover, the DSM V replaced the ASD subtypes from DSM with three levels of severity ("Requiring support", "Requiring substantial support" and "Requiring very substantial support") with a guide for severity specifiers. The severity for Criteria A and B are rated separately and account for variations of severity by context or over time. The diagnosis should also specify if the patient presents with or without accompanying intellectual or language impairment, another neurodevelopmental, behavioural or mental disorder or catatonia (American Psychiatric Association 2013). Research has clearly demonstrated that an ASD diagnosis based on these guidelines is valid and can be made reliably after the age of two years (Charman, Taylor et al. 2005, Lord, Risi et al. 2006). Studies also demonstrated that despite the high heterogeneity in behavioural symptoms and developmental patterns, approximately 88% of children who received an ASD diagnosis at the age of two years in the West, remained on the spectrum at follow-up at the age of nine years (Turner, Stone et al. 2006).

In order for Criterion A to be fulfilled, the abnormalities in communication and social interaction have to be constant and pervasive and the diagnosis gains validity when they are confirmed by multiple sources such as clinical observations, patient history and, if possible, self-report. There is usually high heterogeneity in manifestations depending on the patient's

age, language abilities, intellectual levels as well as environmental factors and treatment history. The symptoms range from language delay to complete lack of speech or impaired use of language for social communication. Social-emotional impairments involve lack of emotional reciprocity, no initiations of social interactions, lack of imitation of peers' behaviour or difficulties understanding and responding to social cues, particularly in novel situations. Abnormalities in nonverbal communication becomes evident through lacking or atypical eye contact, gestures, facial expressions or prosody. Impaired joint attention is one of the first signs of ASD and it involves failure to trail someone's gaze or to direct someone's attention by pointing or bringing objects. Integrating "body language" into social communication becomes tricky to ASD patients (American Psychiatric Association 2013). For these reasons, a substantial part of ASD research focuses on executive function.

ASD is also characterised by a restricted and repetitive repertoire of interests, activities and behaviours, as stated by Criterion B. Repetitive behaviours may include motor stereotypes, repetitive speech or use of certain objects. Avoiding changes and patterns in verbal or nonverbal behaviour could indicate a compulsive devotion to routine. Interests are limited and usually abnormal in intensity. Hyperintensity and extreme reactions are also present in regards to certain sensory stimuli such as certain textures, sounds, smells, lights or spinning objects. There is usually the case for adults with ASD to learn to supress these manifestations in public and to direct the intensity of certain interests into a developing career (American Psychiatric Association 2013). This could also be one of the reasons why numerous adults remain undiagnosed.

Apart from the core characteristics, approximately 70% of individuals diagnosed with ASD have at least one comorbid disorder and 40% have two or more comorbidities (Simonoff, Pickles et al.). People with ASD often have intellectual impairment, structural language disorder, Attention Deficit Hyperactivity Disorder (ADHD), developmental coordination

disorder that may trigger literacy or numeracy, anxiety disorder or depression that may induce sleep or eating abnormalities (Simonoff, Pickles et al.). The most prevalent neurological condition is epilepsy, occurring in approximately 30% of the cases (Tuchman and Rapin 2002).

Recent epidemiological studies estimate the prevalence of ASD at approximately 1% of children in the UK and 1 in 68 children in the USA (Baio 2012). The first epidemiological study investigating the prevalence of ASD conducted in 1966 reported only 4-5 per 10000 cases, suggesting it was a rare disorder (Lotter 1966). The increasing numbers over the recent years could be influenced by several factors such as the increased public awareness that can lead to more cases being identified, more inclusive diagnostic criteria for diagnosis to include high functioning individuals, the inclusion criteria and larger sample sizes that more recent studies used for their epidemiological investigations, or a real growth in the frequency of ASD cases in the population (Roth and Rezaie 2011).

ASD present several diagnostic challenges. Firstly, within the autism phenotype, there is considerable heterogeneity between subjects in intelligence, social skills, language ability, as well as a wide range of comorbidities, which makes diagnosis problematic. Moreover, the deficits and behavioural symptoms are prone to variations over time. Particularly in the developmental stages, it may be challenging to establish the importance of certain behavioural aspects in order to differentiate between ASD and, for instance, social anxiety, withdrawal, developmental delay or intellectual or language impairments. The age of identification and diagnosis of ASD relies on parental or professional recognition of abnormal behaviour, assessment tools and depth of the clinical investigation (Roth and Rezaie 2011). A retrospective study performed in 2001 by Gilchrist et al. found that although 70% of parents of adolescents observed behavioural and developmental abnormalities before the age of three, only 35% resorted to professional clinical investigations (Gilchrist, Green et al. 2001).

For an early identification of ASD, once the child has been referred by the caretaker or a professional, the diagnostic process involves two steps: a developmental screening and a comprehensive diagnostic evaluation (Le Couteur 2003). The Developmental Diagnostic and Dimensional Interview (3Di) is one of the tools developed for the initial stage of developmental screening. This computerized test is administered by a trained professional to a parent and focuses on current behaviour. At the end, it generates a report and algorithms using information on symptoms and diagnostic profiles for both ASD and non-ASD comorbidities. The results of this tests indicate if a further, more in depth investigation is necessary (Roth and Rezaie 2011). The Autism Diagnostic Observational Schedule (ADOS) is a semi-structured test widely used in the second stage of the process. It is based on games and activities and targets the two large domains that make up the diagnosis criteria. The results are complemented by patient history and direct observations. The tests also controls for age and language abilities of the patients, providing four modules adapted to different levels of expressive language. The interpretation of the results relies on diagnostic algorithms that summarise the scores for the two criteria according to the DSM V and ICD-10. The test exists in several languages, however some items pertain to social situations that are not common is certain cultures e.g. birthday parties, which may require further work. This test is currently used both as a diagnostic tests as well as an outcome measure and can output estimates of ASD severity (Roth and Rezaie 2011).

Once these tests are administered and there is indication of an ASD diagnosis, further evaluations are necessary in order to create the complete patient profile and develop a personalised management plan, due to the high heterogeneity in symptoms and comorbidities. These evaluations include neuro-cognitive investigations, speech and language examination, mental health assessments, an examination of the patient's profile of skills, interests and deficits, a family assessment and further medicals exams when necessary (Roth and Rezaie 2011).

The current means of diagnosis have only been effective after approximately 18 months of age. There is consistent proof in the literature that early intervention for children with ASD leads to long-term improvements and early intervention relies on early detection (Rogers 1996, Dawson, Rogers et al. 2010). Besides being time consuming and not entirely objective due to behavioural variations from subject to subject, behavioural screenings also require specialised training, which may become a challenge particularly in underserved populations. As atypical neural connections are likely to precede atypical behaviour, a critical developmental window for early intervention appears during the first year of life (Assaf, Jagannathan et al. 2010, Nelson 2016, Sato, Vidal et al. 2017).

Since Kanner's report of ASD in 1943, a large body of research has been struggling to identify the underlying causes of this disorder. Given the high heritability approximations for ASD, ranging from 37% to higher than 90% based on twin concordance rates, one major focus in ASD research is revealing the genetic causes of the disorder and their interaction with environmental factors (Krumm, Turner et al. 2015). Initially, the strategy to find the genetic factors was to study large cohorts for linkage and association studies (Roth and Rezaie 2011). When the results failed the replication test, sample sizes were increased in order to increase the power of the studies; however this was unsuccessful. One of the largest study using nonparametric linkage methods, performed on 1181 multiplex families failed to identify any significant evidence (Peter Szatmari 2007). Therefore, consensus was reached that the inheritance of ASD is not Mendelian (Ritvo, Jorde et al. 1989). The research has moved on to individual approaches, trying to identify rare gene mutations or chromosomal rearrangements. Advances in genetic technologies, such as the development of whole-genome screenings, led to the conclusion that ASD is likely to be the result of a multitude of genetic mutations that hinder the functioning of certain biological pathways of neurodevelopment and plasticity (Persico and Bourgeron 2006). Major discoveries of the past decade partially elucidated the

mystery behind the genetics of ASD. Simultaneously, new questions appeared about the relationship between ASD genotype and phenotype, the role of environmental factors through the multiplicative or additive effect or the role of common variants.

Another large body of research on ASD focuses on structural and functional abnormalities of diagnosed patients, aiming to reveal the underlying causes and characteristics of ASD at the level of brain structures and regions. These studies focus mostly on the network known as the 'social brain' including the amygdala, superior temporal sulcus, fusiform face area and orbito-frontal cortex as well as on the caudate nucleus that is known to be involved in repetitive behaviours (Critchley, Daly et al. 2000). The advancements in magnetic resonance imaging (MRI) and functional magnetic resonance imaging (fMRI) allowed for an investigation of the core characteristics of ASD, that are considered neurodevelopmental in origin, and their impact or correlations to brain function. Most findings to date have been inconsistent, none being universally replicated. Studies investigating spatial attention in ASD showed hypoactivation in prefrontal and parietal regions in ASD comparted to neurotypical individuals. These results were interpreted suggesting that decreased parietal activation may cause abnormalities in attention shifting in ASD (Shafritz, Dichter et al. 2008). Other studies showed an atypical organization of the region involved in face processing in ASD, with reduced activations in the fusiform face area and the occipital face area. In 2000, Schultz et al. proposed a theory that ASD patients process faces the same way they process objects, analysing each individual feature rather than the whole. This hypothesis was confirmed by fMRI findings showing that when processing faces ASD patients recruit a wide variety of other areas, usually involved in processing objects (Schultz, Gauthier et al. 2000, Pierce, Müller et al. 2001). Structurally, studies have identified higher mean brain volume for individuals with ASD compared to controls, particularly when looking at infant head circumferences that are strongly correlated with brain size in the developmental stages (Courchesne, Carper et al. 2003).

ASD is typically described as a set of core behavioural components. Therefore a large body of research in psychology emerged, trying to create theories that would explain ASD behaviour, particularly in a social context. Simon Baron-Cohen proposed what has now become one of the central theories of ASD, the Theory of Mind Hypothesis. In his milestone study in 1985, Baron-Cohen found that 85% of the ASD cohort investigated showed difficulties performing the false-belief task, although their verbal mental age was over 4-5 years old, a stage when they should theoretically be able to perform well on the task (Baron-Cohen, Leslie et al. 1985). Based on these findings, he proposed that the core characteristics of autism could be explained by one main cognitive impairment in the capacity to understand other people's minds (Baron-Cohen 1997). Many studies that followed confirmed this theory, demonstrating that ASD patients fail or underperform on tasks that require a representational understanding of other minds (Baron-Cohen 2000, Tager-Flusberg 2007). The Central Coherence Theory, proposed by Frith in 1989, is another hypothesis aiming to explain some traits of ASD. Shah and Frith performed a study comparing the performance of children diagnosed with ASD with that of children with moderate learning difficulties (MLD) matched for non-verbal mental age, on the Embedded Figures Test (EFT). They were surprised to discover that children with ASD outperformed children with MLD (Shah and Frith 1983). Based on these findings, Frith proposed the idea that neurotypical individuals are characterised by 'central coherence', meaning they have a natural tendency to process stimuli in a Gestalt manner, regarding them as wholes rather than individual pieces. ASD patients lack or display weak central coherence as they process local aspects rather than the global image (Frith 1989). These are two of the many theories of ASD proposed over time. Numerous studies tried to replicate and confirm these theories, branch out into their different applications, as well as, look at many individual aspects that could explain ASD behaviour such as executive function, motor skills, attention or visual processing.

ASD can also be defined as a dynamical disorder and analysed according to complex dynamical systems theory (Bosl, Tierney et al. 2011, Sato, Vidal et al. 2015). One of the diagnostic challenges presented by ASD is the fact that behavioural criteria by which it is currently diagnosed, manifest long after the neurodevelopmental stages leading to those behaviours have completed. Connectivity abnormalities are some of the factors that may lead to behavioural abnormalities and could be identified prior to behavioural evidence (Boutros, Lajiness-O'Neill et al. 2015). In turn these abnormalities could manifest through and quantified by measureable changes in cortical excitability, as neural connectivity and neural dynamics are strongly interconnected. Several studies showed that properties of complex networks, such as chaotic time series, can vary considerably when altering key network connections, such as the initial conditions (Motter and Albert 2012). Therefore, abnormal neural connectivity underlying ASD could be inferred from dynamical system characteristics of the brain measured from electroencephalography (EEG) time series. Compared to diffusion tensor imaging (DTI) on MRI that provides direct measures of neural connectivity, nonlinear time series measured with EEG devices can be used to identify differences between ASD patients and neurotypical individuals on several levels through quantitative analysis of signal complexity (Lippé, Kovacevic et al. 2009, Takahashi 2013). One measure of physiological complexity is entropy. Entropy is defined as a physical variable that quantifies the order, or regularity, of a system. Ordered systems have lower entropy values, whereas irregular, chaotic systems have very high entropy values (Costa, Goldberger et al. 2005).

Reliable and relatively low cost, simple EEG measurements have the potential to provide important clinical biomarkers for early identification, risk assessment and for monitoring the progression of ASD, while spanning the spectrum's heterogeneity of severity. This method could help reveal the underlying mechanisms of the disorder and explain the behavioural symptoms that are currently used for clinical diagnosis.

1.2. Electroencephalography (EEG)

Scalp electrophysiology using EEG electrodes records the summed potentials of several millions of neurons in the cortex. The physiological interpretations of the recorded signal characterise both intrinsic features of the neuronal populations such as their ionic conductance, as well as connectivity properties and neural networks interactions (Coben and Myers 2008). These EEG recordings are usually classified in five 'standard' frequency bands: delta (0-4 Hz), theta (4-8 Hz), alpha (8-12 Hz), beta (12-30 112 Hz) and gamma (30-100 Hz), but these criteria vary between studies. These frequencies describe different states of the brain, each with a specific function, physiology and cortical topography. Additionally, newer methods of EEG signal analysis, such as using multiscale entropy, filter the signal into "scales" rather than the traditional frequency bands (Bosl, Tierney et al. 2011, Okazaki, Takahashi et al. 2015).

Clinically, EEG has been used for decades now to confirm epilepsy diagnoses. However, this tool's potential to provide valuable information of brain function for many other disorders has been underestimated. Fundamentally, the brain functions through electrical impulses, as it comprises of networks that exert fine control over electrical patterns determining all behaviours and thoughts. As the mind is analogous to a constantly changing pattern of electrical potentials, quantifying the electrical activity in the brain could provide information on cognitive phenotypes in the signal patterns that correlate with them (Bosl 2016).

Quantitative EEG (qEEG) is a collection of computerised methods and algorithms to analyse the EEG signal across multiple frequency bands, its power and connectivity between brain regions (Billeci, Sicca et al. 2013). Using qEEG, researchers identify quantitative features associated with abnormalities in ASD behaviour and to find patterns that could be transformed into clinical biomarkers of ASD. The values calculated using qEEG methods of analysis may be collectively referred to as EEG signal features. qEEG methods could be divided into three

large categories that now form large bodies of research: spectral analysis, functional connectivity analysis and, more recently, information dynamics.

1.3. The Brain in the Context of Complex Dynamical Systems

Cognitive and behavioural phenotypes are discrete cognitive or behavioural traits that can be identified with some degree of precision and quantitatively measured, the most important traits being the ones that delineate types of neuropsychiatric illness and neurotypical functioning (Bosl 2016). The Society for the Study of Behavioural Phenotype (SSBP) defined behavioural phenotype as "a characteristic pattern of motor, cognitive, linguistic and/or social abnormalities which is consistently associated with a biological disorder" (Fletcher, Loschen et al. 2007). Importantly, this definition identifies cognitive and behavioural phenotypes as patterns of actions, continuous processes, rather than static entities. These processes can be observed and analysed by outlining certain features of behaviour at appropriate time points. Identifying these feature involves the separation of a specific sequence of movements or thoughts in a specific context or situation. The connections between behaviours or cognitive processes and brain dynamics is therefore one between well-defined dynamical entities. These aspects are relevant for the identification of connections between phenotypes and dynamical processes in the brain (Bosl 2016).

Dynamical systems theory defines a complex dynamical system as a collection of N variables, each represented by a single real number value, that are mathematically or physically coupled and whose values change over time. The values of all the system's components can be represented with a single N-dimensional vector of real numbers called "state vector" (Juarrero 2012). An example of a state vector is showed below:

$$[x_1, x_2, x_3, \ldots, x_N]$$

$$\longleftarrow N \longrightarrow$$

At any given time, the state of a complex dynamical system is given by the value of its state vector and the sequence of state vectors through time forms the trajectory of the system. Graphically, the system's state over time could be plotted in the system's phase space, which is the space of all passible values the N variables of the state vector could assume at any given time and would look like a trajectory in an N-dimensional phase space (Bosl 2016).

According to the dynamical systems theory, the brain could be defined as an adaptive open complex dynamical system with sensory inputs from the environment and motor outputs, allowing the brain to feel and react to the environment, with dynamical characteristics that continuously change affected by learning and development. The neurons could be considered the smallest units of the brain. They play an important role in information processing, by continually changing their electrical potential through oscillating and their spiking rate has been hypothesised to be the way single neurons encode information (Kello, Rodny et al. 2012). Therefore, the basic quantitative unit of the dynamic brain is the electrical potential of each neuron in the brain at any given time, representing the brain's state at that time (Bosl 2016). In this case, the brain's trajectory through phase space, represented by a continual change in the neurons' electrical potentials underlie all movements and behaviours, as a strong connection between brain activity and cognitive and behavioural processes has already been established. Moreover, the brain is a coupled dynamical system because the future state of each of its neurons is determined both by its current state as well as the state of all other neurons in the system (Bosl 2016).

Another aspect that supports the statement that the brain is a complex dynamical system is the fact that the dynamics of the entire system cannot be deciphered solely from its components and their interactions alone. The whole is more than the sum of the parts, meaning that below a certain scale some system functions are lost. Even through some components play a critical role individually and their function is clearly established, certain functions are not determined

by single components but emerge when some components connect in a specific functional configuration (Bosl 2016). A large body of neuroscientific, psychiatric and psychological research has been dedicated to localizing cognitive processes in brain regions, which had numerous clinical benefits. However, many higher-level cognitive processes have challenged localization, as they could not be attributed to a single brain regions. For example, the prefrontal cortex where research demonstrated that neurons are not anatomically arranged, but they display mixed selectivity for several cognitive functions (Rigotti, Barak et al. 2013).

The state of the brain as a complex dynamical system can be represented at a given time as a 10^{11} dimensional state vector, where a single floating point x_i represents the electrical potential or spiking rate of one single neuron. Each neuron receives inputs from many thousand other neurons and sends its outputs to other neurons. The way the neurons influence each other's activity is determined by the connectivity pattern that is in turn shaped by learning, synaptic strength and chemical influences such as the specific neurotransmitters, excitatory or inhibitory that mediates the connection (Bosl 2016). The connectivity pattern and external factors together determine the state transition rule that regulates the brain's states over time:

$$B^{t+1} = F\,(B^t) + \sigma^t$$

Here, F is the function underlying the connectivity pattern, which determines the future state of every single neuron at t+1. σ^t represents the cumulative sensory inputs from the environment which influence the state of sensory neurons. Even though this is a very simplified model of how the brain works, it is a realistic illustration of how the neural network states change over time (Bosl 2016).

The phase space of the brain is the collection of all possible brain states. According to the model above, the brain's phase space is determined by all points that can be written as 10^{11} dimensional vectors B^t. In reality, neither the brain, nor complex systems in general, will

assume all points in the phase space, but it will cover trajectories that represent only a very small part of the phase space (Kello, Rodny et al. 2012). In the context of the human brain, each person has a unique state transition function that determines unique dynamical trajectories of the brain through phase space. However, many people react to certain stimuli in fundamentally the same way. Therefore, all the brain trajectories in phase space determined by individuals' neural firing patterns that correspond to activities such as chewing or eye saccades, will be very similar in most individuals, as firing patterns underlie cognitive responses to stimuli. These similar patterns in brain state trajectory, underlying cognitive processes and elicited by certain stimuli, are called attractors. "Attractors are typical patterns of dynamical, interdependent behaviours of limited dimensionality and carved out from a much larger space of possible patterns and dimensions. These global structural patterns, which emerge from interactions among the system's components through phase space, can be characterized as emergent collectives" (Juarrero 2012). According to this definition, then, any condition or stimulus that triggers an analogous cognitive or behavioural response must also result in a similar response in the brain; the trajectory of the neural response moves into an attractor of the dynamical system, the brain.

Complex neurological and mental disorders have long been associated with abnormal brain connectivity in different regions and at different frequencies (Noonan, Haist et al. 2009). Identifying and quantifying these neural connectivity abnormalities could be a useful method to detect abnormal brain function and behaviour compared to normal function. This statement relies on the above hypothesis that if we could plot the trajectory a brain follows in state space, which is highly influenced by brain connectivity, we might be able to visualize where normal and abnormal brains respond differently to the same stimuli. By comparing attractors we might be able to identify atypical brain function (Bosl 2016).

Behaviours and responses to stimuli can only be defined as normal because they are the same in the vast majority of people. A neurotypical 5 year old child will respond to a friendly familiar face with an emotional reaction. However, a child with ASD will respond differently. These patterns of reactions reflect underlying brain function. As the brain trajectory falls into an attractor whenever it is presented with the same stimulus, the response to the same stimulus of an ASD patient is different from a neurotypical individual's response in a way that is also recurrent (Bosl 2016). The goal to find neural correlates of behaviour and differences between healthy and clinical populations becomes one of finding patterns of neural activity that correlate with distinguishable behaviours.

The strong connection between brain function and cognitive processes and behaviour has long been established (Kandel, Schwartz et al. 2000). Thus the brain's state trajectory over time corresponds directly to every thought or behaviour elicited at the specific moment in time, even if the electrical potential of each neuron is not directly measurable using non-invasive methods. Nevertheless, it may be possible to mathematically infer specific dynamical properties of the attractors in the brain's dynamics from measurements of electrical potentials obtained from the surface of the brain or scalp.

Advances in dynamical systems theory demonstrate that such inferences are possible (Bosl 2016). Embedding theorems fuelled these advances and have particular relevance in the field of electrophysiology and time series. The reconstruction theorems state that multiple features of the unobservable multidimensional state space of the brain can be derived from one-dimensional time series from EEG recordings (Eckmann, Kamphorst et al. 1987). This has strong implications in the way we analyse EEG signal and its potential in revealing more information about underlying causes of brain abnormalities, as it states that EEG may contain information about the dynamics of the whole brain. Computational advances derived from embedding theorems such as recurrence plots, different measures of signal complexity such as

entropy and Recurrence Quantitative Analysis (RQA) enabled researchers to investigate higher-level brain functioning by extracting multiple features of EEG time series that clearly describe the dynamical brain (Schinkel, Marwan et al. 2007, Schinkel, Marwan et al. 2009, Webber Jr and Marwan 2015).

One novel nonlinear approach to investigate the properties of complex dynamical systems, based on statistical analysis of recurrence plots, is called recurrence quantitative analysis (RQA) (Zbilut, Thomasson et al. 2002, Marwan, Romano et al. 2007, Schinkel, Marwan et al. 2009). RQA is an empirical method of time series data analysis, in principle capable of revealing all the essential dynamical characteristics of a complex system, and has great utility for analysing "real-world, noisy, high dimensional data" (Webber Jr and Zbilut 2005). It has already yielded great results in physics, geophysics, engineering and biology (Marwan, Romano et al. 2007, Komalapriya, Thiel et al. 2008). Its use in neurology and neuroscience are in the early stages. In theory, RQA is capable of identifying significant changes in the states of a dynamical system therefore it may be an appropriate and powerful tool for delineating developmental changes in brain function that are associated with chronic neurological and mental dysfunction (Marwan, Romano et al. 2007, Schinkel, Marwan et al. 2009).

1.4. Aim, Hypotheses and Impact

The explicit goal of this project is to use Multiscale Entropy (MSE) measures and Recurrence Quantitative Analysis (RQA) on electroencephalography (EEG) to identify quantifiable neural correlates of behaviours associated with an ASD diagnosis.

Hypothesis 1. MSE measures a functional brain invariant that is associated with an ASD diagnosis and can be used to distinguish subjects in two categories; ASD and non-ASD. This hypothesis is motivated by previous work showing that these measures can predict risk status in ASD and previous studies on MSE as a tool for analysing physiological signals.

Hypothesis 2. A wider range of EEG signal features derived from RQA are other brain invariants that are associated with an ASD diagnosis and distinguish ASD and non-ASD subjects with a higher accuracy. RQA is a general framework for analysing complex systems from time series. Entropy, such as MSE, is one of several variables that can be calculated from RQA. This hypothesis will determine if additional values derived from EEG data will increase the accuracy or be more specifically associated with ASD diagnosis.

Developing new methods for early diagnosis of ASD has become a priority in this field of research. The pragmatic goal of this project is to develop a new method to identify neural correlates associated with ASD, which could be used as early biomarkers for diagnosis before the behavioural symptoms arise. These finding could pave the way for new therapies and early interventions that could effectively ameliorate symptoms from the first year of life and introduce the possibility of monitoring the effectiveness of these interventions.

2. Systematic Review

The first part of this project consisted in assessing the utility of EEG as a clinical tool to identify ASD and delineate several subtypes of severity. A systematic review on the literature was conducted on three major EEG signal analysis methods: functional connectivity, spectral analysis and information dynamics. The explicit questions that we set out to address in the review were: a) can analysis of EEG signal be used to identify subjects with ASD, particularly, is it useful in diagnosis; and b) can EEG features delineate subtypes of ASD? The results of this review stand as proof for the great potential EEG has as a clinical tool, as well as for the further directions that research should take to identify neurophysiological biomarkers of ASD. It also emphasizes the novelty of the methods used in this project.

The systematic review was published in the journal Frontiers in Psychiatry, in the Child and Adolescent Psychiatry section (Appendix). The Methods and Results sections of the paper are presented below.

The literature search was conducted in three peer-reviewed databases: PubMed, Embase and PsycInfo. Keyword searches were performed in order to identify the most suitable studies for this review. The key terms used were 'ASD', 'Asperger', 'autism', 'EEG', 'encephalography', 'spectral analysis', 'functional connectivity', 'information dynamics'. On each database, the searches consisted of each of the three key terms describing the disorder and subtypes plus each of the terms describing the methods (Table 1). Additionally, to select the studies to be reviewed, the following inclusion criteria were used:

1. The studies were performed on humans, either children or adults;
2. A comparison was performed between either: i) ASD patients and healthy controls; or ii) ASD patient with different subtypes;
3. The studies' outcome consisted of specific EEG features of ASD, not its comorbidities;
4. The studies included patients diagnosed according to the clinical criteria from DSM III onwards;
5. The studies were published between 1980-May 2016;
6. The studies were performed using EEG and the signal was analysed using spectral analysis, functional connectivity measures or information dynamics methods.

Table 1: Description of the search strategy

Search element	PubMed	Embase	PsycInfo
Disorder	ASD Autism Asperger	ASD Autism Asperger	ASD Autism Asperger
Method	EEG Encephalography Spectral analysis Functional connectivity Information dynamics	EEG Encephalography Spectral analysis Functional connectivity Information dynamics	EEG Encephalography Spectral analysis Functional connectivity Information dynamics

In order to filter the initial number of titles obtained (Table 2), according to the six eligibility criteria, a three step strategy was followed (Figure 1). Firstly, the titles of each of the papers yielded by the initial search were examined for relevance to the topic. The absence of any of the key words from the titles led to the exclusion of the studies. Secondly, the abstracts were scanned for relevance, as they briefly indicate the methods used in the study and their results. Animal studies, review papers or studies combining different methods of analysis were excluded. The review papers were used as sources for relevant papers to be examined. Lastly, a full text analysis was performed, allowing a closer examination of diagnostic criteria of the patients and the quality of their results. This process yielded the final collection of studies used for data extraction in the review (Fig.1).

Table 2: Total number of papers identified from each database before and after the exclusion of duplicates

Database	Total number of titles	Total number of titles-duplicates
Pubmed	2155	1523
Embase	2095	1467
PsycInfo	964	649

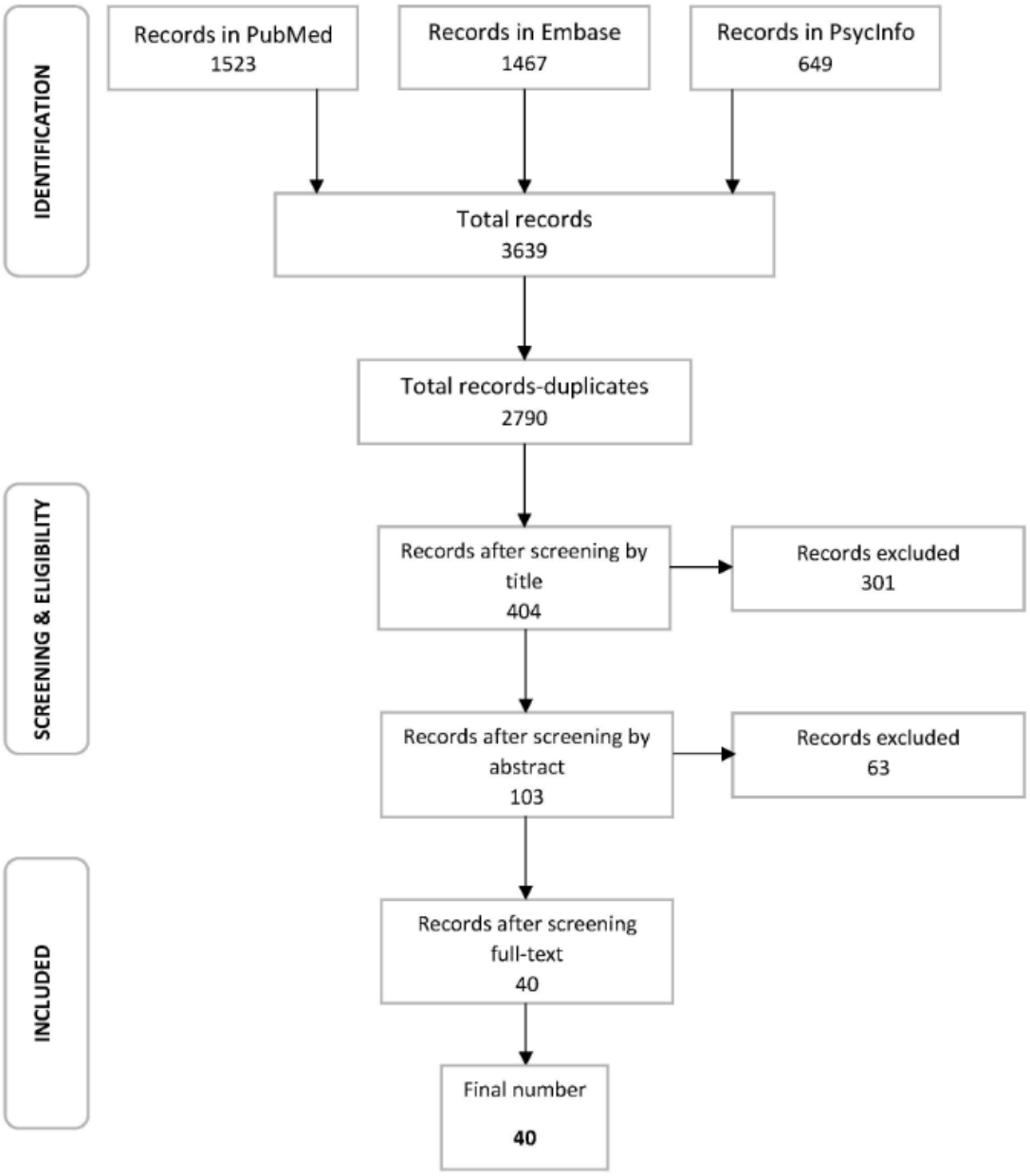

Figure 1: Flow diagram presenting the process of study selection including the three-step strategy used to reach the final collection of studies and number of records in every step

Following the selection stage, the relevant data was extracted from each paper. For this purpose, in consistency with the PRISMA 2009 checklist (http://www.prisma-statement.org/), a template with a number of descriptive variables for each study such as its authors and publishing year; a detailed section describing the methods used in the study including

description of the patient and the control groups, the task performed, methods of EEG analysis as well as statistical tests; and a summary of the results was used. For consistency, all data was extracted from the studies using this template.

Inspection of the literature selected for data extraction revealed three types of EEG signal analysis used for detection of ASD: i) spectral analysis; ii) functional connectivity and coherence analysis; and iii) a larger category, information dynamics, including several methods based on dynamical systems theory and mathematical concepts.

Functional connectivity evaluates the relationship between the signals recorded at different brain regions simultaneously. Usually these relationships are quantified in terms of some measure of synchronization between two signals. Synchronization may be defined in several different ways (Pikovsky, Rosenblum et al. 2003, Wen, Zhou et al. 2015), which includes coherence, phase locking index, phase synchronisation, phase lag index and synchronisation index. Functional connectivity analysis also involves measures of embedded data such as cross recurrence diagrams and synchronisation likelihood. Often signals are decomposed into standard frequency bands.

Spectral analysis is the most common quantitative method used for EEG signal analysis and interpretation. It breaks the continuous range of frequencies into defined bands and evaluates the signal distribution over several frequency bands, usually as the five divisions described above. The spectral power may be computed for each frequency band at each sensor (Rapp, Keyser et al. 2015). Sometimes the total power in each frequency band is summed over all sensors, giving a single power value over the entire scalp for each frequency band. For example, a power value for the alpha band over the entire scalp, may be reported. Or, power in the alpha band at each sensor location may be reported. Group differences between populations with

autism and typically developing controls were assessed. Results were presented either as absolute power or relative power (the ratio of band power to total power over bands).

Information dynamics methods make use of nonlinear analysis methods. These include various measures of entropy, or other dynamical concepts such as Lyapunov exponents or recurrence plot analysis, among others. The meaning of these concepts has been derived from physical systems, but it is not clear how they related to neural systems. Thus, significant correlations between nonlinear features and neural or behavioural observations are sought using machine learning algorithms and mathematical classifiers based on neural networks, graph theory, fractals or Bayesian methods. Machine learning algorithms and classifiers use a set of rules characterising members of one or more categories and then apply these rules to a dataset for classification. The most commonly used nonlinear feature used in neuroscience has been multiscale entropy, a measure of signal complexity. The original EEG signal is used to create a sequence of coarse-grained time series. Each scale of entropy is obtained as follows: scale 2 is calculated by averaging every two values, scale 3 time series is obtained by averaging every three values etc. The sample entropy is then computed for each time series to produce entropy as a function of time. This coarse graining procedure was first introduced to signal analysis by (Costa, Goldberger et al. 2005). Although this procedure is commonly used, it has only recently been noted that for powers of two (1, 2, 4, 8, …) the coarse graining procedure is mathematically identical to the Haar wavelet transform (Bosl, Loddenkemper et al. 2017). Much is known about wavelet transforms and their relationship to frequency decomposition (Al-Fahoum and Al-Fraihat 2014). Multiscale entropy is thus a computation of sample entropy on each of the wavelet transform scales.

According to the PRISMA 2009 checklist, the analysis of the utility of each of these methods includes: a general description, a critical evaluation of statistically significant evidence to differentiate between ASD patients and non-ASD subjects, or different ASD subtypes extracted

from the literature, advantages the technique holds over others, as well as gaps and future lines of improvement followed by a conclusion summarising the overall prospects of using it as a tool in ASD detection.

An evaluation of the selected literature led to the presentation of the papers in three EEG signal analysis methods used to characterise ASD described above.

2.1. Functional connectivity

Of the 40 studies selected for review, 12 studies compared functional connectivity between ASD patients and non-ASD subjects. All studies reported at least one statistically significant difference in ASD connectivity in at least one frequency band. Of the 12 studies employing this method of analysis, 10 use coherence as a measure of connectivity, one calculated the phase lag index of the time series and one calculated clustering to determine the level of synchronisation. EEG recordings were performed under relaxed, no task conditions, with eyes either open or closed, during sleep or during an object recognition, audio or video task. The overall patterns in results are presented in Table 3 together with the condition of the EEG recording and the principal measure of each study.

Although the results are variable, some generalisations can be inferred. ASD is usually associated with reduced long-range connections in the alpha band between the frontal lobe and other brain regions. This finding supports the under connectivity theory of ASD, which is supported by fMRI studies (Just, Keller et al. 2012). Seven out of 11 studies performed coherence analyses in the alpha band, of which 4 supported the presence of under connectivity. For instance, Murias et al. studied coherence in ASD in a relaxed eyes closed condition, using a high density EEG montage (124 electrodes) in male adults and found significant differences in the alpha band between patients and controls, with reduced long range connections particularly from the frontal areas. Some of the patients were taking medication, which may

have influenced the results (Murias, Webb et al. 2007). Catarino et al. also identified an overall decrease in brain connectivity in the alpha band, in subjects with ASD performing two object recognition tasks (Catarino, Andrade et al. 2013). In a more recent study, Carson et al. performed a study on a younger pool of participants that replicated the decrease in the long-range connectivity in the alpha band, while they were attending to a video of either a familiar or unfamiliar person readying a story (Carson, Salowitz et al. 2014). The fourth study to support this theory calculates clustering as a measure of brain connectivity. Boersma et al. used graph analytical tools to demonstrate reduced whole brain connectivity in toddlers, particularly in the alpha band (Boersma, Kemner et al. 2013). However, three of the six studies, show contradictory results. Orekhova et al. performed a longitudinal study, testing participants at high and low risk of developing ASD at 14 months and at 38 months, after part of the high risk participants were diagnosed with ASD. The study showed significant differences between the children diagnosed with ASD and the other participants, with hyper-connectivity in the alpha band between the frontal and central areas in those at risk of developing autism (Orekhova, Elsabbagh et al. 2014). Testing participants in a relaxed eyes open condition, Cantor et al. supports the decrease in alpha connectivity, this time within and between hemispheres (Cantor, Thatcher et al. 1986). Buckley et al. tested participants aged 2-6 years old during three sleep state conditions and found an increase in coherence in ASD patients compared to neurotypical subjects, particularly in long-range connections in the frontal-parietal areas (Buckley, Scott et al. 2015).

Anatomical and functional studies have also demonstrated short-range, local over connectivity, reflected in increases of short range association fibres (Herbert, Ziegler et al. 2004). Moreover, it is known that theta oscillations underlie locally dominant processes (Collura 1996). Six out of 11 studies investigated connectivity differences in this frequency band: 3 of the studies supporting previous fMRI findings (Murias, Webb et al. 2007, Léveillé, Barbeau et al. 2010,

Chan, Han et al. 2011) and 3 not finding any evidence of over connectivity (Coben, Clarke et al. 2008, Boersma, Kemner et al. 2013, Catarino, Andrade et al. 2013). Murias et al. identified significant over connectivity in the theta band in the frontal and temporal areas of the left hemisphere (Murias, Webb et al. 2007). Leveille et al. studied participants during rapid eye movement (REM) sleep and identified increased long-range connectivity between the visual area V1 in the occipital lobe and other parts of the brain (Léveillé, Barbeau et al. 2010). During an object recognition task, Chan found increased frontal coherence in the theta band, confirming fMRI findings (Chan, Han et al. 2011); but 3 studies found whole brain under connectivity in the theta band, the first two employing object recognition tasks (Boersma, Kemner et al. 2013, Catarino, Andrade et al. 2013), whilst Coben et al. demonstrated under-connectivity in the frontal, temporal and parietal regions (Coben, Clarke et al. 2008).

The delta and beta bands yielded significant results in 6 of the 11 functional connectivity studies, but lacked consistency. Barttfeld et al. showed ambivalent results in the delta band, with decreased long-range delta connectivity between the frontal and occipital areas and increased short-range delta connectivity in the frontal region (Barttfeld, Amoruso et al. 2013). In a sleep study, Leveille et al. had contradictory results, showing increased long-range delta connectivity between the occipital area and the rest of the brain (Léveillé, Barbeau et al. 2010). Coben also shows decreased frontal and temporal coherence in the theta band (Coben, Clarke et al. 2008). Decreases in connectivity were detected by Boersma et al., Coben et al. and Lazarev et al. (Coben, Clarke et al. 2008, Boersma, Kemner et al. 2013, Lazarev, Pontes et al. 2015) in the analysis of the beta band. Despite these results, it is notable that 9 of the 11 papers did not find any significant difference in the beta band. Generalisation, in this case, could not be inferred because of the different conditions of the EEG recordings and the age differences between the participants of each study.

Table 3: Studies using functional connectivity

Paper	Patients characteristics	Controls characteristics	Condition	Measure	Changes in ASD
Orekhova et al.	n=28 mean age =14.4 m sex=18F, 10M High-risk (HR) n=26 mean age=14.7 m sex=14F, 12M Low-risk (LR)	n=10 Mean age=38 m sex=3F, 7M High-risk ASD (HR-ASD) n=18 Mean age =38 m sex=15F, 3M High-risk non ASD (HR-non-ASD)	3 video stimuli	De-biased weighted phase lag index	HR-ASD: hyper-connectivity in alpha band in frontal and central areas ($p<0.05$). The degree of hyper-connectivity correlated with the severity of ASD symptoms in later diagnosed.
Righi et al.	n=not specified Adults High-risk of ASD Had an older sibling with ASD	n=not specified Adults Low-risk of ASD	Speech sounds	Coherence	Infants at risk: reduced connectivity ($p<0.005$). Connectivity: HR-ASD<HR-NASD<LR.
Barttfeld	n=10 mean age=23.8 yrs sex=1F, 9M subtypes= autism, Asperger's syndrome	n=10 mean age =25.3 yrs sex=1F, 9M	Relaxed eyes closed	Coherence (synchronisation likelihood)	Delta band: decreased long-range connectivity (fronto-occipital) and increased short-range connectivity (frontal lateral) in ASD ($p<0.05$).
Murias et al.	n=18 Adults sex=18 M diagnosis=ASD Some were taking medication	n=18 Age-matched sex=18M	Relaxed eyes closed	Coherence	Theta: increased connectivity in frontal and temporal left hemisphere ($p<0.025$). Alpha: decreased long range connections of the frontal area ($p<0.025$).
Leville et al.	n=9 mean age=21.1 yrs diagnosis=ASD	n=13 mean age =21.5 yrs	Rapid Eye Movement (REM) sleep	Coherence	Theta and delta: increased long-range coherence between the occipital region and the rest of the brain and decreased the frontal area ($p<0.05$).
Boersma et al.	n=12 mean age =3.5 yrs sex=2F, 10M subtypes= autism(2), Asperger's Syndrome (1), PDD-NOS(9) average IQ=85	n=19 mean age =3.5 yrs sex=19M average IQ=108	Pictures of cars	Clustering	Overall whole brain under-connectivity in beta, theta and alpha bands ($p<0.01$).
Catarino et al.	n=15 mean age=31 m diagnosis=ASD	n=15 mean age =29 m	Object recognition	Coherence	Decreased coherence for both tasks in alpha and theta bands ($p<0.05$).
Carson et al.	n=19 mean age =9.9 yrs sex=1F, 19M diagnosis=ASD	n=13 mean age =10 yrs sex=4F, 9M	Videos of someone reading a story	Coherence	Decreased coherence in alpha band in frontal and temporal lobes at baseline ($p<0.05$).

Cantor et al.	n=11 age range=4-12 yrs sex=2F, 9M subtypes= autism	n=119 classification=normal children (n=88, age range=5-15 yrs, a matched group of intellectually disabled children (n=18, age range=5-15 yrs) and a group of mentally age-matched normal toddlers (n=13, age range=16 m-5 yrs)	Relaxed eyes open	Coherence	Higher coherence between and within hemispheres in delta and alpha bands ($p<0.05$).
Chan et al.	n=21 mean age = 10.27 yrs sex=2F, 19M	n=21 mean age = 9.85 yrs sex=7F, 14M	Object recognition	Coherence	Increased frontal coherence in left hemisphere in theta bands ($p<0.05$).
Coben et al.	n=20 mean age=6-11 yrs sex=6F, 14M	n=20 mean age=6-11 yrs sex=6F, 14M	Relaxed eyes close	Coherence	Decreased coherence in theta and delta bands in frontal region ($p<0.005$), delta, theta and alpha in temporal region ($p<0.05$) and delta, theta and beta in parietal and occipital regions ($p<0.05$).
Buckley et al.	n=87 age range=2-6 yrs diagnostic=ASD n=21 age range=2-6 yrs diagnosis=developmental delay without ASD (DD)	n=29 age range=2-6 yrs (TYP)	Awake, slow wave sleep, and REM sleep	Coherence, phase lag,	Increased coherence observed in ASD compared to TYP, almost exclusively during slow wave sleep, in the frontal–parietal areas, in long-distance pairs
Lazarev et al.	n=14 age range=6-14 yrs sex=14M diagnosis=ASD	n=19 age range=6-14 yrs sex=19M	Intermittent photic stimulation	Coherence	Significantly lower coherence in ASD than the control group in the beta frequencies

*n=number of subjects; F=female; M=male; yrs=years; m=months; PDD-NOS=Pervasive Developmental Disorder Not Otherwise Specified; REM=rapid eye movement

2.2. Spectral analysis

Twenty-one of the selected studies used spectral analysis to characterise ASD. All studies recorded statistically significant variants in spectral power in ASD patients compared to non-ASD subjects in at least one frequency band. The studies measured differences in relative or absolute spectral power across frequency band, power spectrum density or spectral properties such as amplitude. The signal was recorded during relaxed conditions with eyes either open or

closed, during sleep, cognitive tasks or while attending to video or audio stimuli. The overall trend of results can be visualised in Table 4, along with participants' characteristics, recording condition and the main measure of the study.

Inconsistencies are observed in the spectral band findings, although some generalisations can be inferred. Firstly, significant differences in the alpha band were shown by 5 studies with relaxed eyes open condition (Cantor, Thatcher et al. 1986, Dawson, Klinger et al. 1995, Chan, Sze et al. 2007, Mathewson, Jetha et al. 2012, Matlis, Boric et al. 2015). While four studies show a decrease in absolute spectral power in ASD in children of similar ages (Cantor, Thatcher et al. 1986, Dawson, Klinger et al. 1995, Chan, Sze et al. 2007, Matlis, Boric et al. 2015), another showed elevated absolute alpha power in adults (Mathewson, Jetha et al. 2012).

The inconsistencies might be attributed to the age differences between participants and differing developmental trajectories in children with ASD. Yang et al. tested participants while they were performing a cognitive task and showed an increase in alpha power compared to non-ASD controls, but insufficient studies calculated similar measures under the same conditions to make robust conclusions (Yang, Savostyanov et al. 2011).

Calculating spectral amplitudes in all frequency bands, Chan et al. also found significantly increased amplitudes in the ASD population. Moreover, using discriminant function analyses, the study finds that beta amplitudes had high specificity (98.1%) and sensitivity (77.8%) in differentiating ASD from non-ASD subjects (Chan and Leung 2006). The most consistent result that could lead to a generalisation is an increase in absolute gamma power in ASD compared to non-ASD subjects. Sheikhani et al. tested their participants in a variety of conditions and found statistically significant elevated gamma power, particularly in the relaxed eyes open condition (Sheikhani, Behnam et al. 2009). van Diessen et al. confirms the increase in gamma power, particularly in the frontal, parietal and temporal regions in the relaxed eyes

open condition (van Diessen, Senders et al. 2015). Orekhova et al., replicate this finding, using a visual attention task (Orekhova, Stroganova et al. 2007), whilst Lushchekina et 341 al. supports these findings in two studies involving a cognitive task (Lushchekina, Podreznaya et al. 2014).

As for the theta band, none of the results could be validated due to inconsistencies. While Daoust et al., Tani et al., Elhabashy et al. and Yang et al. show increased power in the theta band in two studies performed during sleep, one during a relaxed eyes open and one involving a cognitive task (Daoust, Limoges et al. 2004, Tani, Lindberg et al. 2004, Yang, Savostyanov et al. 2011, Elhabashy, Raafat et al. 2015); Three studies show a reduction in theta power in relaxed eyes open conditions and during a cognitive task (Dawson, Klinger et al. 1995, Lushchekina, Podreznaya et al. 2014, Machado, Estévez et al. 2015). Variations in the participants' age, as well as small sample sizes might lead to the lack of consistency in these results.

Table 4: Studies using spectral analysis

Paper	**Patients characteristics**	**Controls characteristics**	**Condition**	**Measure**	**Changes in ASD**
Matlis et al.	n=27 mean age =4-8 yrs sex=2F, 25M subtypes= autism	n=55 mean age=4-8yrs sex=26F, 29M	Relaxed, eyes open	Spectral properties	Reduced posterior/anterior power ratio in the alpha frequency range (8–14 Hz) ($p \leq 0.0025$).
Sheikhani et al.	n=15 age range=6-11yrs sex =5F, 10M subtypes= Asperger's Syndrome verbal IQ>85 handedness=1 LH, 14RH	n=11 age range=6-11yrs sex =4F, 7M handedness=1LH, 1AD, 9RH	Eyes closed, relaxed-eyes opened, looking at 3 puzzle shapes, looking at mother's and stranger's pictures upright and inverted	Spectral power	Higher power in gamma band while resting with eyes open ($P<0.05$).
Cantor et al.	n=11 age range=4-12yrs sex=2F, 9M mean IQ=37.5 subtypes= autism	n=119 classification=normal children (n = 88, age range=5-15 yrs, age matched group of mentally disabled children (n=18, age range=5-15 yrs) and a group of	Relaxed, eyes opened	1.relative power 2.total power	ANCOVAs and t-tests: Lower alpha power in all regions in ASD subjects compared to age-matched normal and age-matched mentally disabled children ($p<0.001$) Higher power than the normal or mentally

		mentally age-matched normal toddlers (n=13, age range=16 m-5 yrs)			handicapped children in the bilateral fronto-temporal and left temporal regions (p<0.005). Lower power in the bilateral occipital regions normal (p<0.05). Lower power than toddlers in the left central, midline central, and left fronto-temporal regions (p<0.05).
Chan et al.	n=17 mean age=7.1 yrs sex=3F, 14M	n=105 mean age=7.7yrs sex=61F, 44M	Relaxed, eyes opened	Spectral profiles: absolute delta, theta, alpha, sensorimotor rhythm, beta; relative delta, theta, alpha, sensorimotor rhythm, beta bands.	Absolute amplitudes: higher amplitudes in all five frequency bands (P<0.005).
Chan et al.	n=66 age range=5-18 yrs sex=6F, 60M	n=90 age range=6-12 yrs sex=42F, 48M	Relaxed, eyes opened	Mean absolute and relative power of typically developing children and children with ASD	ASD less relative alpha (91% sensitivity, 73% specificity) and more relative delta(76% sensitivity, 78% specificity)
Daoust et al.	n=9 age range=12-53 yrs sex=1F, 8M diagnosis=ASD subtypes= autism, Asperger's Syndrome	n=8 age range=8-56 yrs sex=1F, 7M	Relaxed, eyes closed morning and evening and sleep	1. Awake absolute spectral power 2.REM sleep spectral amplitude	Higher absolute theta over the left frontal pole region during evening wakefulness, but not during morning wakefulness. Lower absolute beta spectral amplitude over the primary (p<0.05) and associative (p<0.03) visual areas.
van Diessen et al.	n=19 mean age=10.6yrs sex=3F,16M	n=19 mean age=10.1yrs sex=3F,16M 7 taking medication	Relaxed, eyes closed	Spectral power	Higher relative gamma power in frontal, parietal and temporal regions (p=0.002).
Jetha et al.	n=15 mean age=18-51 yrs sex=3F, 12M subtypes= autism, Asperger's Syndrome, PDD-NOS medication=8 handedness=13RH, 2LH	n=16 mean age=22-47 yrs sex=4F, 12M handedness=14RH, 2LH	Relaxed, eyes opened and eyes closed	Differences in alpha power	Alpha power in each region greater in ASD than in control in the eyes open condition (p<0.05).
Klinger et al.	n=28 mean age=11 yrs sex=5F, 23M diagnosis=ASD subtypes= autism, PDD-NOS Peabody Picture Vocabulary Test-Revised (PPVT-R) scores=39 to 108 verbal age average=5.8	1.n=28 mean age=11 yrs sex=5F, 23M verbal age average=16 2.n=24 mean age=4.6 yrs sex=2F, 22M verbal age average=5.7	Relaxed eyes opened	Chronological-age-matched power spectra group comparison	Delta: ASD reduced power in the frontal and temporal regions (p<0.1). Theta: ASD reduced power in all three brain regions (p<0.05). Alpha: ASD reduced power in the frontal and temporal regions (p<0.05). Beta: no significant differences.

Machado et al.	n=11 mean age=70.3 m sex=4F, 7M diagnosis=ASD subtypes= autism	n=14 mean age=66.7 m sex=5F, 9M	Control: relaxed eyes opened; watching a popular cartoon; watching the cartoon without audio	Power spectral density (PSD)	Decreased PSD in the central region for delta and theta, and in the posterior region for sigma and beta bands, lateralized to the right hemisphere ($p<0.05$).
Maxwell et al.	n=15 mean age= 15.1 yrs sex=15M diagnosis=ASD subtypes= 14 Asperger's Syndrome, 1 autism	n=18 mean age=14.2 yrs sex=18M	Relaxed eyes opened	Resting gamma power	Decreased gamma power at the right lateral electrodes ($p=0.04$).
Scope et al.	n=20 mean age=12 yrs sex=2F, 18M subtypes= 9 autism, 8 Asperger's Syndrome, 3 PDD-NOS	n=20 mean age=13 yrs sex=2F, 18M	Looking at Gabor patches of different frequencies	Differences in changes in alpha and gamma frequencies of independent components	Induced alpha power of components that were in or near the cingulate gyrus was increased in ASD ($p<0.05$).
Stroganova et al.	n=40 age range=3-8 yrs sex=40 M subtypes= 38 autism, 2 PDD=NOS	n=40 age range=3-8 yrs sex=40M	Sustained visual attention	Spectral power	Increase of gamma at the electrode locations distant from the sources of myogenic artefacts ($p<0.05$).
Stroganova et al.	n=44 age range=3-8 yrs sex=44M diagnosis=ASD subtypes=42 autism, 2 PDD-NOS	n=44 age range=3-8 yrs sex=44M	Sustained visual attention	Spectral power	Higher amount of prefrontal delta in autism ($p<0.05$).
Tani et al.	n=20 mean age=27.2 yrs subtype= Asperger's syndrome diagnosis=ASD	n=10 mean age =26.5 yrs	Asleep	Spectral power	Non-significant trend towards decreased relative delta power and increased theta power in slow-wave sleep was found in the AS group.
Yang et al.	n=5 age range=16-22 yrs sex=1F, 4M subtype= Asperger's syndrome	n=7 age-matched	Looking at photographs of familiar faces	Spectral power	Decrease following the stimulus onset in two time-frequency intervals—(1) 150–300ms in the 1–16Hz frequency range and (2) 300–650ms in the 1–8Hz range ($p<0.01$).
Tierney et al.	n=168 diagnosis=ASD	Longitudinal studies: same patients at 6, 9,12, 18,24 months	Resting state	Change over time in spectral power	Across all bands, spectral power was lower in high-risk infants as compared to low-risk infants at 6-months of age ($p<0.01$).
Sheikhani et al.	n=17 age range=6-11 yrs sex=4F, 13M diagnosis=ASD handedness=1LH, 1 AD, 15 RH	n=11 age range=6-11 yrs sex=4F, 7M	Relaxed eyes opened	Accuracy in differentiating ASD using spectrogram criteria	Alpha frequency band had the best distinction level of 96.4% in relaxed eye-opened condition using spectrogram criteria. ASD had significant lower spectrogram criteria values in left hemisphere ($p<0.01$), at F3, T3, FP1, F7, C3, Cz and T5 electrodes ($p<0.05$).

Lushchekina et al.	n=27 mean age=5.8 yrs diagnosis=ASD subtypes= autism	n=24 mean age=6.1 yrs	Relaxed eyes closed, mental loading (counting, adding and subtracting numbers)	Spectral power in theta and gamma bands	ASD- lower theta spectral power in baseline (p=0.001) and higher gamma spectral power in baseline (p=0.005); cognitive loading presented no changes from baseline in either bands.
Lushchekina et al.	n=27 age range=5-7 yrs sex=27M diagnosis=ASD subtypes= autism	n=19 age range=5-7 yrs sex=19M	Relaxed eyes closed, mental loading (counting, adding and subtracting numbers)	Spectral power in alpha, beta and gamma bands	The cognitive task led to increases in spectral power in alpha1 and alpha 3 but no changes in alpha 2. ASD-gamma spectral power higher than control and did not change during the task ($p<0.05$).
Elhabashy et al.	n=21 age range=4-12 yrs diagnosis=ASD	n=21 age range=4-12 yrs	Relaxed eyes open	Absolute and relative spectral power	Increased absolute delta and theta power in ASD especially at the frontal region

*n=number of subjects; F=female; M=male; yrs=years; m=months; LH=left-handed; RH=right-handed; AD=ambidextrous; PDD-NOS=Pervasive Developmental Disorder Not Otherwise Specified

2.3. Information dynamics

Information dynamics comprises a collection of new methods derived from analysis of nonlinear physical systems using new computational methods from the mathematics of complex dynamical systems (Marwan, Romano et al. 2007, Webber Jr and Marwan 2015). Of the all studies representing the final literature pool considered in this review, six studies used these interdisciplinary methods to compare ASD patients and non-ASD subjects. These studies may use machine learning algorithms, neural networks, graph theory, or Bayesian methods to find group differences from features computed with nonlinear algorithms such as multiscale entropy or fractal analysis. The challenge with these methods is to determine neurophysiological meaning associated with the measures. All studies reported at least one statistically significant difference in at least one variable measured and very high classification capabilities based on those variables. Of the six studies employing such methods of analysis, only two have a common measure. The other four studies use distinct variables and concepts with the same goal. EEG recordings were performed under relaxed, no task conditions, with

eyes either open or closed, or during an object recognition or audio task. The overall patterns in results are presented in Table 3, which show the condition of the EEG recording and the main measure of each study or means of classification.

Multiscale entropy measurements were employed by Catarino et al. and Bosl et al. to measure brain signal complexity in children with autism, infants at high risk of developing ASD and non-ASD subjects during a relaxed eyes open condition and an object detection task respectively. Catarino et al. found significantly decreased multiscale entropy in ASD diagnosed participants compared to controls, predominantly in temporo-parietal and occipital areas of the brain (Catarino, Churches et al. 2011). Bosl et al., found the same results in multiscale entropy, averaged over the entire scalp. The latter found that the greatest differences are observed between 9 and 12 months of age, as multiscale entropy shows an overall different developmental trajectory for infants at high-risk of developing ASD compared to low-risk infants. Bosl et al., used classification algorithms to show that children with a high risk of developing autism based on family history could be detected with high accuracy at 9 to 12 months of age, leading to the more important question of whether an autistic neuroelectrophysiological phenotype could be detected early in infancy. This supervised learning experiment yielded a sensitivity value of over 80% at 9 month of age, remaining very high (70-90%) until 12 month of age (Bosl, Tierney et al. 2011).

Elridge et al. used Bayesian methods to perform a similar classification between ASD and typically developing children, between 6-10 years old. This study extracted robust features such as variance in time, entropy or sum of 391 signed differences from the EEG signal and then used logistic regression and a native Bayes classifier to divide the two groups with a 79% accuracy (Eldridge, Lane et al. 2014). Ahmadlou et al. used a different method of classification based on complexity and chaos theory. Two types of fractal dimensions were used to assess dynamical changes in the brains of ASD children and non-ASD subjects in all frequency sub-

bands: Higuchi's Fractal Dimension and Katz's Fractal Dimension, which indicate non-integers or fractional dimensions of time series, based on regularity or self-similarity of a time series. After computation of fractal dimensions, the most significant characteristics were extracted using analysis of variance (ANOVA). Finally, a Radial Basis Function Neural Network classifier was used to separate ASD from non-ASD subjects. The accuracy of this classification was 90% (Ahmadlou, Adeli et al. 2010).

Table 5: Studies using information dynamics

Paper	**Patients characteristics**	**Controls characteristics**	**Condition**	**Measure**	**Changes in ASD**
Bosl et al.	n=46 age range=6-24 m diagnosis=high risk for autism (HRA)	n=33 age range=6-24 m	Infants' attention was engaged by the researcher blowing bubbles.	1.Modified multiscale entropy (mMSE) 2.Machine learning classification accuracy	1.HRA lower mean complexity over all channels; most prominent differences between groups was the change in mMSE between 9 and 12 months 2.Machine learning techniques threshold P = 0.05: HRA and control groups classified at age 9 months for boys and girls together and for boys separately with accuracies of 80% and well over 90%, respectively.
Eldridge et al.	n=19 age range=6-10 yrs diagnosis=ASD	n=30 age range=6-10 yrs	Auditory paradigm (oddball paradigm)	1. Classification accuracy using robust features, a support vector machine, logistic regression, and a naive Bayes classifier	1. Bayesian classification: sensitivity of 79% was achieved for classifying ASD and non-ASD subjects.
Gregory et al.	n=56 age range=2-22 yrs diagnosis=ASD	n=56 age range=2-22 yrs	Relaxed eyes open	1. Differences in posterior dominant EEG rhythm (PDR) between groups	1.2-sampled t-tests: across the entire pool of participants: significantly different PDR between ASD and non-ASD subjects (p=0.014) ages 2–5.9 years (n = 22): significantly different PDR between ASD and non-ASD subjects (p = 0.047). ages 6–22 years (n = 34):no significant differences in PDR between ASD and non-ASD subjects (p> 0.05)
Ahmadlou et al.	n=9 age range=7-13 yrs subtypes= autism	n=9 age range=7-13 yrs	Resting state, eyes closed	1. Discriminative capacity of functional connectivity within and between regions. 2. Accuracy of EPNN classification of ASD and non-ASD.	1. One way ANOVAs: Theta band right-temporal- right-temporal; Occipital-Frontal; Parietal- Right-temporal; Occipital-Central (P<0.0005) 2. 95.5% sensitivity with 1.2% variance of classification of ASD and non-ASD subjects.
Ahmadlou et al.	n=9	n=8	Resting state, eyes closed	1. Discriminative capacity	1. One way ANOVAs significant differences using

	age range=6-13 yrs sex=2F, 7M	age range=7-13 yrs sex=2F, 6M		of Fractal Dimensions (FD) in 5 sub-bands 2. accuracy of Radial Basis Function Neural Network classification of ASD and non-ASD	Katz's Fractal Dimension: gamma in temporal regions, delta in frontal and central regions (P<0.001) 2. 90% accuracy in the 3 parameter feature space with 0.15% variance
Catarino et al.	n=15 mean age=31.4 yrs diagnosis=ASD	n=15 mean age=29.4 yrs	Face and chair detection task	Signal complexity (multiscale entropy)	1. ASD decreased multiscale entropy over temporo-parietal and occipital regions (P=0.036)

*n=number of subjects; F=female; M=male; yrs=years; m=months

In conclusion, the results of these suggest the high utility of EEG signal analysis in characterising the disorder and the facts that it is a vital complement to other existing technologies. The current literature supports further research, suggesting different electrophysiological features of high importance and major gaps that can be filled. Therefore, we set out to use new, advanced methods of analysis in combination with already established ones to make one step closer to the final goal: early detection of emerging autism, which may open a window for early intervention and prevention.

3. Materials and Methods

3.1. Data Collection

The data used in this study consists of two cohorts. The first cohort contains data collected in Kilifi, Kenya from both healthy neurotypical children as well as children diagnosed with ASD. The second comes from the National Database for Autism Research (NDAR), also containing data from both neurotypical children and those with ASD.

The Kenyan Cohort

The data in the Kenyan cohort were collected from 22 different children, 11 ASD patients and 11 healthy controls, recruited by clinicians in Kilifi, Kenya. The data was collected in Kilifi, Kenya within the KEMRI-Wellcome Trust Research Program, Centre for Geographic Medicine Research. The patients were recruited after a two stage screening process. Firstly, the children were screened using the Neurodevelopmental Screening Questionnaire (NDST), conducted in the community households (Juneja, Mishra et al. 2014). Those who screened positive for specific questions on features of autism were further assessed using the 3Di and Autism Diagnostic Observation Schedule (ADOS) in the Neuro-assessment clinic (Skuse, Warrington et al. 2004, Falkmer, Anderson et al. 2013, Slappendel, Mandy et al. 2016). The 3Di is a computer-based test, developed for administration by trained personnel that outputs symptom and diagnostic profiles for several social communication disorders, both autism and non-autistic, over a wide range of IQs. The test uses short questions that refer to a very specific feature of behaviour, decreasing rater inference, and therefore increasing its validity (Santosh, Mandy et al. 2009). ADOS is a semi-structured test widely used in the second stage of the diagnostic process. It is based on games and activities and targets the two large domains that make up the diagnosis criteria (Roth and Rezaie 2011). The screening sensitivity of the NDST for all Neurodevelopmental Disorders was 93.7% (92.7-94.7%) and was approximately 98.7% (95%CI, 98.2-99.2%)) against ADOS. The diagnosis of autism was based upon clinical criteria according to the DSM-V, with data from the 3Di and ADOS.

The ASD study group included 11 participants diagnosed with ASD after the two stage process described above, aged 6-9 years old (mean age=8, SD=1, 8 females, 3 males) and 11 typically developing children, referred to as controls age-matched (mean age=8.1, SD=1.1, 6 females, 5 males). Six of the 11 patients were also diagnosed with epilepsy, two had a history of acute illness and four were delivered prematurely.

Continuous EEG was recorded using a 19-channel digital recording system (Grass Technologies, Warwick, RI, USA) with electrodes placed according to the international 10–20 system (Jasper 1958). Recordings were conducted for at least 20 minutes, during which all participants were asked to hyperventilate for 3 minutes and had photic stimulation (Binnie, Rowan et al. 1982). The data were amplified, filtered with a 0.1-100.0 Hz bandpass filter and sampled at a frequency of 200 Hz. Two minutes of baseline activity were recorded and continuous sample segments of 30 seconds were selected from the resting state data and used to compute the entropy and RQA values.

The NDAR Cohort

The data in this cohort come from the NDAR, a research data repository funded by the National Institute of Health (NIH) encouraging progress in ASD research through data sharing, data harmonization, and sharing of research outputs. NDAR also serves as a scientific community platform for multiple other research repositories, allowing for aggregation and secondary analysis of data. This dataset consists of 49 individuals, 23 diagnosed with ASD aged 4.42-11.42 years old (mean age=8.07, SD=2.24, 5 females, 18 males) and 26 typically developing aged 4.08-11.50 years old (mean age=6.65, SD=1.99, 9 females, 17 males). This data was obtained by Dr. William Bosl, who is a member of the NDAR.

3.2. Feature extraction

This part of the analysis was performed by Dr. William Bosl, a collaborator from University of San Francisco. Each of the EEG samples was processed in an identical manner by the following steps. Thirty-second segments were selected from the beginning of the EEG recordings for each subject. Previous research studies that analyzed EEG data for autism biomarkers found that 30 seconds of data was sufficient. It was found that the nonlinear features computed from 30 seconds of resting state data were relatively stable (Bosl, Loddenkemper et

al. 2017). Further research on this specific topic would be beneficial, as it is not known if longer segments, or multiple shorter segments, might improve the diagnostic potential of nonlinear EEG analysis. The optimal size of segment lengths has yet to be determined. The original study of multiscale entropy as a biomarker for autism used only 10 second segments and found significant results (Bosl, Tierney et al. 2011). Average referencing was computed and used for all EEG time series. A quantitative analysis was performed on every EEG signal segment using multiscale entropy (MSE) values and Recurrence Quantitative Analysis (RQA).

As defined in the Introduction, entropy is a physical measure of a system's complexity, with ordered systems displaying low entropy values and irregular systems showing very high entropy values. However, regularity is not always correlated with complexity. Random phenomena like white noise are highly irregular and will therefore present very high values of entropy, but they lack in structural richness of information over multiple spatial and temporal scales, which is an essential characteristic of complex systems (Costa, Goldberger et al. 2002, Costa, Goldberger et al. 2005). To make a clear differentiation between white noise and real complexity, Costa proposed the method of MSE, which uses a coarse-graining procedure to measure the complexity of a signal across multiple time-scales. This methods is based on the idea that complex biological systems are controlled by several mechanisms that interact across multiple time-scales, yielding complex data consisting of overlapping signals. Multiscale methods will then show great entropy values for progressively coarser time-scales. Decreasing entropy values will characterize random signals such as white noise as the time-scales increase, because white noise only contains information on the shortest time-scales, therefore the standard deviation of the signal decreases (Costa, Goldberger et al. 2005).

The scaling method typically uses the coarse-graining algorithm showed in Figure 2 and it can be applied to numerous variables, not just entropy. For power-of-two scales (2, 4, 8, 16, …)

the time series produced by this method are identical to the Haar wavelet transform (Struzik and Siebes 1999).

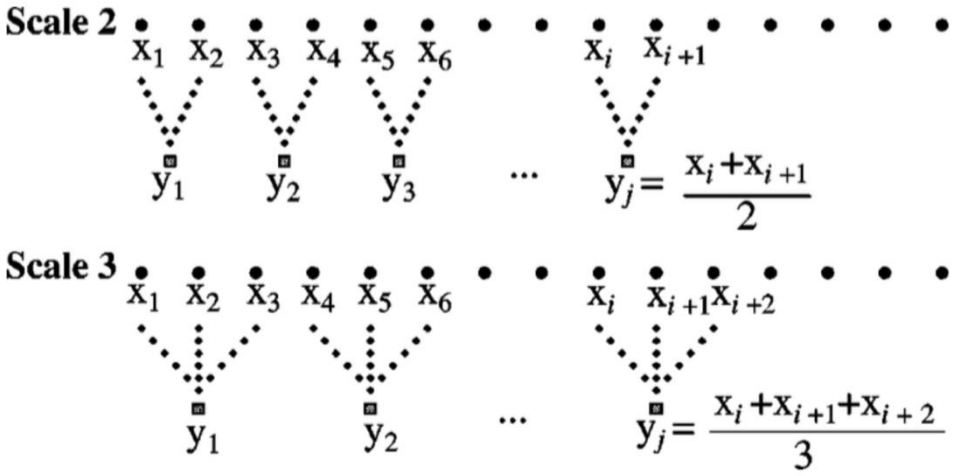

Figure 2: The coarse-graining procedure introduced by Costa, et al. (2005) is illustrated. For powers of 2, the resulting scaled time series are identical to Haar wavelet transform approximations.

There is a lot of information about the properties of wavelet transforms and their use in neurophysiological signal analysis is important e.g. wavelets can be associated with the 'classic' frequency bands. For example, according to the Niquist limit, if an EEG signal has a sampling rate of 200 Hz, then the signal contains frequencies up to 100 Hz (Srinivasan 2005). Scale 2 in the coarse-graining procedure corresponds to wavelet approximation level 1, and comprises of all frequencies up to half of the original signal, so 0 to 50 Hz, while the highest frequencies are removed in the averaging process. The complete averaging method yields the results shown in Table 6, which shows the relationship between coarse-graining scales and the 'classic' frequency bands.

Table 6: The coarse-graining procedure is mathematically identical to the Haar wavelet transform. For signal collected with a sampling rate of 256 samples per second, the frequency bands contained in the scales, wavelet approximations, and wavelet details are shown.

Coarse-grain averaging scales	**Wavelet level**	**Frequency range**		
		Wavelet approximation	**Wavelet detail**	
			Frequencies	EEG Band
1	0	0 – 128 Hz	Original signal	
2	1	0 – 64 Hz	64 - 128 Hz	High gamma
3	2	0 – 32 Hz	32 - 64 Hz	Gamma
4	3	0 – 16 Hz	16 - 32 Hz	Beta
8	4	0 – 8 Hz	8 – 16 Hz	alpha
16	5	0 – 4 Hz (delta)	4 – 8 Hz	Theta

Wavelet transforms and coarse-graining procedure decompose a time series in very similar ways. However the wavelet transform has the advantage of retaining, not only the approximations which are equivalent to the multiscale ranges, but also the details that have been removed in each step which contain the higher frequencies that have been removed. Therefore, a wavelet transform could perfectly replace the coarse-graining procedure introduced by Costa, if both the details and the approximations are used.

For this study, we used the DB20 wavelet transform to compute the wavelet details, which are power-of-two frequency bands. The closest traditional labels (delta, theta, alpha, beta, gamma, and high gamma) to the wavelet detail are shown in table. For the remainder of this thesis, six non-overlapping frequency bands are used for all analysis and the traditional frequency band labels are used in figures. All data was sampled at 200 Hz. Recurrence plots were computed from the original signal and from each of the wavelet transforms that effectively created averaged signals of successively coarser resolution by powers of two.

Recurrence quantitative analysis (RQA) values were calculated for all of the frequencies derived from each EEG channel. The software for computing recurrence plot statistics is publicly available from a web site (http://www.recurrence-plot.tk/). Seven of the most commonly used recurrence plot values (RR, DET, LAM, L_max, L_entr, L_mean, and TT) were computed and used in this study, as well as multiscale entropy, denoted from now on as

sample entropy (SampE). SampE was computed using publicly available software "Nonlinear measures for dynamical systems" or nolds, version 0.3.2 (https://pypi.python.org/pypi/nolds).

Therefore, eight nonlinear values, describing neural activity, were computed on each of the six frequency bands from each EEG sensor time series. Brief definitions of SampE, RR, DET, LAM, L_max, L_entr, L_mean, and TT and what processes they underlie are given in Table 7.

Table 7: Nonlinear invariant measures of a time series and their physical interpretation.

Nonlinear Variable	Symbol	Definition
Invariant measures computed with the nolds software package		
Sample Entropy	SampE	Sample entropy measures the complexity of a time-series, based on approximate entropy (Bosl, Tierney et al. 2011, Bosl, Tager-Flusberg et al. 2011)
Invariant measures derived from Recurrence Quantitative Analysis (RQA)		
Entropy derived from recurrence plot	L_entr	A measure of entropy computed from the diagonal lines of the recurrence plot, closely associated with the Shannon entropy. It is associated to other measures of entropy, such as sample entropy.
Max line length	L_max	L_max is related to the largest Lyapunov exponent of a chaotic signal, which is a dynamic complexity measure that describes the divergence of trajectories starting at nearby initial states, (Gomez and Hornero 2010). Lower L_max values are typically associated with pathological conditions (Goldberger 1997, Peng, Costa et al. 2009).
Mean line length	L_mean	The time that two segments of the recurrence plot trajectory are close to each other, and can be interpreted as the mean prediction time of the signal, a measure of chaos or divergence from an initial point.
Recurrence rate	RR	The probability that a system state recurs in a finite time. RR has been found useful for detecting evoked response potentials (ERPs) using single trials (Schinkel, Marwan et al. 2009). The concept is similar to periodicity.
Determinism	DET	DET comes from repeating patterns in the system and is an indication of its predictability. Regular, deterministic signals, such as sine waves or deterministic chaos, will have higher determinism values, while uncorrelated time series, such as random numbers, will have low detreminism.
Laminarity	LAM	Laminarity represents fast transitions and instabilities, or the frequency of transitions from one state to another, without describing the length of these transition phases. More frequent appearance of laminar states may relate to more frequent "seeds" for synchronized dynamics (Hirata and Aihara 2011).
Trapping time	TT	Trapping time is an estimate of the time that a system will remain in a given state, such as the length of transition states, as opposed to the time for the transition to take place.

These variables characterize the dynamical features of the EEG time series, which should correlate to functional characteristics of the neural network of the brain that produced the time

series. Statistical methods will be used to compare the two samples and find patterns that are associated with typically developing and atypically developing brains.

The total feature set computed from each EEG session consists of 8 invariant measures computed on 6 frequency bands for each of 19 sensors, totaling 912 features. Many of these features are likely to be correlated to some extent. Spatially close sensors might reasonably be expected to have some overlapping tendencies. Some nonlinear measures may also be correlated. For example, SampE and L_entr are both measures of entropy, though derived by entirely different algorithms. However, many of these features may contribute with different, independent information about neural function.

3.3. Data Analysis

The statistical analysis was performed in three steps. All statistical analysis was performed using the commercial software packages Matlab (MATLAB 9.1, The MathWorks Inc., Natick, MA, 2016) and SPSS (IBM Corp. Released 2013. IBM SPSS Statistics for Windows, Version 22.0. Armonk, NY: IBM Corp)

The first step of the analysis involved averaging the values of each variable and frequency across electrode contacts to obtain whole brain measurements of the respective variables for each frequency for each individual. In order to determine which variables measured over the whole brain accurately delineate the two groups, binary logistic regressions were performed, each model consisting of the values at all six frequencies for each variable at a time. Six predictors were therefore tested using this method for each variable. A whole brain analysis was considered useful as it could identify whole brain markers of ASD that could then be used with any EEG electrode montage. As numerous EEG headsets are now available with different numbers of electrodes, this measure could provide a universal marker to span heterogeneity in data collection methods.

The second step of the analysis involved a closer look at each variable individually and more specifically, accounting for brain regions and electrode locations. This step was performed in order to conclude in which scalp locations and in which frequencies the variables have the capacity to distinguish the two groups, as well as for comparison with the previous findings that looked at the overall dataset, across all electrodes. An exploratory factor analysis using principal components (PCA) was performed for each individual variable, including all the data points for the electrode locations and frequencies. The PCA was performed using the correlation matrix, as this is a useful default method because it takes the standardized form of the matrix. Therefore, if variables were measured using different scales this will not affect the analysis. Additionally, even variables measured using the same scale can have very different variances and this can also cause problems when performing a PCA. Using the correlation matrix addresses this problem. The orthogonal varimax rotation was used because this method tries to maximize the distribution of loadings within factors, hence loading a smaller number of variables highly onto each factor resulting in clusters more accessible for interpretation. The univariate descriptives were also analyzed. Moreover, if data points were missing, a list wise elimination would be performed. Initially, Kaiser's criteria was used and only factors with an eigenvalue higher than 1 were retained. After each PCA was performed, a variable number of factors were further selected from each variable using the criteria that the amount of cumulative variance explained by them is approximately 80%. The regression scores were saved for each of these factors and formed a binary logistic regression model that determined their prediction capacity. The factors that contributed significantly to the main effect of successful models were then selected and the loadings of the features that compose them were plotted. For a better understanding and interpretation of the results, another filtering step was necessary consisting of the selection and plotting of the data points that had a component loading higher than 0.3 or lower than -0.3, as the component loadings represent

correlations between the variables and the identified components. This was done in order to determine visually and conclude which features contributed significantly to the delineation.

4. Results

The dataset consisted of two cohorts, with individuals classified as ASD patients or controls. The first cohort consisted of data collected in Kenya from 11 ASD patients and 11 typically developing children, referred to as controls The ASD patients were aged 6-9 years old (mean age=8, SD=1, 8 females, 3 males) and the controls were age-matched (mean age=8.1, SD=1.1, 6 females, 5 males), without statistically significant differences in age. The second cohort consisted of 49 individuals, 23 ASD patients aged 4.42-11.42 years old (mean age=8.07, SD=2.24, 5 females, 18 males) and 26 controls aged 4.08-11.50 years old (mean age=6.65, SD=1.99, 9 females, 17 males). All individuals from both cohorts were characterized using eight variables, six frequency bands and 19 scalp locations.

The two cohorts were not combined to form a larger one for analysis, for the following reasons: i) the data was collected in very different environments; ii) no other information could be obtained about the data collection for the NDAR cohort or about the medical history of the patients. Avoiding the risk of obtaining a heterogeneous dataset, the two cohorts were analyzed separately and the results were compared in the Discussion.

The analysis was performed in two steps, investigating the utility of these variables to delineate an ASD diagnosis at a whole brain level and at individual electrode locations. The results of the analysis are presented below.

4.1. Whole Brain Analysis

The aim of this investigation was to see if the two groups could be delineated based on a set of eight variables derived from EEG signals (sample entropy, recurrence rate, determinism, laminarity, l_max, l_mean, l_ent and trapping time) measured across the whole brain for the six frequency bands. The outcome variable was the ASD diagnosis (ASD vs controls). The predictor variables were the measurements of each variable at a time for each frequency band across participants. The values for each variable formed one separate individual model.

As the study is investigating the prediction of a binary categorical outcome based on continuous predictor variables, a binary logistic regression using a forced entry method was performed to assess the impact of the six predictor variables on the likelihood participants had an ASD diagnosis. Each model contained six independent (predictor) continuous variables consisting of the values of the eight measures used in this study for the six frequency bands.

4.1.1 Sample Entropy

The first variable investigated was sample entropy. The main statistics of the first binary regression analyses performed are presented in Table 8. The results for the two cohorts are presented together for comparison.

Table 8: Results for sample entropy of binary logistic regression with a dichotomous outcome and six predictor variables for: Kenyan cohort: overall model fit: chi^2= 14.794, p=0.022; additional fit statistics: Cox&Snell R^2=0.490, Nagelkerke R^2=0.653; linearity fit: R^2 p=0.759 (Hosmer-Lemeshow); classification sensitivity=90.9%, specificity=72.7%, accuracy=81.8%; NDAR cohort: overall model fit: chi^2= 13.905 p=0.031; additional fit statistics: Cox&Snell R^2=0.247, Nagelkerke R^2=0.330; Linearity fit: R^2 p=0.632 (Hosmer-Lemeshow); classification sensitivity=52.2%, specificity=73.1%, accuracy=63.3%.

Variable	Cohort	Frequency	b	Wald statistic	p-value (df=1)	95% CI for Odds ratio		
						Lower	Odds ratio(ExpB)	Upper
Sample entropy	**Kenyan**	Delta	-41.540	1.698	0.193	0.000	9.1036e-19	1236873127.503
		Theta	15.596	0.291	0.590	0.000	5930824.190	2.51e+31
		Alpha	21.348	2.268	0.132	0.002	1867387730.330	2.174e+21
		Beta	-15.032	2.036	0.154	0.000	2.9626e-7	275.058
		Gamma	29.670	3.411	0.065	0.163	7.684e+12	3.632e+26
		High gamma	-17.478	1.993	0.158	0.000	2.5675e-8	886.345
	NDAR	Delta	-1.236	0.505	0.477	0.010	0.291	8.787
		Theta	-2.529	0.669	0.413	0.000	0.080	34.117
		Alpha	-10.249	5.198	0.023	0.000	0.000035	0.237
		Beta	7.674	4.136	0.042	1.320	2150.763	3503579.594
		Gamma	-9.675	4.712	0.030	0.000	0.000063	0.391
		High gamma	5.516	3.347	0.067	0.675	248.742	91669.710

Two models containing six predictors were tested for sample entropy, one for each cohort. The predictors consisted of the values obtained for sample entropy for each frequency band across the whole brain. The model for the Kenyan cohort was statistically significant (chi-square=14.794, p=0.022) indicating that the alternative model is a significantly better fit than the baseline model (without the predictors). Furthermore, the Hosmer-Lemeshow test is not significant (p=0.759) which reinforces the fact that the alternative model is a good fit of the data. The R square statistics suggest that approximately 49% (Cox and Snell R square) to 65% (Nagelkerke R square) of the variance in the data is explained by the model. In the alternative model, 81.8% of the cases were correctly classified compared to the baseline model (50%), with a 72.7% specificity and 90.9% sensitivity, which reinforces the accuracy of the alternative model. Table 8 indicates that, although the overall model fit was significant, none of the independent variables were significant predictors (all p-values>0.05). However sample entropy in the gamma band was almost significant (p=0.065). Although not significant, this factor seems to play an important role in the main effect of the model.

The second model, for the NDAR cohort was also statistically significant (chi-square=13.905, p=0.031) indicating that the alternative model is a significantly better fit than the baseline model. Furthermore, the Hosmer-Lemeshow test is not significant (p=0.632) which supports the alternative model as a good fit of the data. The R square statistics imply that approximately 24% (Cox and Snell R^2) to 33% (Nagelkerke R^2) of the variance in the data is explained by the model. This model had an overall classification accuracy of 63.3%, a specificity of 73.1% and a sensitivity of 52.2%. Table 9 suggests that three of the six predictors contributed significantly to the accuracy of the model. The strongest predictor was sample entropy in the alpha band (Wald statistic=5.198, df=1, p =0.023). This has an odd ratio <0.001, suggesting with sample entropy increasing in the alpha band, the chances for an individual to carry an ASD diagnosis decrease substantially. The other two significant predictors were the values of sample entropy in the beta (Wald statistic=4.136, df=1, p=0.042) and gamma (Wald statistic=4.712, df=1, p=0.030) bands. The odds ratio obtained for sample entropy in the beta band are >1, suggesting that when the level of entropy increases in the beta band, so does the chance for an individual to be diagnosed with ASD; whereas an increase in entropy in the gamma band corresponds to a decrease in the chances of having ASD as the odds ratio <0.001. The 95% confidence intervals for sample entropy values in the alpha and gamma bands' odds ratios do not cross one, which also suggests they are significant predictors, with a negative association with the outcome. The 95% confidence intervals for the beta band are >1 on both limits of the interval confirming a positive association with the ASD outcome.

4.1.2 Trapping time

The second variable that showed significant results was sample entropy. The main statistics of the binary regression analyses performed are presented in Table 9. The results for the two cohorts are presented together for comparison.

Table 9: Results for trapping time of binary logistic regression with a dichotomous outcome and six predictor variables for: Kenyan cohort: overall model fit: chi^2= 14.322, p=.026; additional fit statistics: Cox&Snell R^2=0.478, Nagelkerke R^2=0.638; linearity fit: R^2 p=0.554 (Hosmer-Lemeshow); classification sensitivity=81.8%, specificity=81.8%, accuracy=81.8%; NDAR cohort: overall model fit: chi^2= 4.305 p=0.636; additional fit statistics: Cox&Snell R^2=0.084, Nagelkerke R^2=0.112; linearity fit: R^2 p=0.073 (Hosmer-Lemeshow); classification sensitivity=47.8%, specificity=50.0%, accuracy=49.0%.

Variable	**Cohort**	**Frequency**	**b**	**Wald statistics**	**p-value (df=1)**	**95% CI for Odds ratio**		
						Lower	**Odds ratio(ExpB)**	**Upper**
Trapping time	**Kenyan**	Delta	-2.292	1.752	0.186	0.003	0.101	3.010
		Theta	-2.096	1.954	0.162	0.007	0.123	2.322
		Alpha	0.299	1.682	0.195	0.858	1.349	2.119
		Beta	0.292	0.886	0.347	0.729	1.339	2.457
		Gamma	-0.014	4.082	0.043	0.973	0.986	1.000
		High gamma	0.004	3.250	0.071	1.000	1.004	1.009
	NDAR	Delta	-0.033	0.094	0.759	0.786	0.968	1.192
		Theta	-0.024	0.101	0.751	0.840	0.976	1.134
		Alpha	0.009	0.256	0.613	0.974	1.009	1.046
		Beta	0.004	0.452	0.501	0.993	1.004	1.015
		Gamma	-0.003	1.474	0.225	0.991	0.997	1.002
		High gamma	0.000	0.218	0.641	0.999	1.000	1.002

Table 9 illustrates the results obtained after performing two logistic regressions using six predictors for each model, consisting of the values of trapping time for all six frequency bands for the two cohorts. The model using the Kenyan data was statistically significant (chi^2= 14.322, p=.026), suggesting that trapping time could potentially be used to successfully classify individuals in the two groups. Moreover the non-significant Hosmer-Lemeshow p-value (p=0.554) suggests that this model is a better fit than the baseline. The trapping time model explains between 48% (Cox&Snell R^2) and 64% (Nagelkerke R^2) of the variance in the Kenyan data. The model's sensitivity, specificity and accuracy values were identical, of 81.8%. Out of the six predictors, only trapping time in the gamma band contributed significantly to the effect of the model (Wald statistic=4.082, df=1, p=0.043). This predictor has an odd ratio <1, suggesting with sample entropy increasing in the alpha band, the chances for an individual to carry an ASD diagnosis decrease. The 95% interval of the variable in the gamma band confirms the negative association between the predictor and the outcome. The results propose that

trapping time could potentially be used to classify individuals in the two groups, particularly using the measurements in the gamma band.

However, the model using as predictors the measures of trapping time in the six frequencies in the NDAR cohort was non-significant ($p>0.05$). Although non-significant, the Hosmer-Lemenshow test yielded a value close to the significance threshold ($p=0.073$), demonstrating that the model is not a good fit compared to the baseline. Additional fit statistics show that only 8% (Cox&Snell R^2) to 11% (Nagelkerke R^2) of the variance can be explained by this model. Furthermore, none of the six predictors showed a significant contribution to the main effect of the model (p-values>0.05). This contradicts the initial findings using the Kenyan cohort, indicating that trapping time does not have a high utility in classifying individuals in the two groups, in this cohort.

None of the other six variables tested (recurrence rate, determinism, laminarity, l_max, l_mean, l_entropy) yielded statistically significant results. None of the models with predictors consisting of values of these variables across the six frequency bands for either of the two cohorts proved to be statistically significant in separating the data in the two groups. All of the models were better fitted in comparison to the baseline models. Moreover, none of the individual predictors had a significant contribution to the main effect of the models. The results of these tests are presented in the Appendix.

The diagram in Table 10 presents a summary of all the whole brain analysis results.

Table 10: A summary of all the results obtained after the whole brain analysis including a logistic regression for each variable across all frequency bands.

Kenyan cohort		**NDAR cohort**	
Variable	**Frequency**	**Variable**	**Frequency**
Sample entropy	-	SampE	Alpha (-), beta (+), gamma (-)
Trapping time	Gamma (-)	TT	-

4.2. Single Electrode Analysis

The aim of this analysis step was to identify individual electrode regions and frequency bands within each variable (sample entropy, recurrence rate, determinism, laminarity, l_max, l_mean, l_ent and trapping time) that best distinguished ASD children from the neurotypical controls. The first step included reducing the dimensions of the datasets for each variable, by grouping them statistically into different components according to the variance they explain. For this purpose exploratory factor analyses using principal components were performed (PCA) based on the correlation matrices, using a varimax rotation. Initially the factors were retained based on Kaiser's criteria of eigenvalues greater than 1. A further filter was applied and the number of factors was determined by their cumulative variance explained, which had to be approximately 80%. The regression scores were saved for these factors and used in binary logistic regressions to determine their accuracy in delineating the two groups. After ranking the factors based on their significance levels within the regression models, the first factors were selected and their component loadings were plotted, to visually determine which variables, in which brain region and frequency present a high utility for categorizing the individuals correctly. This strategy was followed for both cohorts and the results are presented below.

4.2.1 Sample Entropy

Kenyan Cohort

Firstly, in the Kenyan cohort sample entropy yielded a total of 13 components with an eigenvalue greater than 1. These 13 components cumulatively accounted for 96.2% of the variance. The univariate descriptive statistics suggested that none of the data points were removed in the analysis. The first four components were then selected for the binary logistic regression model, as they cumulatively explained 81.1% of the variance in the data. The output Scree plot used for guidance can be visualized in Figure 3.

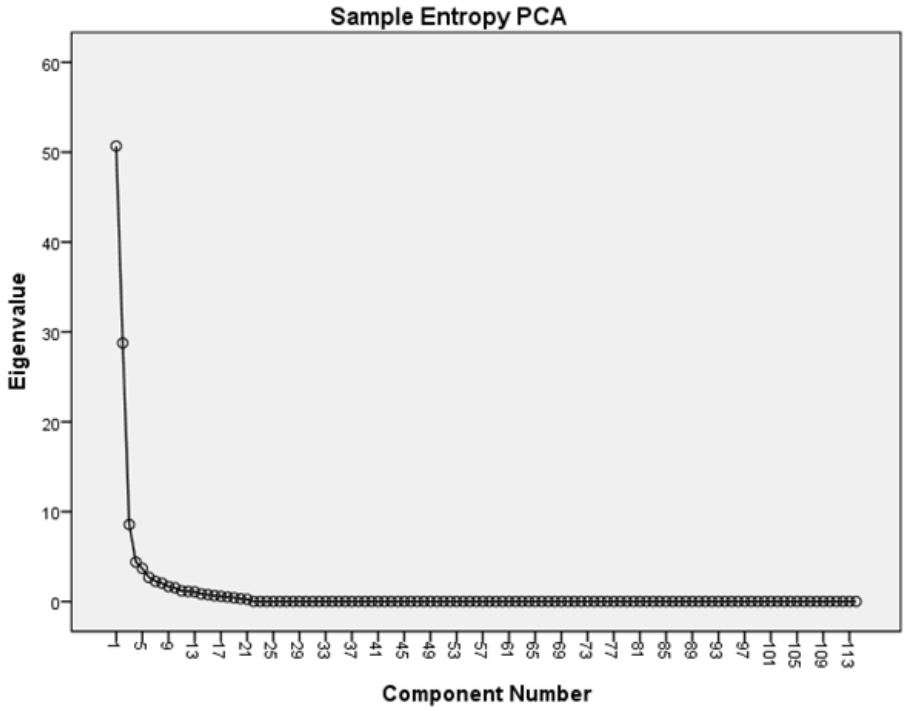

Figure 3: Scree plot obtained from a PCA on all sample entropy data points, for all frequency bands and scalp locations in the Kenyan cohort. This plots the eigenvalues of each component identified.

The regression scores were saved for these four components and used as predictors in a logistic regression model with a dichotomous outcome (ASD or control). The results of the regression are presented in Table 11.

Table 11: Results for sample entropy binary logistic regression with a dichotomous outcome and the PCA regression scores of factors 1,2,3 and 4 as predictors for the Kenyan cohort: overall model fit: chi^2=18.642, p=0.001; additional fit statistics: Cox&Snell R^2=0.571, Nagelkerke R^2=0.762; linearity fit: R^2 p=0.882 (Hosmer-Lemeshow); classification sensitivity=81.8%, specificity=81.8%, accuracy=81.8%.

Variable	Cohort	Component	b	Wald statistics	p-value (df=1)	95% CI for Odds ratio		
						Lower	Odds ratio(ExpB)	Upper
Sample entropy	**Kenyan**	1	1.808	2.388	0.122	0.616	6.096	60.361
		2	4.888	2.558	0.110	0.332	132.746	53059.306
		3	-4.311	3.525	0.060	0.000149	0.013	1.208
		4	-0.866	1.191	0.275	0.089	0.421	1.992

The model consisting of the regression scores from the PCA of the first four components selected as the predictors was statistically significant in delineating the two groups (chi^2=

18.642, p=.001). Moreover, the Hosmer-Lemenshow test was not significant (p=0.882), suggesting that the model is a greater fit compared to the baseline model. Between 76% (Cox&Snell R^2) and 88% (Nagelkerke R^2) of the variance in the data could be explained using this model. The model separated the groups with an 81.8% sensitivity, 81.8% specificity and 81.8% accuracy. Table 11 indicates that, although the overall model was significant, none of the independent variables were significant predictors (all p-values>0.05). However, component 3 was very close to significance (p=0.060). Although not significant, this component seems to play an important role in the high accuracy of the model. Within the PCA, component 3 had an eigenvalue of 8.567 and explained 7.5% of the variance in the data. The loadings of each data point on this factor were plotted and can be observed in Figure 4, in order to understand which frequency bands and scalp locations contributed the most to the delineation of the two groups.

A clear pattern can be observed in the component loadings plotted in Figure 4, with relatively high positive values in the delta and theta frequencies and negative values in the alpha and beta frequencies. In the gamma and high gamma bands most loadings observed show positive values, much lower compared to the low frequency bands. For a better understanding and interpretation of these results, another filtering step was necessary consisting of the selection and plotting of the data points that had a component loading higher than 0.3 or lower than -0.3. The filtered results were then plotted in Figure 5.

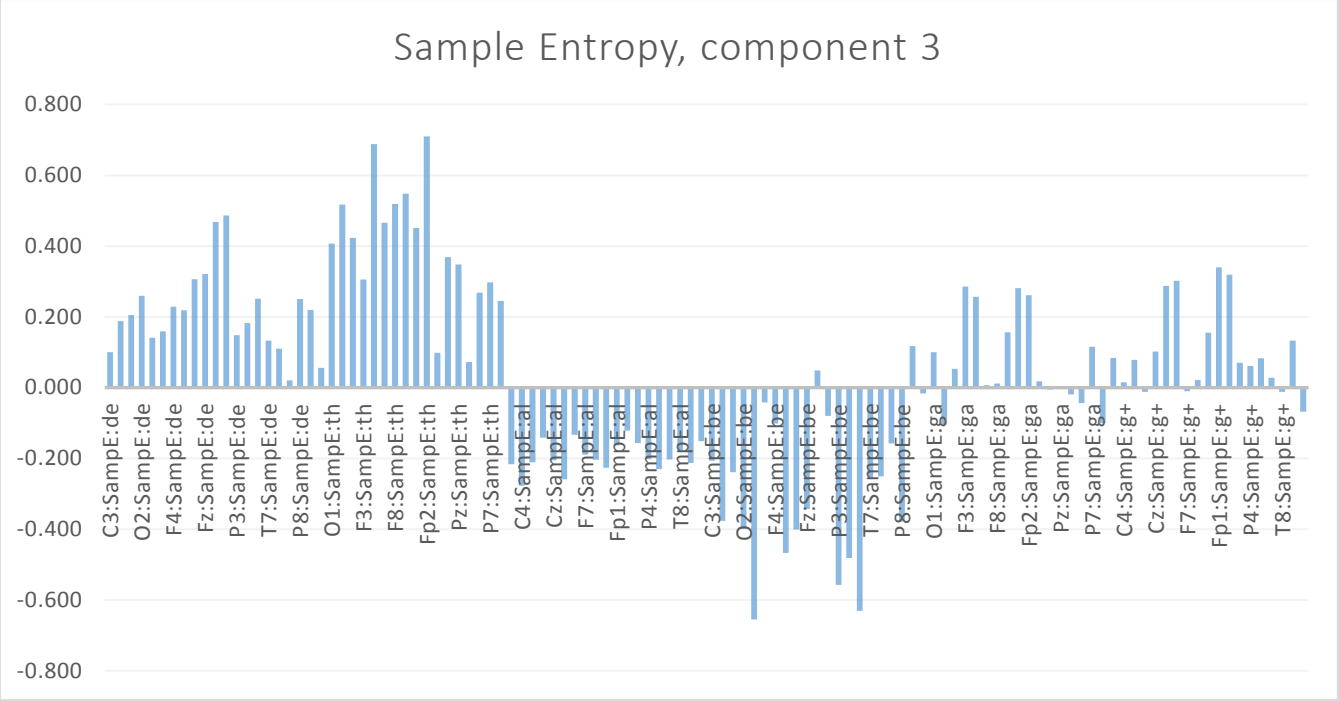

Figure 4: Sample entropy component loadings of each data point on component 3 obtained in the PCA, against the labels of each data point including the abbreviated variable name, frequency band and electrode location, in the Kenyan cohort.

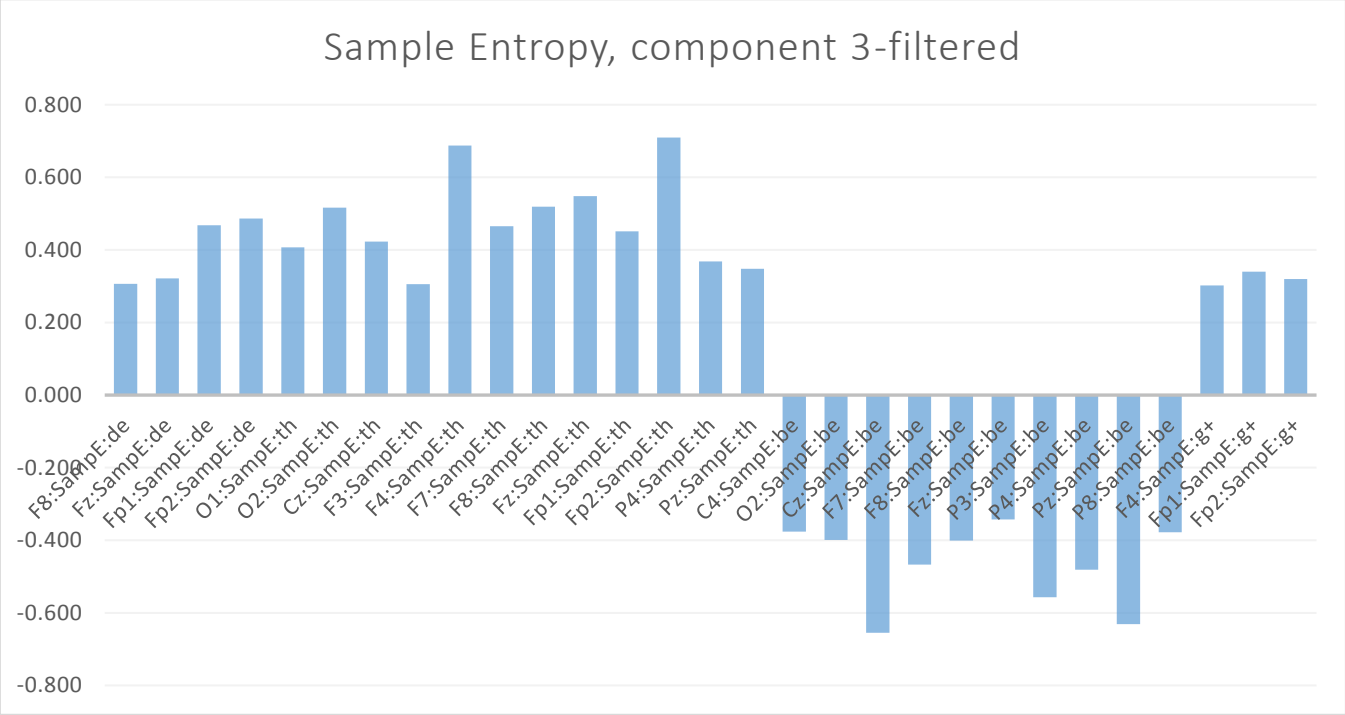

Figure 5: Sample entropy component loadings higher than 0.3 and lower than -0.3 of the data points on component 3 obtained in the PCA, against the labels of each data point including the abbreviated variable name, frequency band and electrode location in the Kenyan cohort.

The pattern observed in Figure 4 becomes more evident in Figure 5, where the variable with the highest component loadings within sample entropy are in the theta band in electrodes Fp2

(component loading=0.710) and F4 (component loading=0.688). The variable that played the most important role in the delta band was sample entropy measured at electrodes Fp2 (component loading=0.487) and Fp1 (component loading=0.468). In contrast, the values in sample entropy in the beta band are very negative. The variables that played the most important role in the beta band were sample entropy recorded in electrodes Cz (component loading=-0.655) and Pz (component loading=-0.631). Overall, all variables that played a significant role in the delta and theta bands show high positive values, as well as three electrodes (F4, Fp1 and Fp2) in the high gamma band, whereas the significant variables in the beta band were highly negative. Sample entropy measures in the alpha and gamma bands did not carry high component loadings for this specific component and were therefore filtered out. However, it is important to note that all values of sample entropy in the alpha band component loadings were negative, whereas approximately all sample entropy variables in the gamma band were positive, carrying very low component loadings. Moreover, it can be observed that all the electrode locations of the variables that were considered after the filter was applied are in the frontal area for the delta and theta bands and fronto-parietal for the beta band.

NDAR cohort

The PCA on the NDAR cohort on sample entropy yielded a total of 18 factors with an eigenvalue greater than 1 which cumulatively accounted for 89.8% of the variance. The univariate descriptive statistics suggested that none of the data points were removed in the analysis. The first ten components were then selected for the binary logistic regression model, as they cumulatively explained 79.3% of the variance in the data. The output Scree plot used for guidance is presented in Figure 6.

The regression scores for these ten components were then used as predictors in a logistic regression model with a binary outcome (ASD or control). The main statistics yielded by this regression are presented in Table 12.

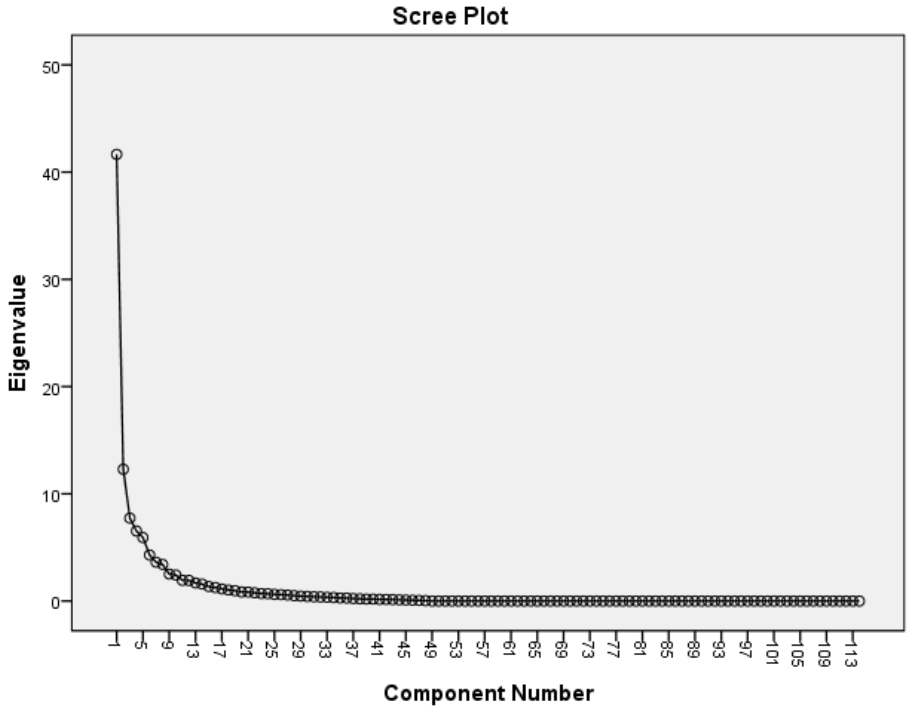

Figure 6: Scree plot obtained from a PCA on all sample entropy data points, for all frequency bands and scalp locations in the NDAR cohort. This plots the eigenvalues of each component identified.

Table 12: Results for sample entropy binary logistic regression with a dichotomous outcome and the PCA regression scores of factors 1-10 as predictors for the NDAR cohort: overall model fit: $chi^2=26.243$, $p=0.003$; additional fit statistics: Cox&Snell $R^2=0.415$, Nagelkerke $R^2=0.554$; linearity fit: R^2 p=0.774 (Hosmer-Lemeshow); classification sensitivity=82.6%, specificity=84.6%, accuracy=83.7%.

Variable	Cohort	Component	b	Wald statistics	p-value (df=1)	95% CI for Odds ratio		
						Lower	Odds ratio(ExpB)	Upper
Sample entropy	**NDAR**	1	-0.889	1.878	0.171	0.115	0.411	1.466
		2	-0.768	3.121	0.077	0.198	0.464	1.088
		3	-0.171	0.130	0.719	0.332	0.843	2.139
		4	-1.742	6.072	0.014	0.044	0.175	0.700
		5	-0.797	3.486	0.062	0.195	0.451	1.040
		6	1.656	2.884	0.089	0.775	5.240	35.441
		7	-1.485	5.225	0.022	0.063	0.226	0.809
		8	0.604	1.298	0.255	0.647	1.830	5.177
		9	0.203	0.292	0.589	0.587	1.225	2.559
		10	0.289	0.454	0.500	0.576	1.335	3.096

The NDAR model using the regression scores from the PCA of the first ten components as the predictors was statistically significant in delineating the two groups (chi^2= 26.243, p=.003). The Hosmer-Lemenshow test was not significant (p=0.774), indicating that the model is a better fit compared to the baseline model. This model can explain between 41% (Cox&Snell R^2) and 55% (Nagelkerke R^2) of the variance in the data. The model separated the groups with an 82.6% sensitivity, 84.6% specificity and 83.7% accuracy. Table 12 suggests that two of the ten predictors contributed significantly to the accuracy of the model. The strongest predictor was component 4 (Wald statistic=6.072, df=1, p =0.014). The PCA results showed that component 4 had an eigenvalue of 6.535 and accounted for 5.732% of that variance in the data. The other significant predictor was component 7 (Wald statistic=5.225, df=1, p=0.022), with an eigenvalue of 3.637 and accountable for 3.181% of the variance in the data. The loadings of each data point on these two components were plotted and can be observed in Figures 7-10 in order to understand which frequency bands and scalp locations contributed the most to the delineation of the two groups.

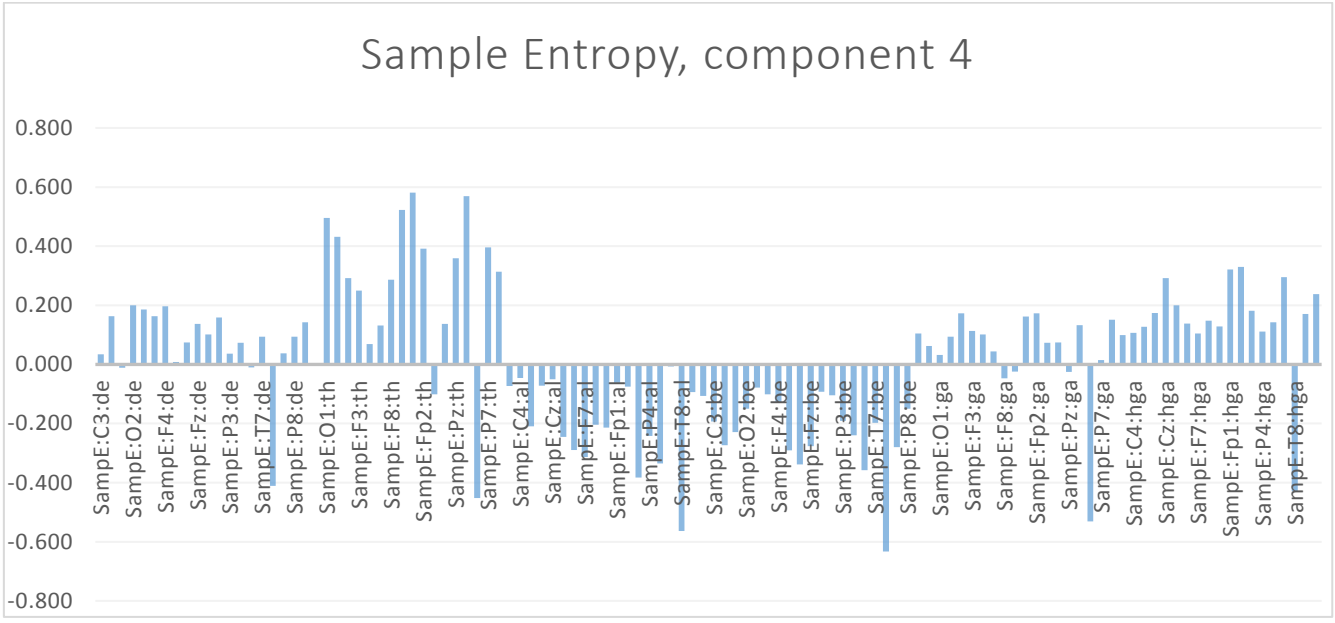

Figure 7: Sample entropy component loadings of each data point on component 4 obtained in the PCA, against the labels of each data point including the abbreviated variable name, frequency band and electrode location, in the NDAR cohort.

A pattern can be observed in Figure 7, with the gamma, delta and theta frequency bands showing positive values, in contrast with the alpha and beta bands that showed only negative values. It can also be observed that the loadings of the delta band are much lower compared to the other frequency bands. For a better interpretation of these results, another filter was applied consisting of the selection and plotting of the data points that had a component loading higher than 0.3 or lower than -0.3. The filtered results were then plotted in Figure 8.

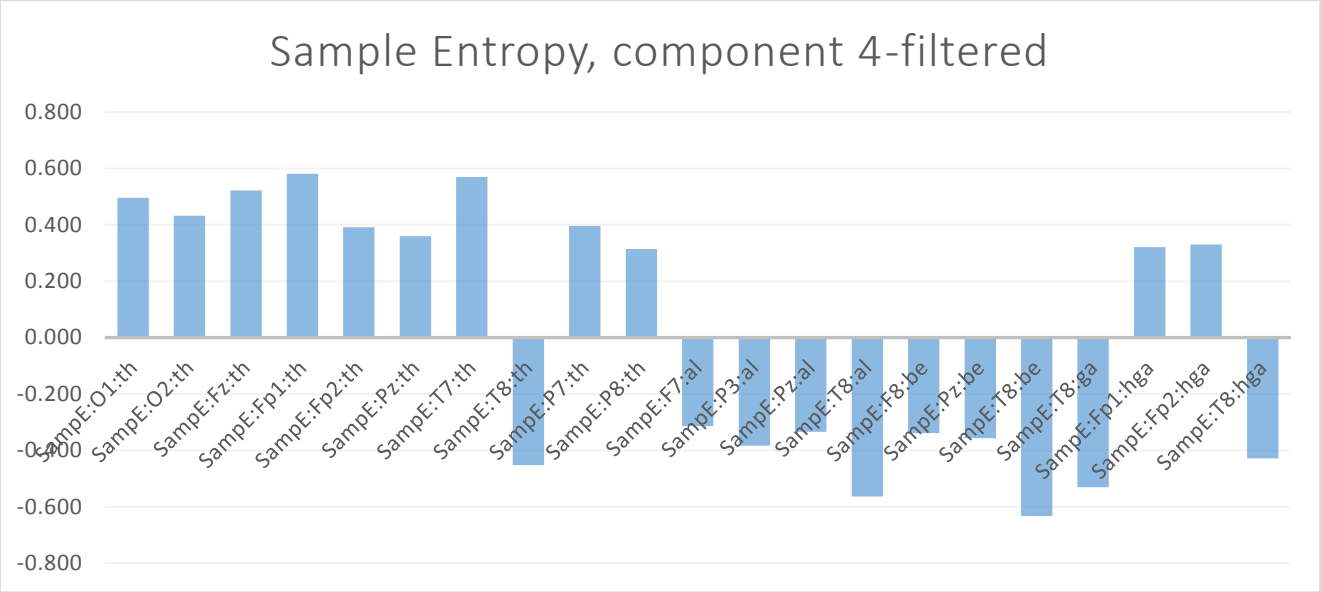

Figure 8: Sample entropy component loadings higher than 0.3 and lower than -0.3 of the data points on component 4 obtained in the PCA, against the labels of each data point including the abbreviated variable name, frequency band and electrode location in the NDAR cohort.

Figure 8 shows a pattern in the theta band, with positive sample entropy component loadings, except for the electrode T8 (component loading=-0.452). Within the theta band, the highest loading was carried by sample entropy measured at Fp1 (component loading=0.582), followed by T7 (component loading=0.570) and Fz (component loading=0.522). Four electrodes (F7, P3, Pz, T8) were highly loaded on component 4 in the alpha band, carrying only negative values, the most correlated one being sample entropy measured at T8 (component loading=-0.564). In the beta band, three electrodes (F8, Pz, T8) were negatively correlated with component 4, the strongest correlation observed being for sample entropy measured at T8

(component loading=-0.633). For the gamma band, the only correlated electrode was T8 (component loading=-0.531). In the high gamma band, Fp1 and Fp2 electrodes were positively correlated with component 4, whereas T8 showed a strong negative correlation (component loading=-0.429). None of the sample entropy measurements in the delta band were strongly correlated with component 4 for the NDAR cohort. The pattern that can be observed is for electrode T8 that showed high negative loadings on component 4 for the theta, alpha, beta, gamma and high gamma bands.

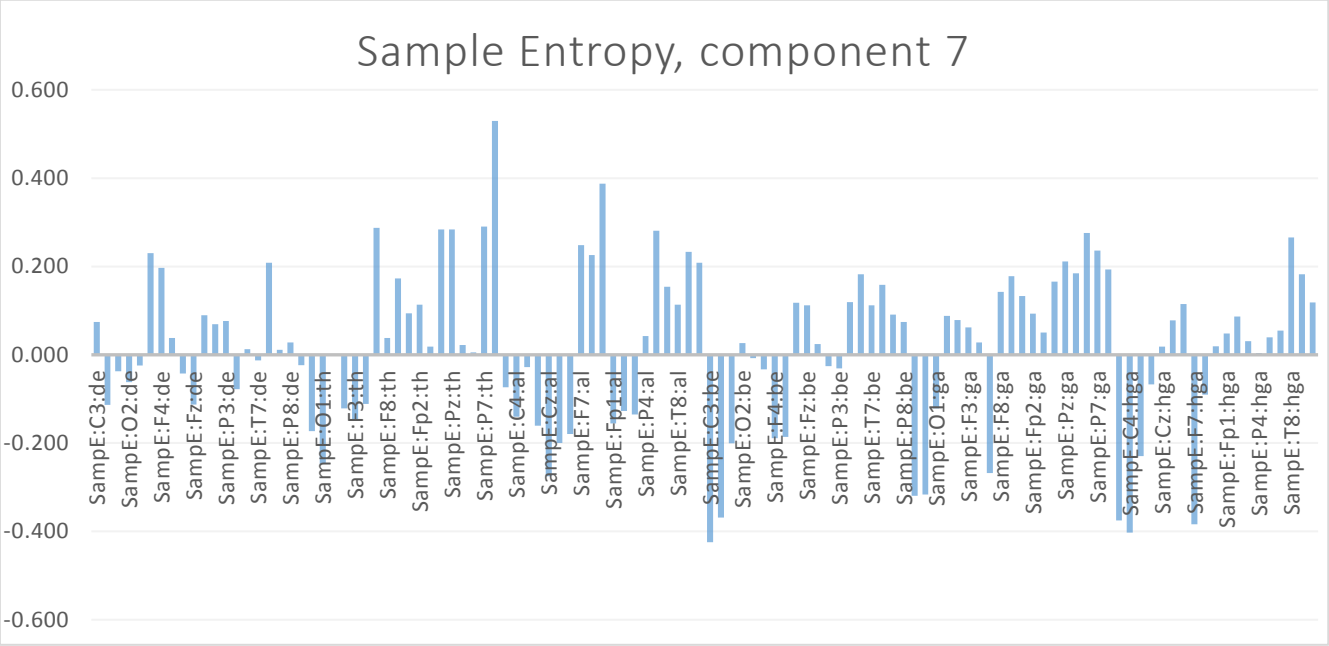

Figure 9: Sample entropy component loadings of each data point on component 7 obtained in the PCA, against the labels of each data point including the abbreviated variable name, frequency band and electrode location, in the NDAR cohort.

Figure 9 shows the component loadings of sample entropy measurements on component 7. A specific pattern cannot be observed in this figure. Therefore, in order to better understand these results, another filter was applied consisting of the selection and plotting of the data points that had a component loading higher than 0.3 or lower than -0.3. The filtered results were then plotted in Figure 10.

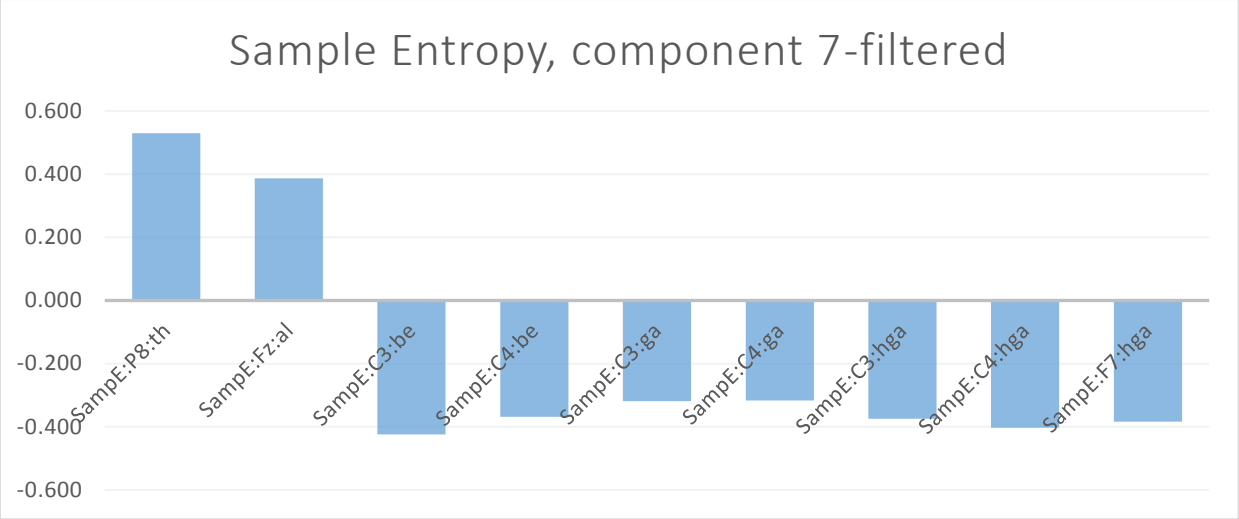

Figure 10: Sample entropy component loadings higher than 0.3 and lower than -0.3 of the data points on component 7 obtained in the PCA, against the labels of each data point including the abbreviated variable name, frequency band and electrode location in the NDAR cohort.

Figure 10 shows the only nine electrodes contributed substantially to the main effect of component 7. In the theta band only electrode P8 showed a high positive correlation with component 7 (component loading=0.529); similarly the alpha band contributed with the electrode Fz (component loading=0.387). Electrodes C3 and C4 were negatively correlated with component 7 in the beta, gamma and high gamma bands. Moreover, it can be observed that all the electrodes that were considered after the filter was applied that correlated negatively with component 7 are in the central area for the beta, gamma and high gamma bands.

4.2.2. Determinism

Kenyan cohort

The next variable tested was determinism. A PCA was performed on determinism values recorded in the Kenyan cohort across all frequencies and electrode locations. A total of 12 factors with an eigenvalue greater than 1 cumulatively accounted for 96.4 % of the variance in the data. The univariate descriptive statistics suggested that none of the data points were removed in the analysis. The first four components were selected to form a binary logistic

regression model, as they cumulatively explained 83.8% of the variance in the data. The main statistics yielded by this regression are presented in Table 13. The Scree plot of the components identified is presented in Figure 11.

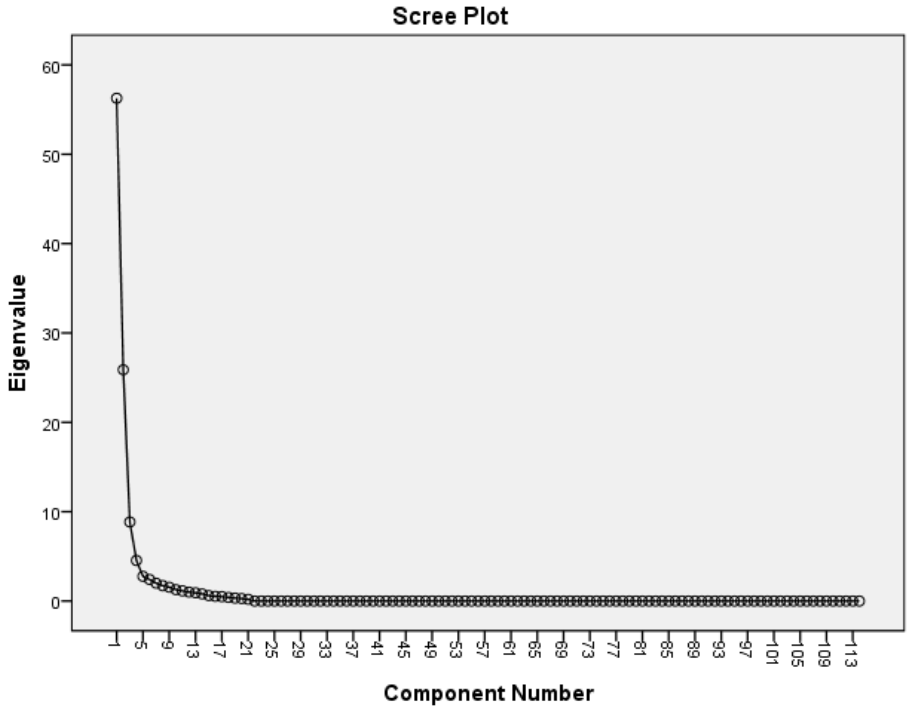

Figure 11: Scree plot obtained from a PCA on all determinism data points, for all frequency bands and scalp locations in the Kenyan cohort. This plots the eigenvalues of each component identified.

Table 13: Results for determinism binary logistic regression with a dichotomous outcome and the PCA regression scores of factors 1-4 as predictors for the Kenyan cohort: overall model fit: chi^2=12.851, p=0.102; additional fit statistics: Cox&Snell R^2=0.442, Nagelkerke R^2=0.590; linearity fit: R^2 p=0.303 (Hosmer-Lemeshow); classification sensitivity=72.7%, specificity=90.9%, accuracy=81.8%.

Variable	Cohort	Component	b	Wald statistic	p-value (df=1)	95% CI for Odds ratio		
						Lower	Odds ratio(ExpB)	Upper
Determinism	**Kenyan**	1	-2.400	1.760	0.185	0.003	0.091	3.144
		2	-15.799	2.419	0.120	3.1019e-16	1.3755e-7	60.996
		3	-1.851	2.678	0.102	0.017	0.157	1.442
		4	-0.406	0.247	0.619	0.135	0.666	3.299

The model consisting of the regression scores from the PCA of the first four components selected as predictors was statistically significant in delineating the two groups (chi^2= 12.851, p=.012). The Hosmer-Lemenshow test was non-significant (p=0.303), suggesting that the model is a good fit of the data. Between 44% (Cox&Snell R^2) and 59% (Nagelkerke R^2) of the

variance in the data could be explained using this model. The model separated the groups with an 72.7% sensitivity, 90.9% specificity and 81.8% accuracy. Table 13 indicates that, although the overall model was significant, none of the independent variables were significant predictors (all p-values>0.05) and they were therefore not investigated further.

NDAR cohort

Determinism values were also tested in the NDAR cohort. A PCA was performed on determinism values across all frequencies and electrode locations. A total of 21 factors with an eigenvalue greater than 1 cumulatively accounted for 91.2% of the variance in the data. The univariate descriptive statistics suggested that none of the data points were removed in the analysis. The first 11 components were selected to form a binary logistic regression model, as they cumulatively explained 77.7% of the variance in the data. The Scree plot of the components identified is presented in Figure 12.

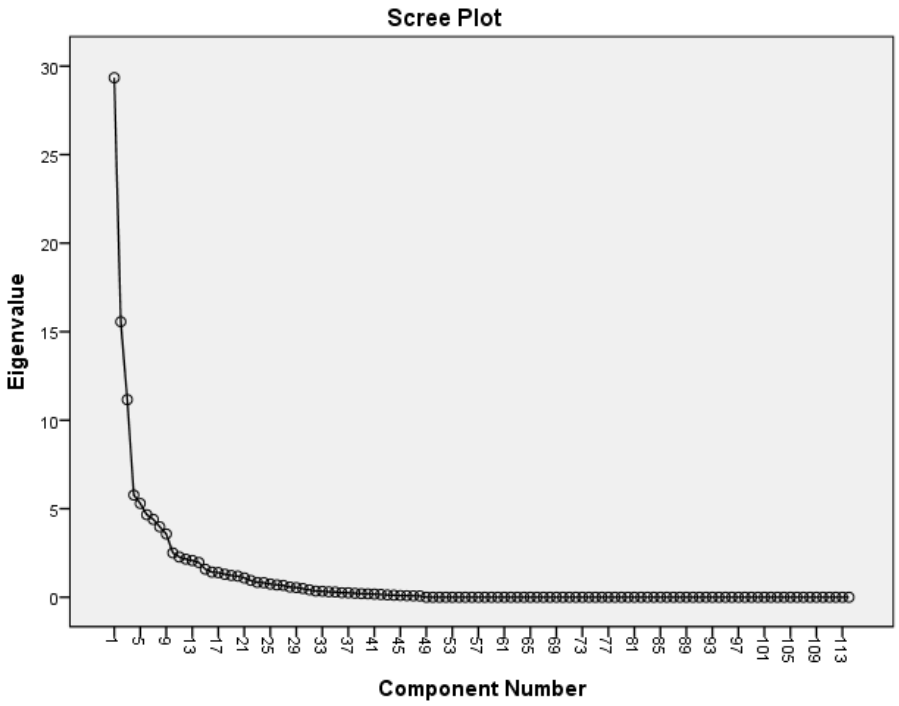

Figure 12: Scree plot obtained from a PCA on all determinism data points, for all frequency bands and scalp locations in the NDAR cohort. This plots the eigenvalues of each component identified.

The regression scores for these 11 components were then used as predictors in a logistic regression model with a binary outcome (ASD or control). The main statistics yielded by this regression are presented in Table 14.

Table 14: Results for determinism binary logistic regression with a dichotomous outcome and the PCA regression scores of factors 1-10 as predictors for the NDAR cohort: overall model fit: chi^2=30.770, p=0.001; additional fit statistics: Cox&Snell R^2=0.466, Nagelkerke R^2=0.623; linearity fit: R^2 p=0.784 (Hosmer-Lemeshow); classification sensitivity=82.6%, specificity=84.6%, accuracy=83.7%.

Variable	Cohort	Component	b	Wald statistics	p-value (df=1)	95% CI for Odds ratio		
						Lower	Odds ratio(ExpB)	Upper
Determinism	**NDAR**	1	-1.284	3.202	0.074	0.068	0.277	1.130
		2	1.940	6.494	0.011	1.565	6.955	30.914
		3	0.244	0.368	0.544	0.580	1.276	2.806
		4	-1.276	4.237	0.040	0.083	0.279	0.941
		5	-0.928	2.526	0.112	0.126	0.395	1.241
		6	0.097	0.031	0.859	0.376	1.102	3.226
		7	1.886	6.911	0.009	1.616	6.592	26.890
		8	1.068	4.325	0.038	1.063	2.909	7.959
		9	1.682	4.216	0.040	1.080	5.377	26.782
		10	0.909	2.567	0.109	0.816	2.481	7.542
		11	-0.087	0.022	0.882	0.293	0.917	2.870

The NDAR model using the regression scores from the PCA of the first 11 components as the predictors was statistically significant in delineating the two groups (chi^2= 30.770, p=.001). The Hosmer-Lemenshow test was not significant (p=0.784), indicating that the model is a better fit compared to the baseline model. This model can explain between 46% (Cox&Snell R^2) and 62% (Nagelkerke R^2) of the variance in the data. The model separated the groups with an 82.6% sensitivity, 84.6% specificity and 83.7% accuracy. Table 14 suggests that four of the 11 predictors contributed significantly to the accuracy of the model. The strongest predictor was component 7 (Wald statistic=6.911, df=1, p =0.009). The PCA results showed that component 7 had an eigenvalue of 4.400 and accounted for 3.86% of that variance in the data. The next significant predictor was component 2 (Wald statistic=6.494, df=1, p=0.011), with an eigenvalue of 15.563 and accountable for 13.6% of the variance in the data. Components 4 (Wald statistic=4.237, df=1, p=0.040, eigenvalue=5.775, variance explained=5.066%) and 9 (Wald statistic=4.216, df=1, p=0.040, eigenvalue=3.576, variance explained=3.137%) were

equally significant. The loadings of each data point on these four components were plotted and can be observed in Figures 13-20 in order to understand which frequency bands and scalp locations contributed the most to the delineation of the two groups.

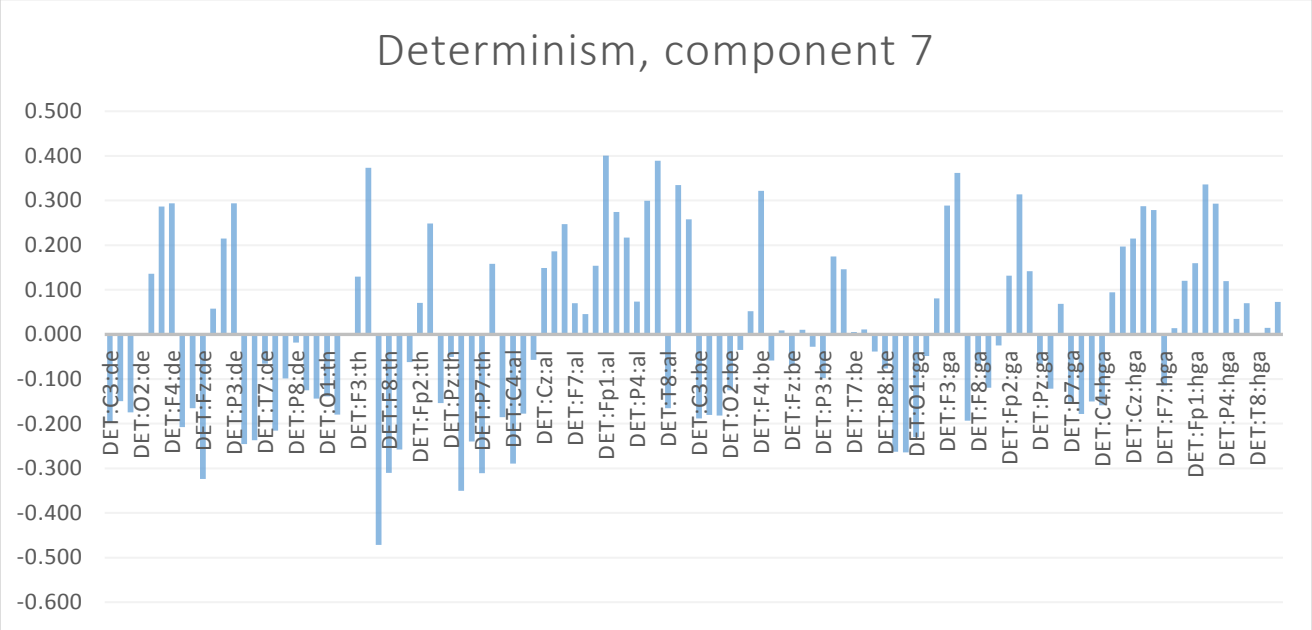

Figure 13: Determinism component loadings of each data point on component 7 obtained in the PCA, against the labels of each data point including the abbreviated variable name, frequency band and electrode location, in the NDAR cohort.

Figure 13 shows the component loadings of determinism measurements on component 7 in the NDAR cohort. A specific pattern cannot be observed in this figure. Therefore, in order to better understand these results, another filter was applied consisting of the selection and plotting of the data points that had a component loading higher than 0.3 or lower than -0.3. The filtered results were then plotted in Figure 14.

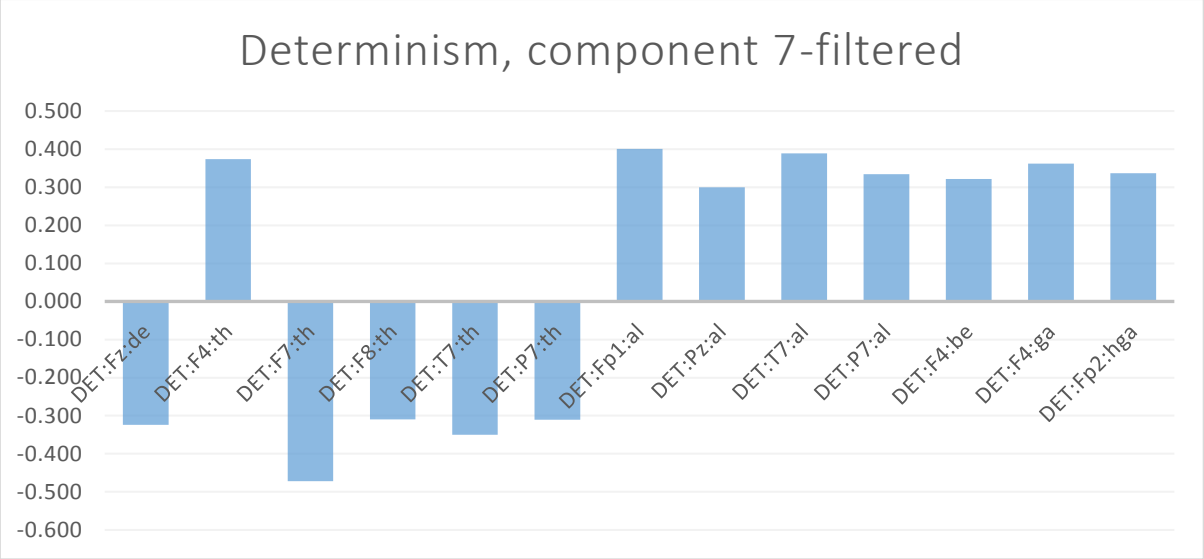

Figure 14: Determinism component loadings higher than 0.3 and lower than -0.3 of the data points on component 7 obtained in the PCA, against the labels of each data point including the abbreviated variable name, frequency band and electrode location in the NDAR cohort.

Figure 14 shows that in the delta band, only one electrode, Fz, was highly loaded on component 7 with a negative value. With the exception of electrode F4, theta band shows a negative correlation with component 7, with the highest component loading being carried by electrode F7 (component loading=-0.472). In contrast, the alpha band only showed positive correlations in electrodes Fp1, Pz, T7 and P7. F4 is the electrode that correlates positively with component 7 in the theta, beta and gamma bands.

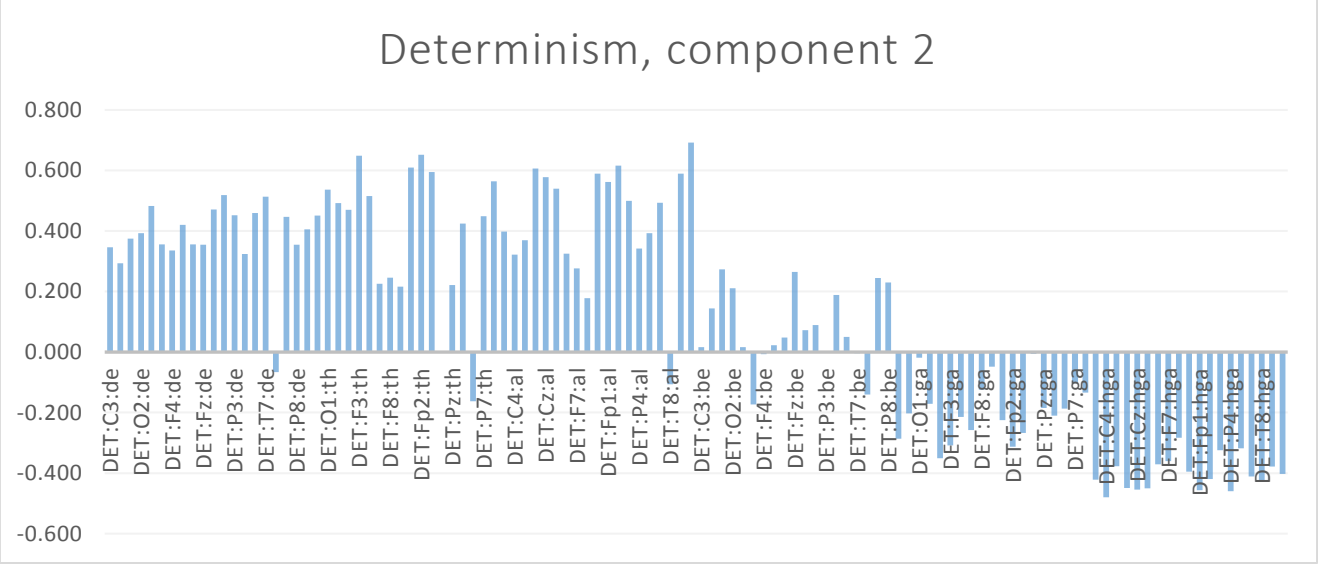

Figure 15: Determinism component loadings of each data point on component 2 obtained in the PCA, against the labels of each data point including the abbreviated variable name, frequency band and electrode location, in the NDAR cohort.

Figure 15 shows the component loadings of determinism measurements for component 2 across all frequencies and electrodes. A clear pattern can be observed in the component loadings plotted in Figure 18, with relatively high positive values in the delta, theta and alpha frequencies and negative values in the gamma and high gamma frequencies. In the beta band most loadings observed show positive values, much lower compared to the low frequency bands. For a better understanding and interpretation of these results, another filtering step was necessary consisting of the selection and plotting of the data points that had a component loading higher than 0.3 or lower than -0.3. The filtered results were then plotted in Figure 16.

The pattern becomes more apparent in Figure 16, where it can be observed that all the electrodes remained in the analysis after the filter from the delta, theta and alpha bands were positively correlated with component 2. None of the electrodes appears in all three frequency bands, however, O2 and F3 carry positive loadings both in delta and theta, and P3 and P7 were positively correlated with component 2 in both theta and alpha bands. In contrast, the electrodes in the gamma and high gamma bands were negatively correlated with component two. The measurements in the beta frequency did not have any component loadings >0.3 or <-0.3 for component 2.

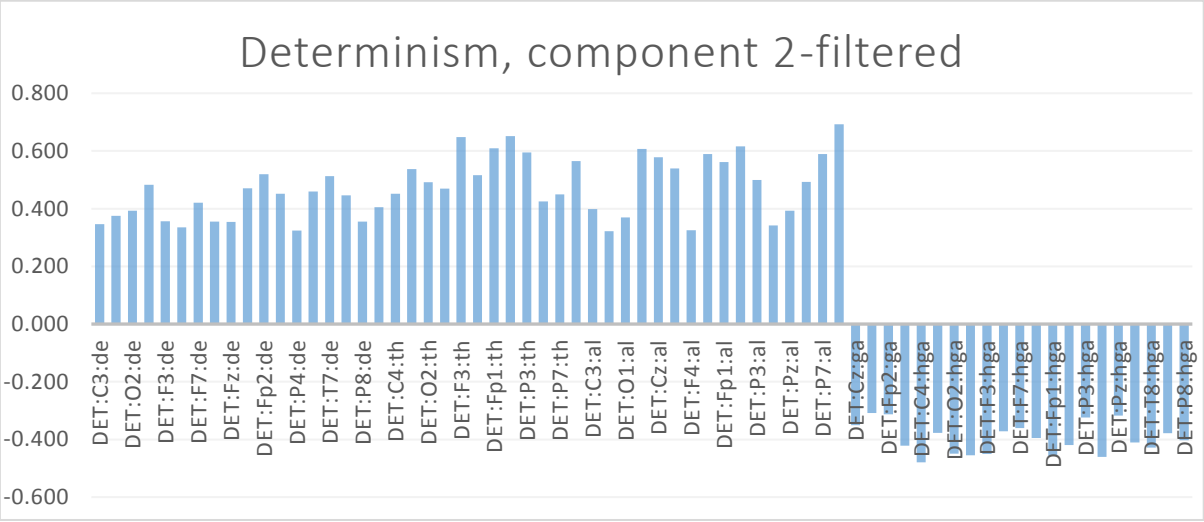

Figure 16: Determinism component loadings higher than 0.3 and lower than -0.3 of the data points on component 2 obtained in the PCA, against the labels of each data point including the abbreviated variable name, frequency band and electrode location in the NDAR cohort.

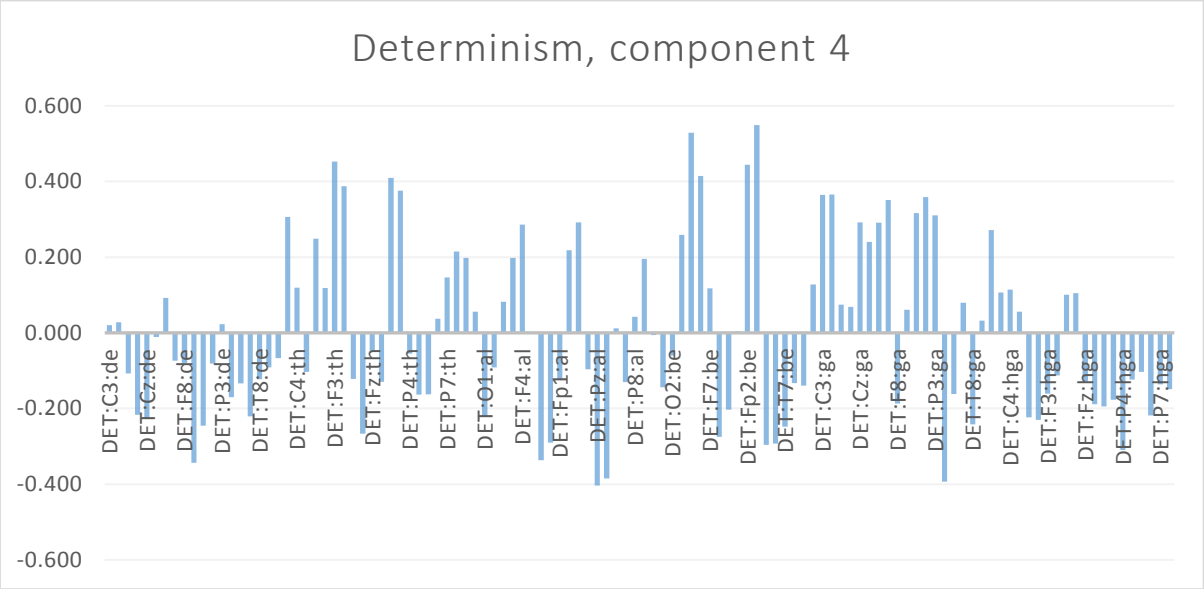

Figure 17: Determinism component loadings of each data point on component 4 obtained in the PCA, against the labels of each data point including the abbreviated variable name, frequency band and electrode location, in the NDAR cohort

Figure 17 shows the component loadings of determinism measurements on component 2 in the NDAR cohort. A specific pattern cannot be observed in this figure. Therefore, in order to better understand these results, another filter was applied consisting of the selection and plotting of the data points that had a component loading higher than 0.3 or lower than -0.3. The filtered results were then plotted in Figure 18.

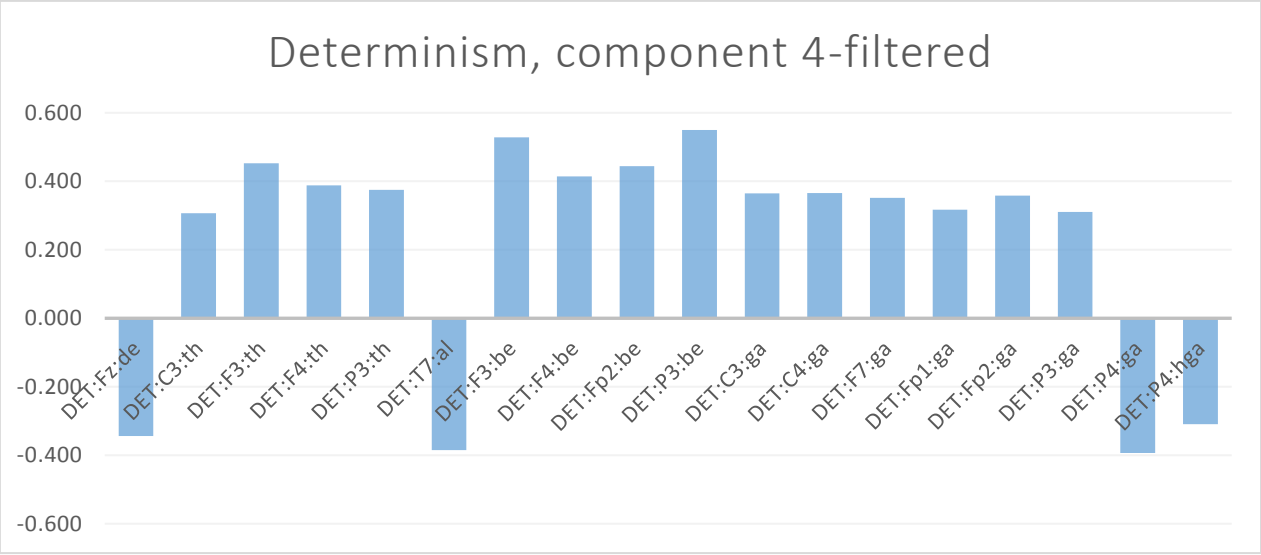

Figure 18: Determinism component loadings higher than 0.3 and lower than -0.3 of the data points on component 4 obtained in the PCA, against the labels of each data point including the abbreviated variable name, frequency band and electrode location in the NDAR cohort.

In Figure 18, it can be observed that determinism measured in the delta frequency only correlates with component 4 at electrode Fz that carries a negative component loading (component loading=-0.344). Theta, beta and gamma bands show positive correlations with component 4, with the exception of electrode P4 in the gamma band, which carries a negative component loading (component loading=-0.394). Moreover, it can be observed that all of the positive correlations in the theta, beta and gamma bands are in the frontal and central regions.

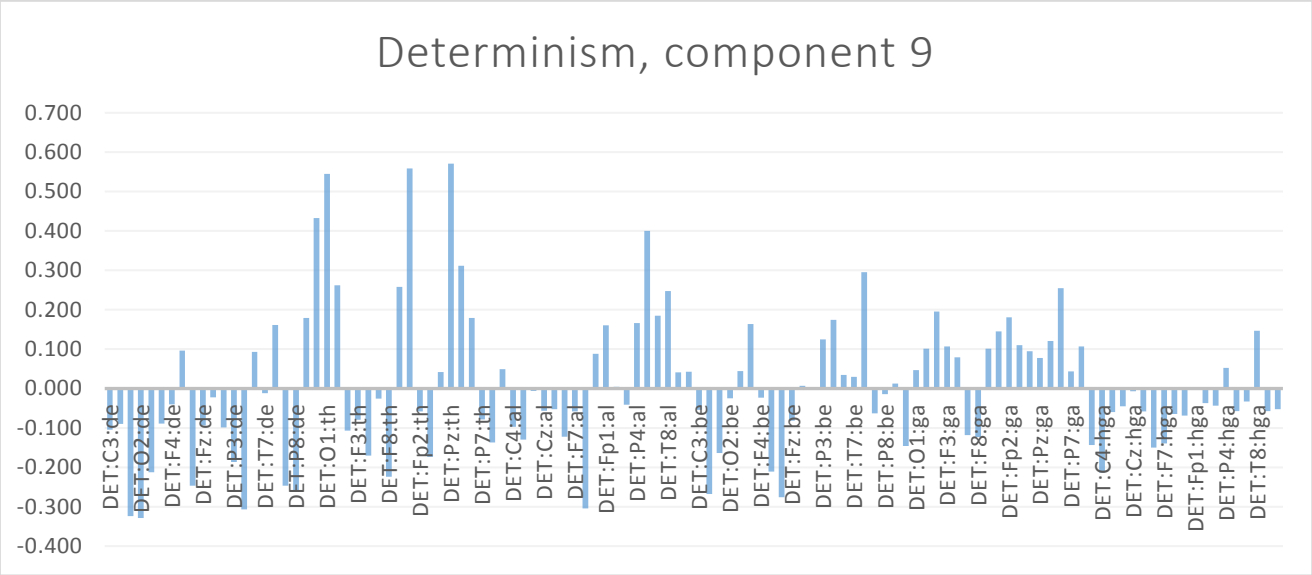

Figure 19: Determinism component loadings of each data point on component 9 obtained in the PCA, against the labels of each data point including the abbreviated variable name, frequency band and electrode location, in the NDAR cohort

Figure 19 shows the component loadings of determinism measurements on component 9 in the NDAR cohort. A specific pattern cannot be observed in this figure. Therefore, in order to better understand these results, another filter was applied consisting of the selection and plotting of the data points that had a component loading higher than 0.3 or lower than -0.3. The filtered results were then plotted in Figure 20.

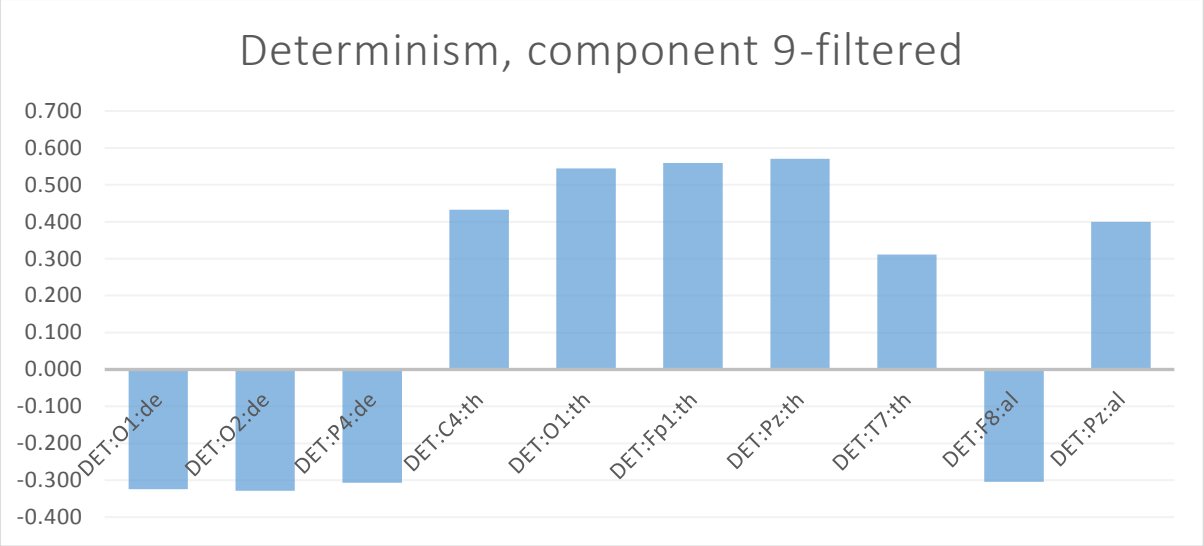

Figure 20: Determinism component loadings higher than 0.3 and lower than -0.3 of the data points on component 9 obtained in the PCA, against the labels of each data point including the abbreviated variable name, frequency band and electrode location in the NDAR cohort.

Figure 20 shows that only 10 data points remained in the analysis after the filter was applied. Delta frequency shows a negative correlation with component 9, on electrodes O1, O2 and P4. In contrast, theta shows high correlations with the component, with the highest loading being carried by electrode Pz (component loading=0.517). Alpha band shows contradictory results as electrode F8 is negatively correlated with the component, whereas Pz carries a positive value.

4.2.3. Laminarity

Kenyan cohort

A PCA was performed on the laminarity values in the Kenyan cohort across all frequencies and electrode locations. A total of 14 factors with an eigenvalue greater than 1 cumulatively accounted for 96.7 % of the variance in the data. The univariate descriptive statistics suggested that none of the data points were removed in the analysis. The first five components were selected for a binary logistic regression model, as they cumulatively explained 78.8% of the variance in the data. The main statistics yielded by this regression are presented in Table 15. The Scree plot of the components identified is presented in Figure 21.

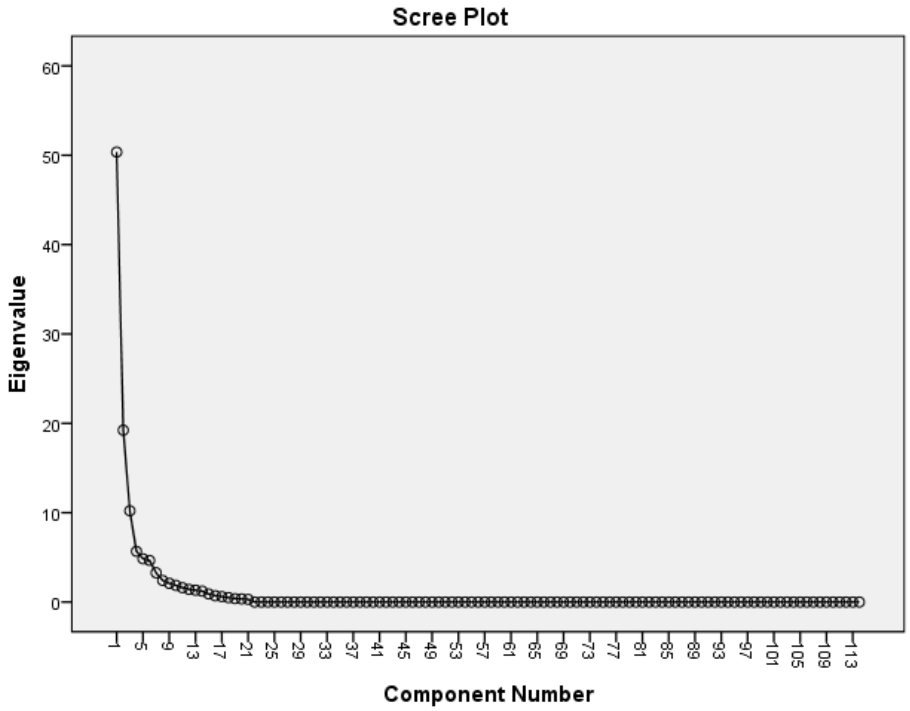

Figure 21: Scree plot obtained from a PCA on all laminarity data points, for all frequency bands and scalp locations in the Kenyan cohort. This plots the eigenvalues of each component identified.

Table 15: Results for laminarity binary logistic regression with a dichotomous outcome and the PCA regression scores of factors 1-5 as predictors for the Kenyan cohort: overall model fit: chi^2=13.875, p=0.016; additional fit statistics: Cox&Snell R^2=0.468, Nagelkerke R^2=0.624; linearity fit: R^2 p=0.160 (Hosmer-Lemeshow); classification sensitivity=72.7%, specificity=90.9%, accuracy=81.8%.

Variable	Cohort	Component	b	Wald statistics	p-value (df=1)	95% CI for Odds ratio		
						Lower	Odds ratio(ExpB)	Upper
Laminarity	**Kenyan**	1	-1.546	2.074	0.150	0.026	0.213	1.747
		2	-5.089	2.003	0.157	0.000	0.006	7.088
		3	-0.547	0.510	0.475	0.129	0.579	2.597
		4	0.866	0.858	0.354	0.380	2.378	14.867
		5	-3.660	1.472	0.225	0.000	0.026	9.501

The model consisting of the regression scores from the PCA of the first five components selected as predictors was statistically significant in delineating the two groups (chi^2= 13.875, p=.016). The Hosmer-Lemenshow test was non-significant (p=0.160), suggesting that the model is a good fit of the data. Between 47% (Cox&Snell R^2) and 62% (Nagelkerke R^2) of the variance in the data could be explained using this model. The model separated the groups with a 72.7% sensitivity, 90.9% specificity and 81.8% accuracy. Table 15 indicates that, although

the overall model was significant, none of the independent variables were significant predictors (all p-values>0.05) and they were therefore not investigated further.

NDAR cohort

Laminarity was also tested in the NDAR cohort. Another PCA was used to test the laminarity values across all frequencies and electrode locations. A total of 19 factors with an eigenvalue greater than 1 cumulatively accounted for 90% of the variance in the data. The univariate descriptive statistics suggested that none of the data points were removed in the analysis. The first ten components were selected for a binary logistic regression model, as they cumulatively explained 77.4% of the variance in the data. The main statistics yielded by this regression are presented in Table 16. The Scree plot of the components identified is presented in Figure 22.

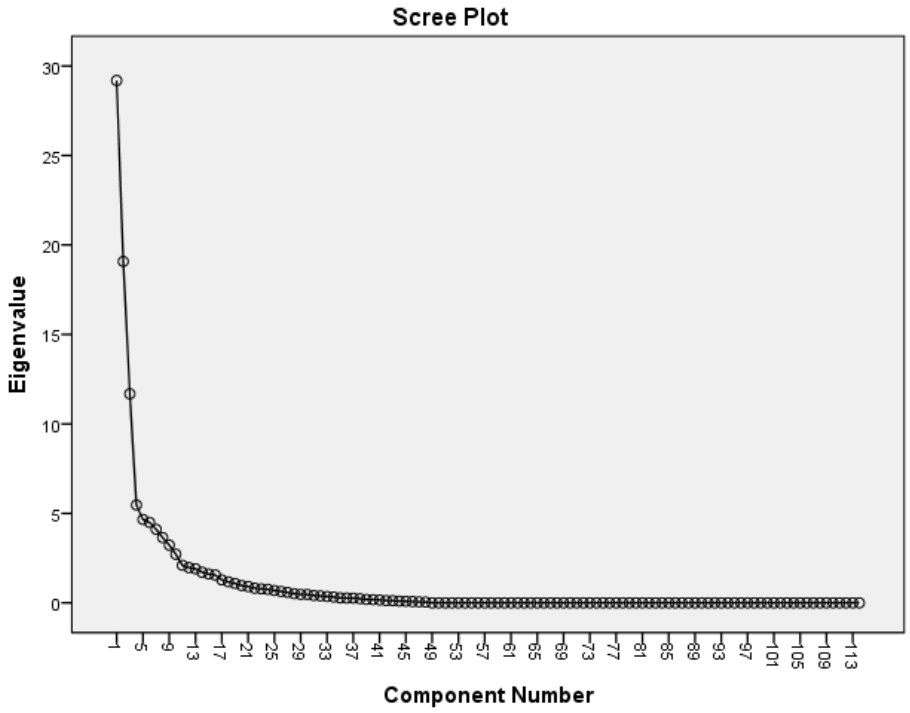

Figure 22: Scree plot obtained from a PCA on all laminarity data points, for all frequency bands and scalp locations in the NDAR cohort. This plots the eigenvalues of each component identified.

Table 16: Results for laminarity binary logistic regression with a dichotomous outcome and the PCA regression scores of factors 1-10 as predictors for the NDAR cohort: overall model fit: chi^2=23.499, p=0.009; additional fit statistics: Cox&Snell R^2=0.381, Nagelkerke R^2=0.509; linearity fit: R^2 p=0.689 (Hosmer-Lemeshow); classification sensitivity=69.6%, specificity=80.8%, accuracy=75.5%.

Variable	Cohort	Component	b	Wald statistics	p-value (df=1)	95% CI for Odds ratio		
						Lower	Odds ratio(ExpB)	Upper
Laminarity	**NDAR**	1	-0.676	1.448	0.229	0.169	0.509	1.530
		2	-0.227	0.255	0.614	0.330	0.797	1.925
		3	0.673	2.266	0.132	0.816	1.961	4.710
		4	-1.022	5.328	0.021	0.151	0.360	0.857
		5	-0.153	0.070	0.792	0.276	0.858	2.669
		6	0.832	2.156	0.142	0.757	2.299	6.983
		7	0.110	0.104	0.747	0.571	1.117	2.184
		8	-0.588	1.621	0.203	0.225	0.555	1.373
		9	1.574	6.755	0.009	1.473	4.825	15.810
		10	0.134	0.126	0.723	0.546	1.143	2.395

The NDAR model using the regression scores from the PCA of the first ten components as the predictors was statistically significant in delineating the two groups (chi^2= 23.499, p=.009). The Hosmer-Lemenshow test was not significant (p=0.689), indicating that the model is a better fit compared to the baseline model. This model can explain between 41% (Cox&Snell R^2) and 51% (Nagelkerke R^2) of the variance in the data. The model separated the groups with a 69.6% sensitivity, 80.8% specificity and 75.5% accuracy. Table 16 suggests that two of the ten predictors contributed significantly to the accuracy of the model. The strongest predictor was component 9 (Wald statistic=6.755, df=1, p=0.009). The PCA results showed that component 9 had an eigenvalue of 3.338 and accounted for 2.83% of the variance in the data. The other significant predictor was component 4 (Wald statistic=5.328, df=1, p=0.021), with an eigenvalue of 5.469 and accountable for 4.8% of the variance in the data. The loadings of each data point on these two components were plotted and can be observed in Figures 23-26 in order to understand which frequency bands and scalp locations contributed the most to the delineation of the two groups.

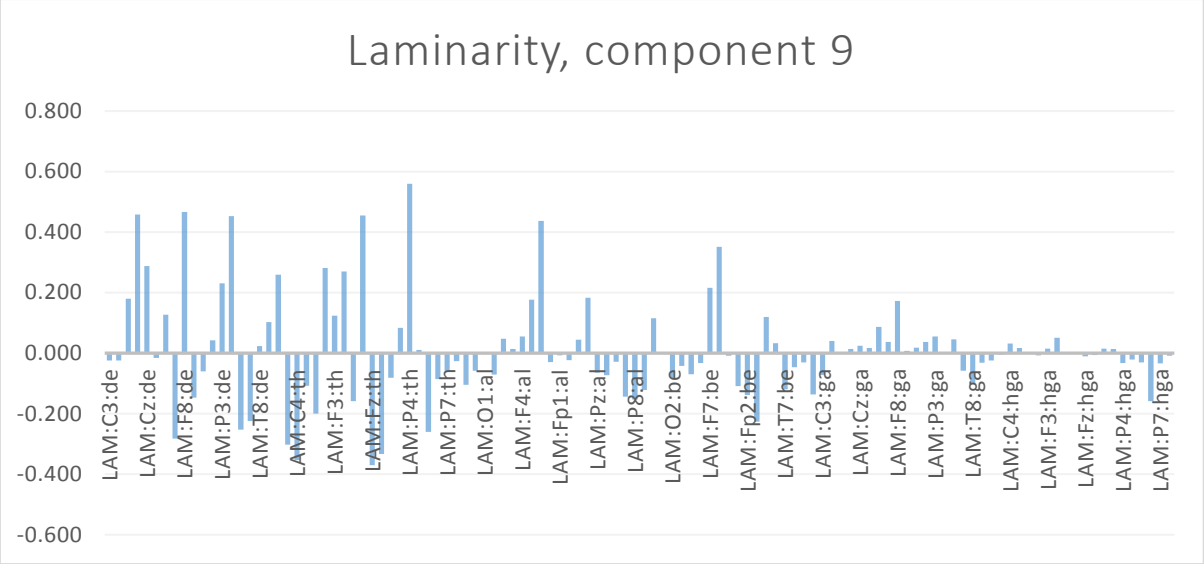

Figure 23: Laminarity component loadings of each data point on component 9 obtained in the PCA, against the labels of each data point including the abbreviated variable name, frequency band and electrode location, in the NDAR cohort.

Figure 23 does not reveal any pattern in the distribution of the component loadings on component 9. It can be noted however that the loadings are much higher in the low frequency bands compared to the high frequency bands where almost none of the electrodes carry values higher than 0.2. In order to better understand these results, another filter was applied consisting of the selection and plotting of the data points that had a component loading higher than 0.3 or lower than -0.3. The filtered results were then plotted in Figure 24.

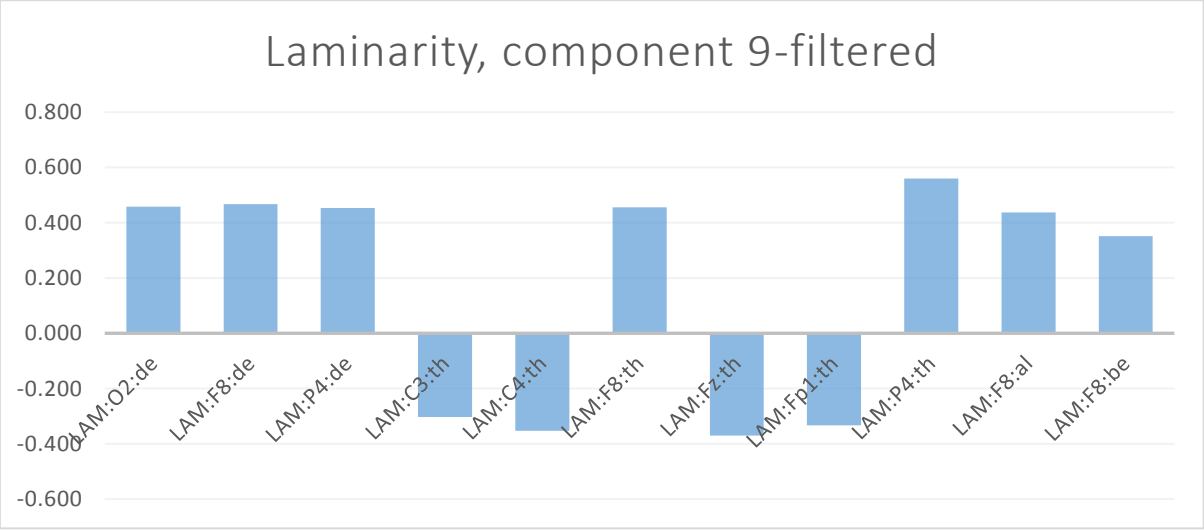

Figure 24: Laminarity component loadings higher than 0.3 and lower than -0.3 of the data points on component 9 obtained in the PCA, against the labels of each data point including the abbreviated variable name, frequency band and electrode location in the NDAR cohort.

Figure 24 shows the remaining component loadings after the filter was applied. All correlations in the delta band are positive, with three electrodes, O2, F8 and P4 showing the highest values. No pattern of directionality cam be observed in the theta band where electrodes C3, C4, Fz and Fp1 appear negative correlated with component 9, whereas electrodes F8 and P4 carry positive component loadings. Electrode F8 is positively correlated with component 9 in the alpha and beta bands as well. None of the electrodes in the gamma and high gamma bands remained in the analysis after the filter was applied, suggesting that they were not highly correlated with component 9.

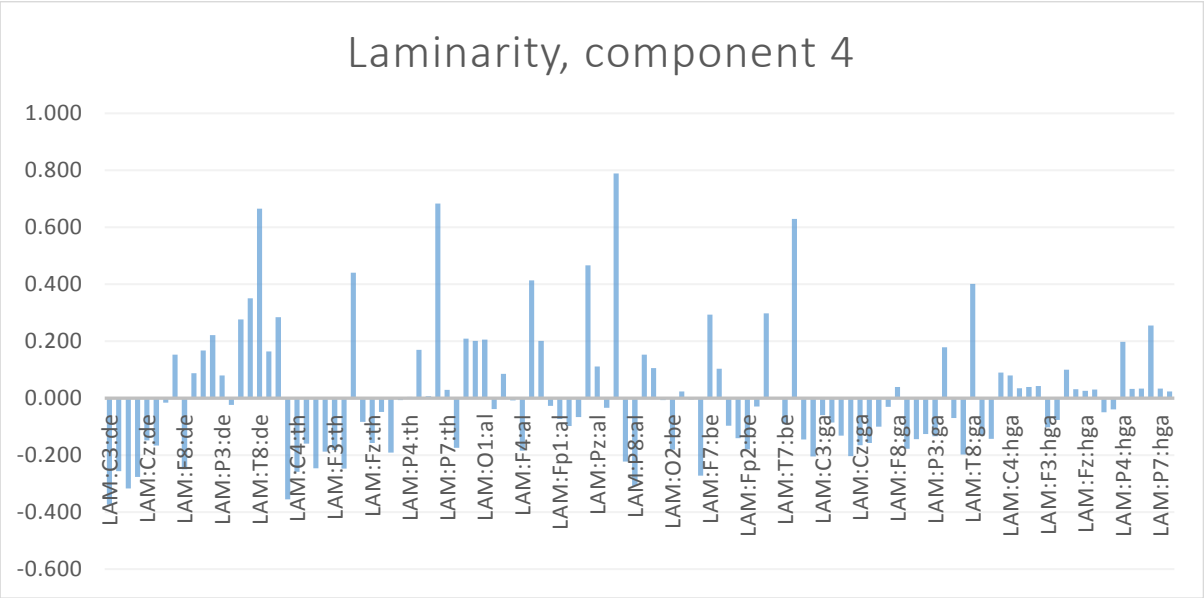

Figure 25: Laminarity component loadings of each data point on component 4 obtained in the PCA, against the labels of each data point including the abbreviated variable name, frequency band and electrode location, in the NDAR cohort.

Similarly to component 9, the distribution of the component loadings for component 4 in Figure 25 do not show any specific pattern. The correlations appear relatively weak, particularly in the high frequency bands, with the exception several electrodes in the delta, theta and alpha bands. For a better understanding of these results, another filter was applied consisting of the selection and plotting of the data points that had a component loading higher than 0.3 or lower than -0.3. The filtered results were then plotted in Figure 26.

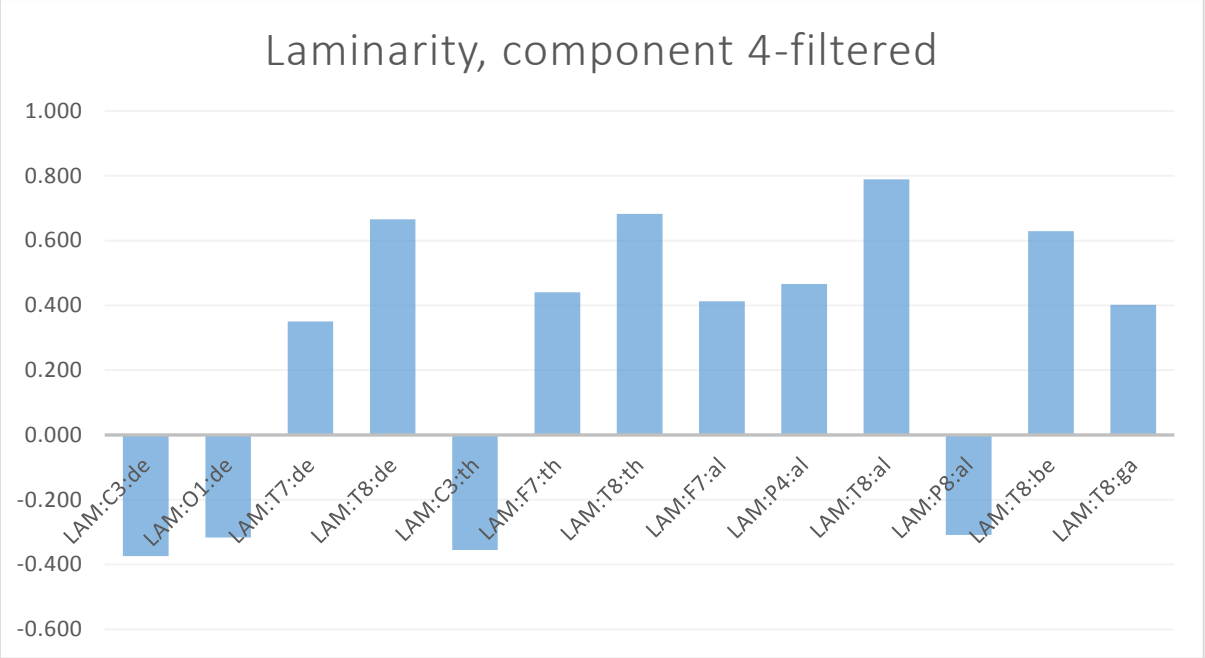

Figure 26: Laminarity component loadings higher than 0.3 and lower than -0.3 of the data points on component 4 obtained in the PCA, against the labels of each data point including the abbreviated variable name, frequency band and electrode location in the NDAR cohort.

Figure 26 does not reveal any further patters in the distribution of component loadings for component 4. The highest correlations as observed for electrode T8 in the delta (component loading=0.665), theta (component loading=0.683), alpha bands (component loading=0.789) and beta bands (component loading=0.629). T8 is also positively correlated with component 4 in the gamma band.

4.2.4. L_entropy

Kenyan cohort

L_entropy was tested in the Kenyan cohort using the same strategy. The PCA returned 16 component that explain 96.8% of the variance in the data. The univariate descriptive statistics suggested that none of the data points were removed in the analysis. The first seven components were selected for a binary logistic regression model, as they cumulatively explained 79.1% of

the variance in the data. The main statistics yielded by this regression are presented in Table 17. The Scree plot of the components identified is presented in Figure 27.

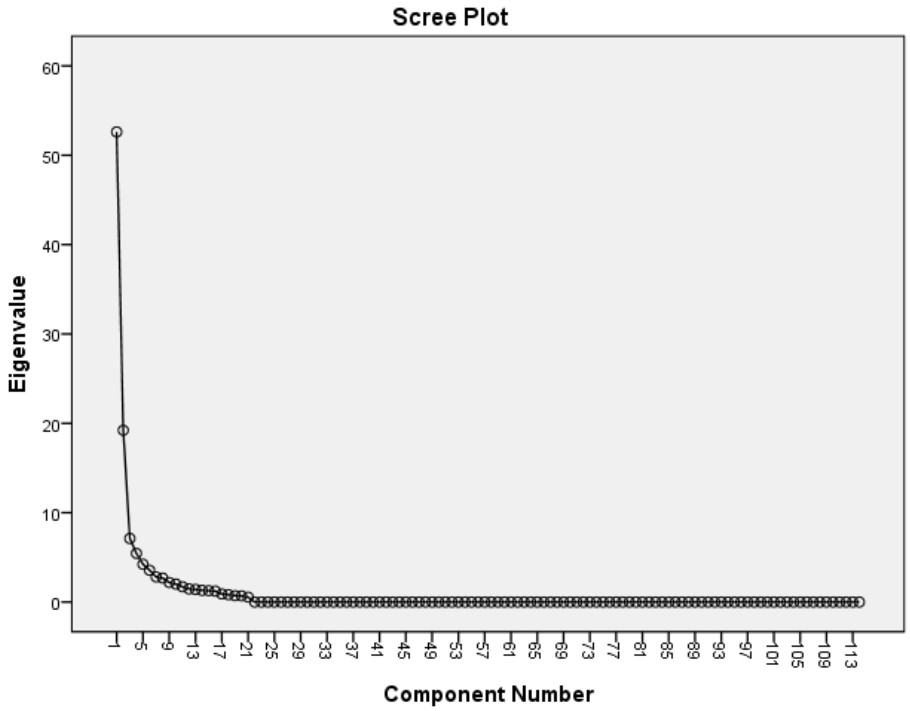

Figure 27: Scree plot obtained from a PCA on all l_entropy data points, for all frequency bands and scalp locations in the Kenyan cohort. This plots the eigenvalues of each component identified.

Table 17: Results for l_entropy binary logistic regression with a dichotomous outcome and the PCA regression scores of factors 1-7 as predictors for the Kenyan cohort: overall model fit: chi^2=17.969, p=0.012; additional fit statistics: Cox&Snell R^2=0.558, Nagelkerke R^2=0.744; linearity fit: R^2 p=0.106 (Hosmer-Lemeshow); classification sensitivity=100%, specificity=90.9%, accuracy=95.5%.

Variable	Cohort	Component	b	Wald statistics	p-value (df=1)	95% CI for Odds ratio		
						Lower	Odds ratio(ExpB)	Upper
L_entropy	**Kenyan**	1	1.387	0.155	0.694	0.004	4.003	3992.898
		2	-2.257	1.501	0.221	0.003	0.105	3.871
		3	-6.788	2.188	0.139	0.000	0.001	9.080
		4	-1.943	0.827	0.363	0.002	0.143	9.428
		5	-6.034	1.849	0.174	0.000	0.002	14.328
		6	-1.312	1.079	0.299	0.023	0.269	3.201
		7	2.898	2.039	0.153	0.340	18.135	967.871

The Kenyan model using the regression scores from the PCA of the first ten components as the predictors was statistically significant in delineating the two groups (chi^2= 17.969, p=.012).

The Hosmer-Lemenshow test was non-significant (p=0.106), indicating that the model is a better fit compared to the baseline model. This model can explain between 56% (Cox&Snell R^2) and 74% (Nagelkerke R^2) of the variance in the data. The model separated the groups with a 100% sensitivity, 90.9% specificity and 95.5% accuracy. Table 17 indicates that, although the overall model was significant, none of the independent variables were significant predictors (all p-values>0.05) and they were therefore not investigated further.

NDAR cohort

L_entropy was also investigated in the NDAR cohort. The PCA returned 18 component that explain 89% of the variance in the data. The univariate descriptive statistics suggested that none of the data points were removed in the analysis. The first 11 components were selected for a binary logistic regression model, as they cumulatively explained 79.8% of the variance in the data. The main statistics yielded by this regression are presented in Table 18. The Scree plot of the components identified is presented in Figure 28.

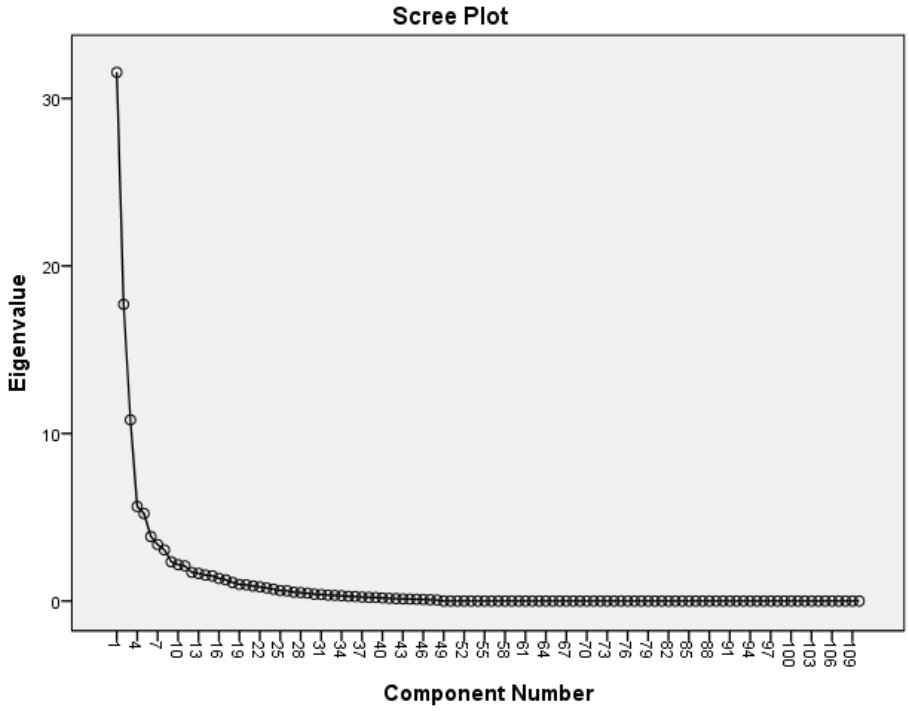

Figure 28: Scree plot obtained from a PCA on all l_entropy data points, for all frequency bands and scalp locations in the NDAR cohort. This plots the eigenvalues of each component identified.

Table 18: Results for l_entropy binary logistic regression with a dichotomous outcome and the PCA regression scores of factors 1-7 as predictors for the NDAR cohort: overall model fit: chi^2=24.969, p=0.009; additional fit statistics: Cox&Snell R^2=0.399, Nagelkerke R^2=0.533; linearity fit: R^2 p=0.736 (Hosmer-Lemeshow); classification sensitivity=69.6%, specificity=76.9%, accuracy=73.5%.

Variable	Cohort	Component	b	Wald statistics	p-value (df=1)	95% CI for Odds ratio		
						Lower	Odds ratio(ExpB)	Upper
L_entropy	**NDAR**	1	-0.684	2.567	0.109	0.219	0.505	1.165
		2	0.202	0.218	0.641	0.525	1.224	2.853
		3	0.059	0.020	0.886	0.471	1.061	2.391
		4	0.026	0.004	0.947	0.476	1.027	2.215
		5	-0.045	0.010	0.919	0.397	0.956	2.301
		6	0.235	0.357	0.550	0.585	1.265	2.739
		7	-0.529	1.628	0.202	0.261	0.589	1.328
		8	-1.368	7.541	0.006	0.096	0.255	0.676
		9	0.987	4.587	0.032	1.087	2.683	6.621
		10	0.701	3.246	0.072	0.940	2.016	4.321
		11	0.428	1.145	0.284	0.701	1.534	3.360

The NDAR model using the regression scores from the PCA of the first 11 components as the predictors was statistically significant in delineating the two groups (chi^2= 24.969, p=.009). The Hosmer-Lemenshow test was not significant (p=0.736), indicating that the model is a better fit compared to the baseline model. This model can explain between 40% (Cox&Snell R^2) and 53% (Nagelkerke R^2) of the variance in the data. The model separated the groups with a 69.6% sensitivity, 76.9% specificity and 73.5% accuracy. Table 18 suggests that two of the ten predictors contributed significantly to the accuracy of the model. The strongest predictor was component 8 (Wald statistic=7.541, df=1, p =0.006). The PCA results showed that component 8 had an eigenvalue of 3.045 and accounted for 2.77% of the variance in the data. The other significant predictor was component 9 (Wald statistic=4.587, df=1, p=0.032), with an eigenvalue of 2.340 and accountable for 2.12% of the variance in the data. The loadings of each data point on these two components were plotted and can be observed in Figures 29-32 in order to understand which frequency bands and scalp locations contributed the most to the delineation of the two groups.

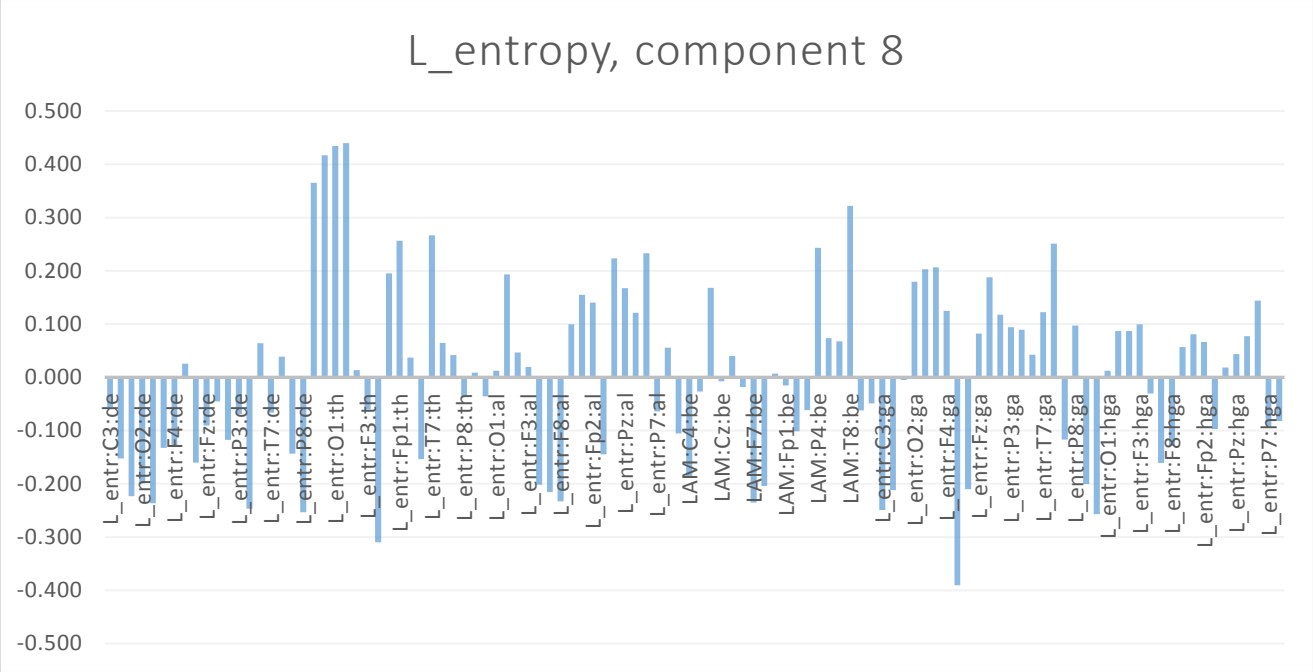

Figure 29: L_entropy component loadings of each data point on component 8 obtained in the PCA, against the labels of each data point including the abbreviated variable name, frequency band and electrode location, in the NDAR cohort.

Figure 29 shows the component loading distribution for component 8. It can be observed that delta band is negatively correlated with component 8, whereas theta shows the strongest positive correlations. For a better interpretation of these patterns, a filter was applied consisting of the selection and plotting of the data points that had a component loading higher than 0.3 or lower than -0.3. The filtered results were then plotted in Figure 30.

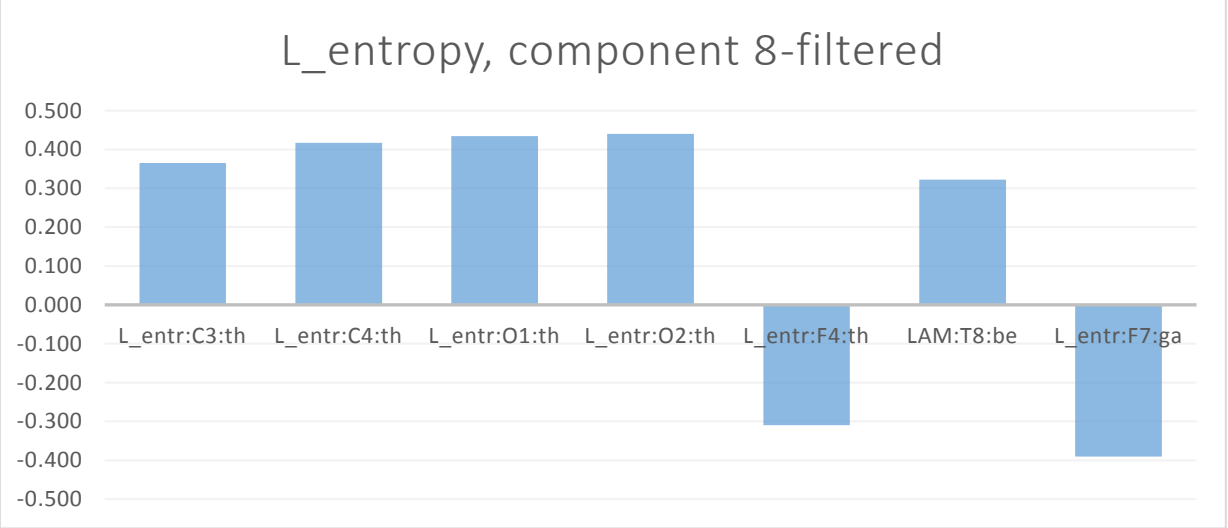

Figure 30: L_entropy component loadings higher than 0.3 and lower than -0.3 of the data points on component 8 obtained in the PCA, against the labels of each data point including the abbreviated variable name, frequency band and electrode location in the NDAR cohort.

Figure 30 shows that only seven electrodes remained in the analysis after the filter was applied. With the exception of F4, all electrodes in the theta band carry negative loadings for component 8. In the beta band, only electrode T8 showed a strong correlation with the component in a positive direction, whereas in the gamma band F7 was negatively correlated. None of the values in for l_entropy in the delta, alpha and high gamma bands remained in the analysis after the filter was applied.

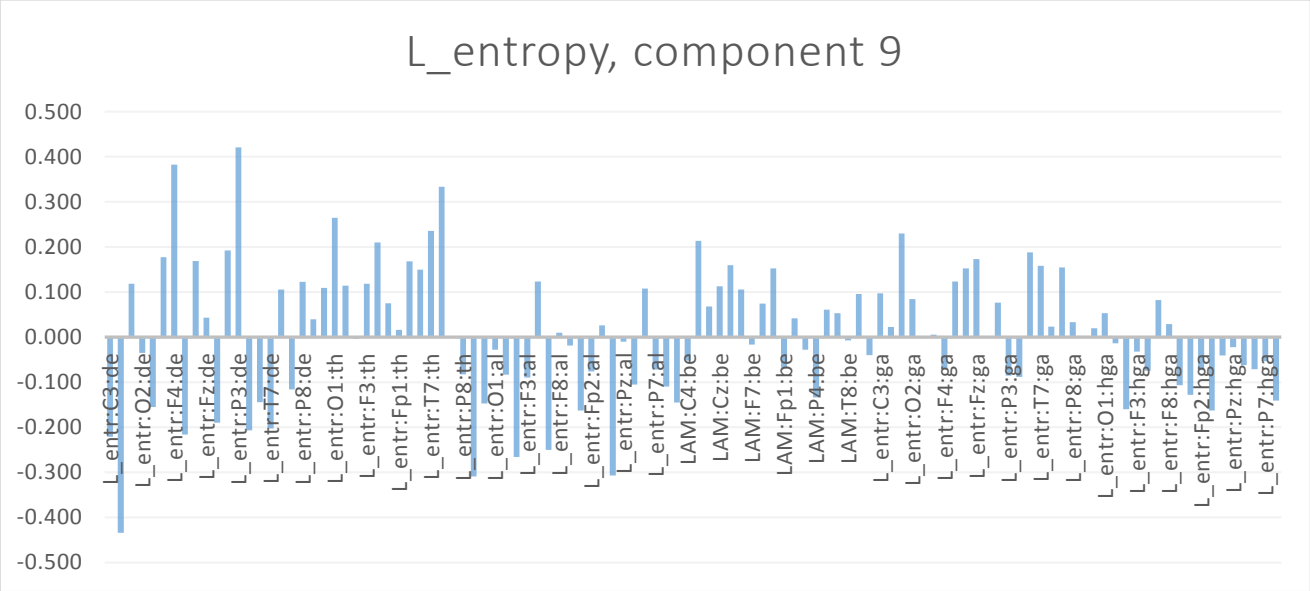

Figure 31: L_entropy component loadings of each data point on component 9 obtained in the PCA, against the labels of each data point including the abbreviated variable name, frequency band and electrode location, in the NDAR cohort.

Figure 31 shows the distribution of component loadings for component 9. A contrast can be observed between the correlations in the alpha and theta bands as well as the ones in the gamma and high gamma bands. For a better interpretation of these patterns, a filter was applied consisting of the selection and plotting of the data points that had a component loading higher than 0.3 or lower than -0.3. The filtered results were then plotted in Figure 32.

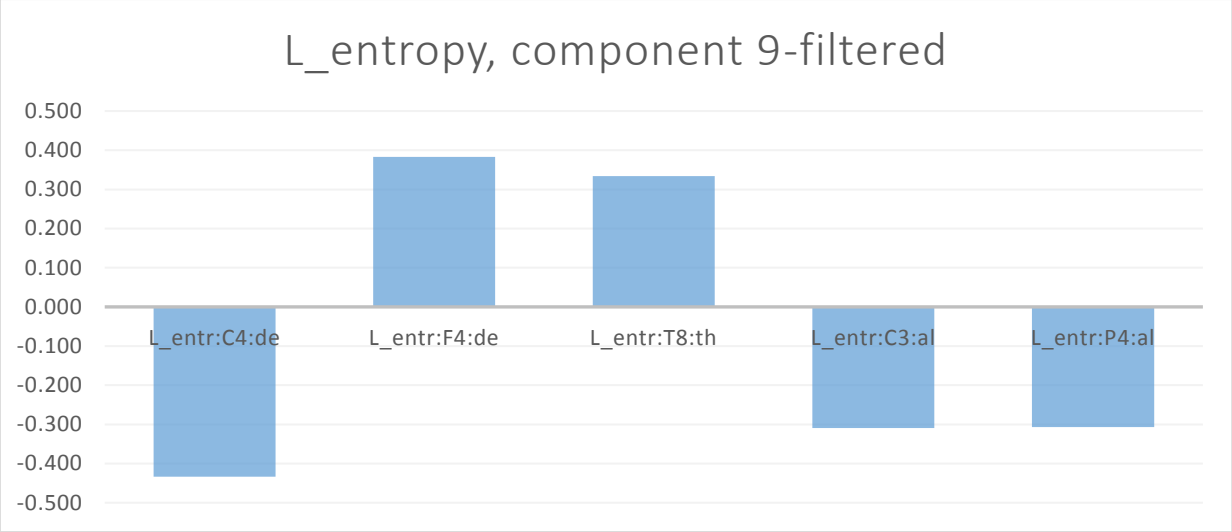

Figure 32: L_entropy component loadings higher than 0.3 and lower than -0.3 of the data points on component 9 obtained in the PCA, against the labels of each data point including the abbreviated variable name, frequency band and electrode location in the NDAR cohort.

For component 9, only five electrodes remained in the analysis after the filter was applied. The two remaining electrodes in the delta band showed contrasting results, as C4 was negatively correlated with the component and F4 was positively correlated. T8 had a positive loading in the theta band, whereas C3 and P4 had negative loadings in the alpha band. No patterns can be observed in these results.

4.2.5. L_max

Kenyan cohort

The next variable tested was l_max. Another PCA was performed on the values in the Kenyan cohort across all frequencies and electrode locations. A total of 18 factors with an eigenvalue greater than 1 cumulatively accounted for 97.8 % of the variance in the data. The univariate descriptive statistics suggested that none of the data points were removed in the analysis. The first nine components were selected for a binary logistic regression model, as they cumulatively explained 80% of the variance in the data. The regression model was not statistically significant and therefore was not investigated further. The statistic of the regression can be found in the Appendix. The Scree plot of the components identified is presented in Figure 33.

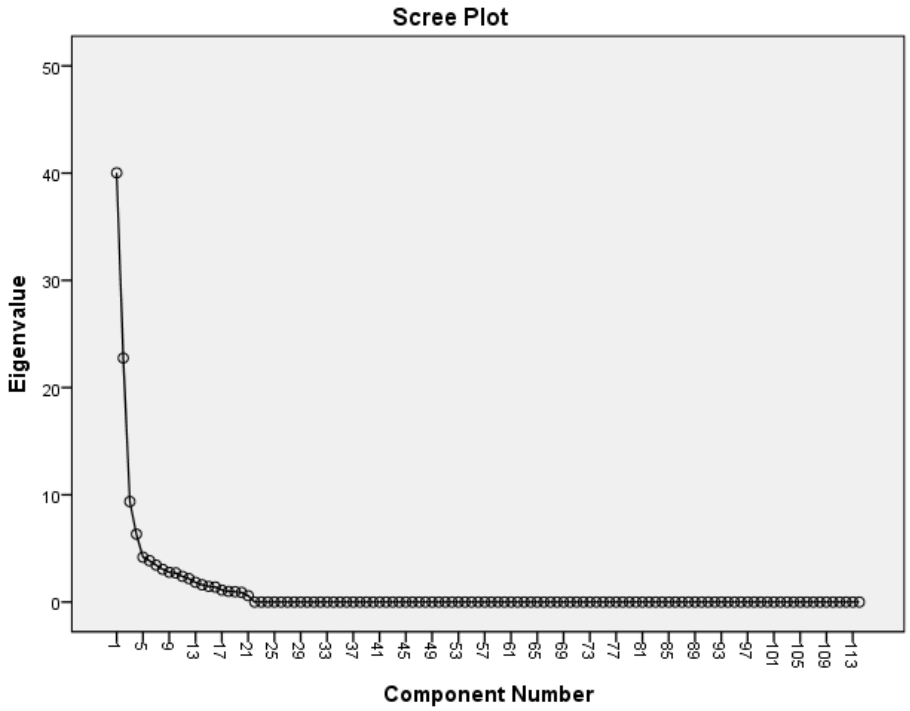

Figure 33: Scree plot obtained from a PCA on all l_max data points, for all frequency bands and scalp locations in the Kenyan cohort. This plots the eigenvalues of each component identified.

NDAR cohort

L_max was also investigated in the NDAR cohort. The PCA returned 22 component that explain 90.2% of the variance in the data. The univariate descriptive statistics suggested that none of the data points were removed in the analysis. The first 14 components were selected for a binary logistic regression model, as they cumulatively explained 81% of the variance in the data. The main statistics yielded by this regression are presented in Table 19. The Scree plot of the components identified is presented in Figure 34.

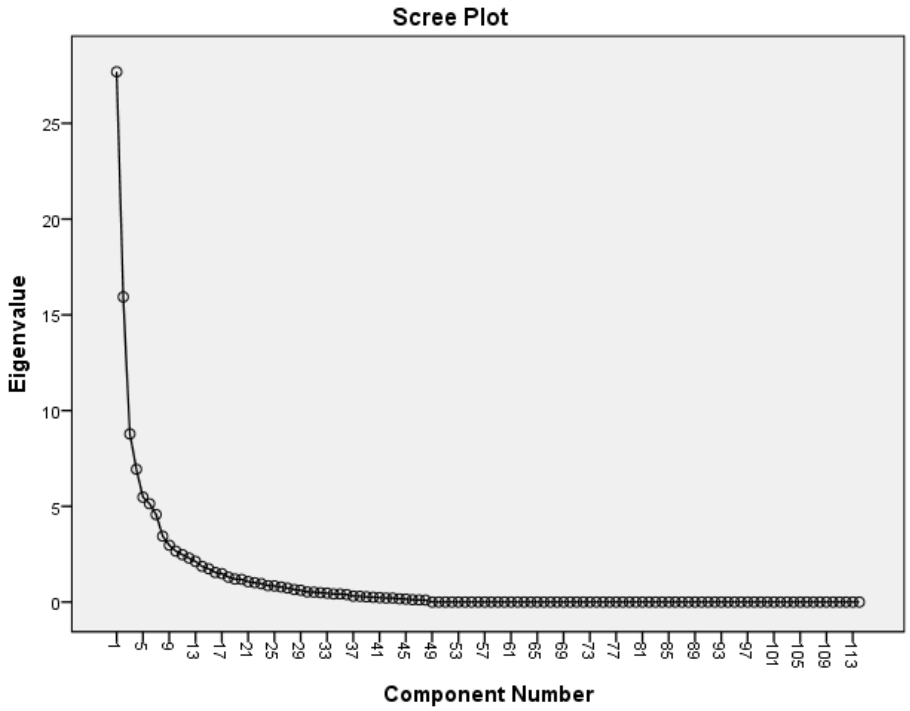

Figure 34: Scree plot obtained from a PCA on all l_max data points, for all frequency bands and scalp locations in the NDAR cohort. This plots the eigenvalues of each component identified.

Table 19: Results for l_max binary logistic regression with a dichotomous outcome and the PCA regression scores of factors 1-14 as predictors for the NDAR cohort: overall model fit: chi^2=25.409, p=0.031; additional fit statistics: Cox&Snell R^2=0.405, Nagelkerke R^2=0.540; linearity fit: R^2 p=0.370 (Hosmer-Lemeshow); classification sensitivity=73.9%, specificity=84.6%, accuracy=79.6%.

Variable	Cohort	Component	b	Wald statistics	p-value (df=1)	95% CI for Odds ratio		
						Lower	Odds ratio(ExpB)	Upper
L_max	**NDAR**	1	-0.358	0.928	0.335	0.338	0.699	1.448
		2	-0.289	0.537	0.464	0.346	0.749	1.622
		3	0.504	1.273	0.259	0.690	1.655	3.971
		4	0.122	0.095	0.758	0.519	1.130	2.463
		5	0.879	0.672	0.412	0.294	2.408	19.701
		6	0.441	0.788	0.375	0.587	1.555	4.121
		7	-0.070	0.046	0.831	0.493	0.933	1.765
		8	-1.412	7.702	0.006	0.090	0.244	0.660
		9	-0.569	0.540	0.463	0.124	0.566	2.583
		10	-0.331	0.453	0.501	0.274	0.718	1.882
		11	-0.269	0.338	0.561	0.309	0.764	1.892
		12	1.042	5.606	0.018	1.196	2.834	6.713
		13	0.335	0.670	0.413	0.627	1.398	3.119
		14	0.219	0.280	0.597	0.553	1.245	2.803

The NDAR model using the regression scores from the PCA of the first 14 components as the predictors was statistically significant in delineating the two groups (chi^2= 25.409, p=.031). The Hosmer-Lemenshow test was non-significant (p=0.370), indicating that the model is a

better fit compared to the baseline model. This model can explain between 40% (Cox&Snell R^2) and 54% (Nagelkerke R^2) of the variance in the data. The model separated the groups with a 73.9% sensitivity, 84.6% specificity and 79.6% accuracy. Table 19 suggests that two of the 14 predictors contributed significantly to the accuracy of the model. The strongest predictor was component 8 (Wald statistic=7.702, df=1, p=0.006). The PCA results showed that component 8 had an eigenvalue of 3.440 and accounted for 3.0% of the variance in the data. The other significant predictor was component 12 (Wald statistic=5.606, df=1, p=0.018), with an eigenvalue of 2.301 and accountable for 2.019% of the variance in the data. The loadings of each data point on these two components were plotted and can be observed in Figures 35-38 in order to understand which frequency bands and scalp locations contributed the most to the delineation of the two groups.

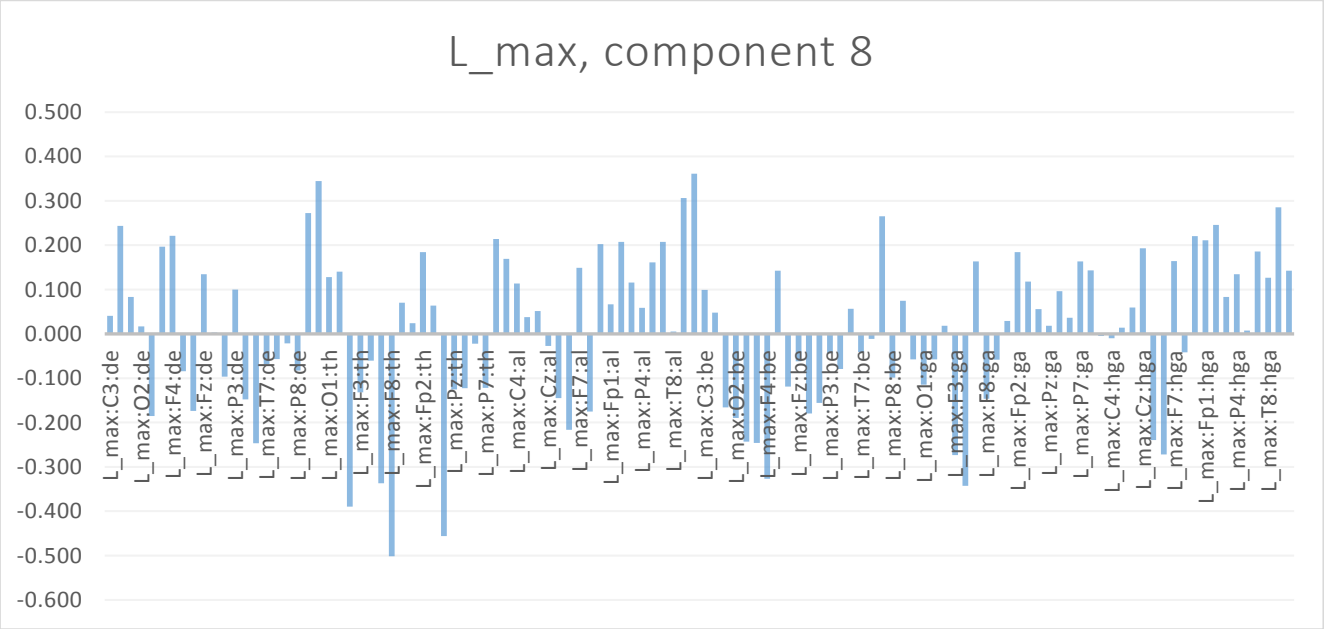

Figure 35: L_max component loadings of each data point on component 8 obtained in the PCA, against the labels of each data point including the abbreviated variable name, frequency band and electrode location, in the NDAR cohort.

Figure 35 shows the distribution of component loadings for component 8. A contrast can be observed between the correlations within the delta and theta bands, with both positive and

negative correlations. For a better interpretation of these patterns, a filter was applied consisting of the selection and plotting of the data points that had a component loading higher than 0.3 or lower than -0.3. The filtered results were then plotted in Figure 36.

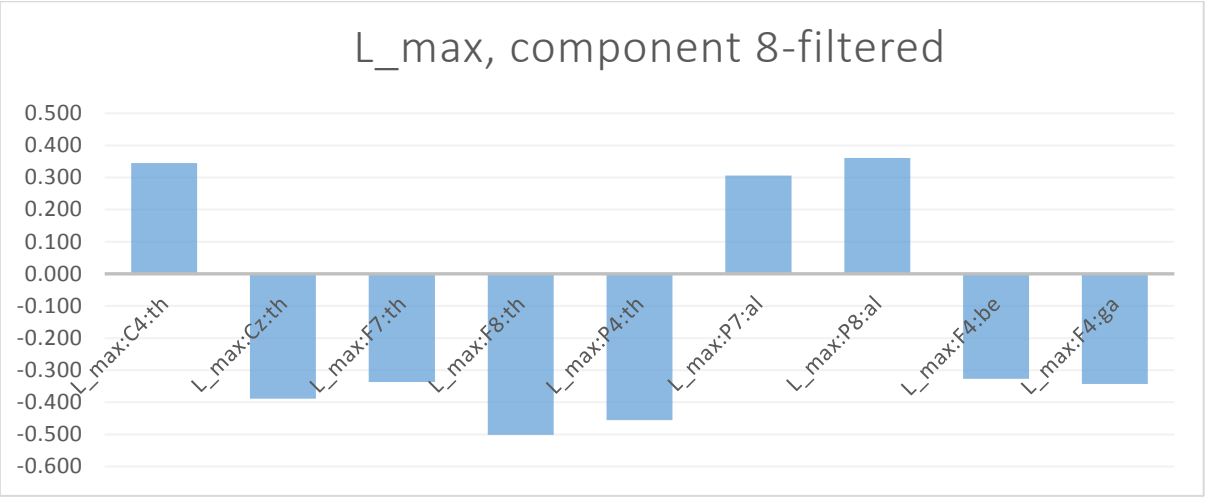

Figure 36: L_max component loadings higher than 0.3 and lower than -0.3 of the data points on component 8 obtained in the PCA, against the labels of each data point including the abbreviated variable name, frequency band and electrode location in the NDAR cohort.

Only nine electrodes remained in the analysis after the filter was applied. With the exception of C4, all four electrodes in the theta band were positively correlated with component 8. P7 and P8 carried positive loading in the alpha band. Moreover, electrode F4 correlated positively with component 8 both in the beta and gamma bands. No specific pattern was distinguished in these results.

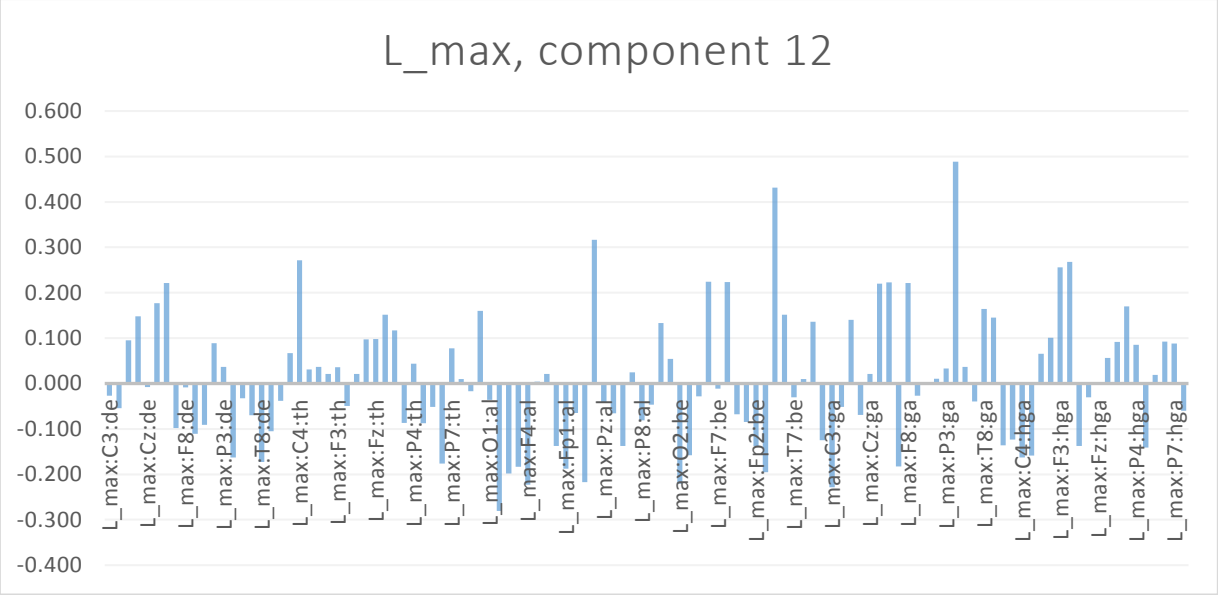

Figure 37: L_max component loadings of each data point on component 12 obtained in the PCA, against the labels of each data point including the abbreviated variable name, frequency band and electrode location, in the NDAR cohort.

In figure 37, it can be observed that the stronger correlations are this time in the higher frequency bands, particularly beta and gamma. For a better interpretation of the results, a filter was applied consisting of the selection and plotting of the data points that had a component loading higher than 0.3 or lower than -0.3. The filtered results were then plotted in Figure 38.

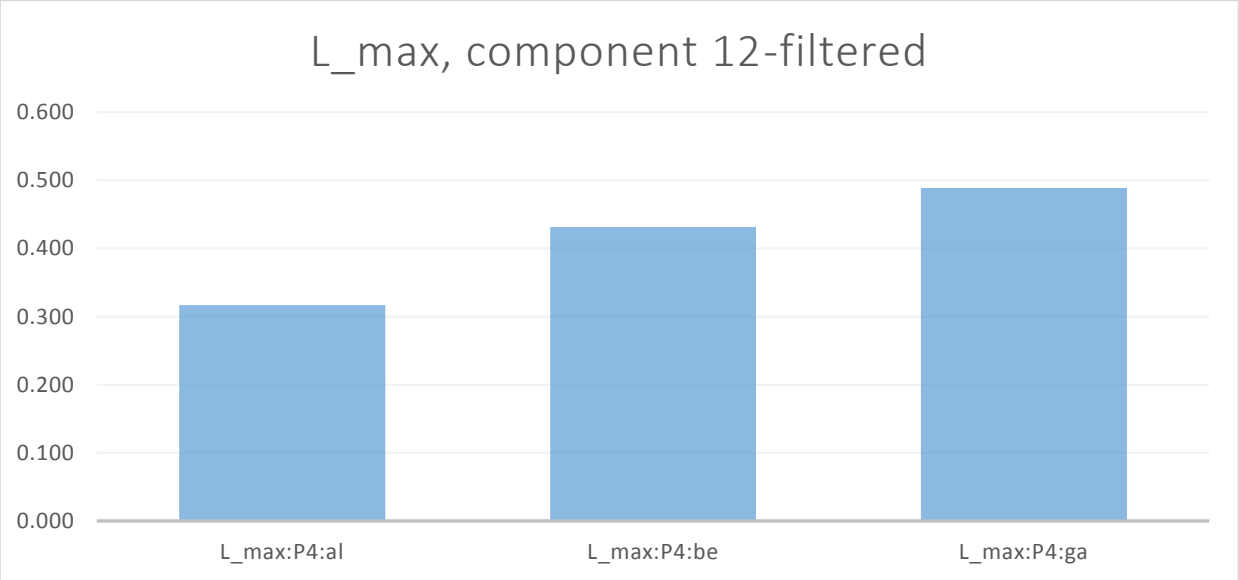

Figure 38: L_max component loadings higher than 0.3 and lower than -0.3 of the data points on component 12 obtained in the PCA, against the labels of each data point including the abbreviated variable name, frequency band and electrode location in the NDAR cohort.

Only three electrodes remained in the analysis after the filter was applied. In fact, electrode P4 was correlated positively with component 12 in alpha, beta and gamma bands. No other electrodes or frequency bands showed strong correlations with component 12 of the PCA.

Recurrence rate, l_mean and trapping time did not yield any significant results in neither of the two cohorts. The statistics of the regressions performed on the components for these three variables in both cohorts are presented in the Appendix. The diagram in Table 20 presents a summary of all the results obtained from the single electrode analysis.

Table 20: A summary of all the results obtained after the single electrode analysis including a PCA and a logistic regression for each variable across all frequencies and electrodes. The results that are consistent in both cohorts are marked with bold text.

Electrode	Kenyan cohort		NDAR cohort	
	Variable	Frequency	Variable	Frequency
C3			SampE	beta (-), gamma (-), high gamma (-)
			DET	delta (+), theta (+), alpha (+), gamma (+)
			LAM	Delta (-), Theta (-)
			L_ent	Theta (+), alpha (-)
C4	SampE	**beta (-)**	SampE	**beta (-)**, gamma (-), high gamma (-)
			DET	Theta (+), gamma (+), high gamma (-)
			LAM	Theta (-)
			L_ent	delta (-), Theta (+)
			L_max	Theta (+)
O1	SampE	**theta(+)**	SampE	**theta (+)**
			DET	Delta (-), theta (+), Alpha (+)
			LAM	Delta (-)
			L_ent	Theta (+)
O2	SampE	**theta (+)**, beta (-)	SampE	**theta (+)**
			DET	Delta (+), theta (+), high gamma (-)
			LAM	Delta (+)
			L_ent	Theta (+)
Cz	SampE	theta (+), beta (-)		
			DET	Alpha (+), gamma (-)
			L_max	Theta(-)
F3	SampE	theta(+)		
			DET	Delta (+), theta (+), beta (+), high gamma (-)
F4	SampE	theta (+), high gamma (+)		
			DET	theta (+), alpha (+), beta (+), gamma (+)
			L_ent	Theta (-), delta (+)
			L_max	Beta (-), gamma (-)
F7	SampE	theta (+), beta (-)	SampE	alpha (-), high gamma (-)
			DET	delta (+), theta (-), gamma (+), high gamma (-)
			LAM	Theta (+), alpha (+)
			L_ent	Gamma (-)
			L_max	Theta (-)
F8	SampE	delta(+), theta (+), beta (-)	SampE	beta (-)
			DET	theta (-), alpha (-)

			LAM	Delta (+), theta (+), alpha (+), beta (+)
			L_max	Theta(-)
Fz	SampE	delta(+), **theta (+),** beta (-)	SampE	**theta (+)**, alpha (+)
			DET	delta (+)
			LAM	Theta (-)
Fp1	SampE	delta(+), **theta (+), high gamma (+)**	SampE	**theta (+), high gamma (+)**
			DET	Theta (+), alpha (+), gamma (+), high gamma (-)
			LAM	Theta (-)
Fp2	SampE	delta(+), **theta (+), high gamma (+)**	SampE	**theta (+), high gamma (+)**
			DET	Delta(+), beta (+), gamma (+), high gamma (+)
P3	SampE	beta (-)	SampE	alpha (-)
			DET	Theta (+), alpha (+), beta (+), gamma (+,)high gamma (-)
P4	SampE	theta (+), beta (-)		
			DET	Delta (+), gamma (-), high gamma (-)
			LAM	Delta (+), theta (+), alpha (+)
			L_ent	Alpha (-)
			L_max	Theta (-), alpha (+), beta (+), gamma (+)
Pz	SampE	**theta (+)**	SampE	**theta (+),** alpha (-), beta (-)
			DET	Theta (+), alpha (+), high gamma (-)
T7			SampE	theta (+)
			DET	Delta (+), theta (-), alpha (+)
			LAM	Delta (+)
T8			SampE	theta (-), alpha (-), beta (-), gamma (-), high gamma (-)
			DET	High gamma (-)
			LAM	Delta (+), theta (+), alpha (+), beta (+), gamma (+)
			L_ent	Beta (+), theta (+)
P7			SampE	theta (+)
			DET	theta (+), alpha (+)
			L_max	Alpha (+)
P8	SampE	beta (-)	SampE	theta (+)
			DET	Delta (+), high gamma (-)
			LAM	Alpha (-)
			L_max	Alpha (+)

5. Discussion

The explicit aims of this study was to use MSE measures and RQA to analyse EEG signals in order to identify quantifiable neural correlates associated with an ASD diagnosis. Two hypotheses were addressed:

Hypothesis 1: MSE represents a functional brain measure that correlates with an ASD diagnosis and can be used to distinguish subjects in two categories, ASD and non-ASD.

Hypothesis 2: A broader range of EEG signal features computed using RQA are other brain invariants that are associated with ASD and separate ASD from non-ASD subjects with a high accuracy. Entropy, such as MSE, is one of several variables that can be extracted from RQA. This hypothesis aimed to determine if additional values derived from EEG data increase the accuracy of delineation.

The first hypothesis addressed in this study was confirmed, the findings showing that sample entropy is useful in distinguishing ASD from non-ASD individuals, both at a whole brain level in the alpha, beta and gamma bands, and at a single electrode level, mainly in the theta band in the frontal (Fp1, Fp2, F7, F3, Fz), occipital (O1, O2) and parietal electrodes (P7, Pz, P4, P8) and in the high gamma band in the frontal (Fp1, Fp2, F7, F4). Testing of RQA variables found that determinism can be used to distinguish ASD from controls in the theta, gamma and high gamma bands in all electrode locations, in the delta band mainly in the left frontal (F7, F3, Fz) and temporal areas (T7) and in the alpha band mainly in the left hemisphere in the occipital (O1), parietal (P7, P3), temporal (T7) and central electrodes (C3, Cz, Pz); laminarity is useful in delineating ASD in the frontal (Fp1, F7, F8), temporal (T8) and parietal regions (P4) in the theta band and the occipital (O1, O2), parietal (P4) and temporal regions (T7, T8) in the delta band; another measure of complexity, l_entropy delineated ASD in the central (C3, C4), temporal (T8) and occipital areas (O1, O2) in the theta frequency; and, lastly, l_max was another brain measure that accurately distinguished the two groups in the frontal (F7, F8) and central areas (Cz, C4) in the theta band and in the parietal region (P7, P4, P8) in the alpha frequency.

The limitations of this study and interpretations of these results are presented below.

5.1. Limitations

5.1.1. Data

The hypotheses addressed in this study were tested on two separate cohorts, the Kenyan and the NDAR cohort. Some of the results presented were replicated in both cohorts. However, most of the results presented are different between the two cohorts, particularly in the single electrode analysis where only sample entropy is identified as a useful marker in the Kenyan cohort. The reasons for these differences may be the limitations this study encountered with the datasets. These limitations should also be considered outside of the comparison between the two cohorts, when evaluating the results and importance of this study.

The first such limitation is sample size, particularly in the Kenyan cohort. When performing statistical tests, such as PCA or logistic regression, the number of variables and the number of cases has to be taken into consideration. This study used two cohorts with sample sizes of 22 and 49 respectively and a number of 114 data points for each variable tested. These numbers clearly suggest that the sample sizes were very small and generalisations of these results should be made with caution. However, this study could be regarded as an initial exploration, as it tests variables that have not been tested in the context of ASD with the aim of measuring their utility in ASD delineation in different frequency bands and scalp locations. That means that the findings presented here should not be generalised for the entire population, instead they should be regarded as suggestive evidence of the utility of new methods of analysis as well as markers of what future research should focus on in order to uncover the full potential of EEG and this non-linear analysis method in ASD.

The sample size limitation could have been addressed by combining the two cohorts. The reason why this was not possible represents another limitation of the study. Previous research has demonstrated that data collected in different environments, using different equipment could

be combined in order to obtain a large dataset. In a previous study, Bosl and colleagues used EEG data collected in different settings, from both clinical patients and healthy controls (Bosl, Loddenkemper et al. 2017). The control groups from both settings were compared and no differences were found, showing that data could theoretically be combined to form large cohorts. The reason why this method was not applied in the current study is because no information could be obtained about the data collection, medical history or any other characteristics of the NDAR cohort. Moreover, the ages of the individuals in the two cohorts were different, which could have an effect on the EEG signal. Avoiding the risk of obtaining a heterogeneous dataset, the two cohorts were analyzed separately.

Another limitation is represented by the age of the children in both cohorts. As mentioned in the Introduction, a reliable diagnosis of ASD is usually made after the age of 2 years. The ages of the individuals in the two cohorts range between 6-9 years old in the Kenyan cohort and 4-12 years old in the NDAR cohort. These are far from the critical age of diagnosis and early intervention has improved and longer-lasting outcomes. Moreover, before generalising results found on individuals in these age groups, different cohorts of younger ages should be investigated, as the brain dynamics change substantially in the first years of life. For example, EEG signal coherence increases during maturation and power distribution tends to shift to higher frequencies (Gasser, Verleger et al. 1988, Marosi, Harmony et al. 1992). In the first 2-3 years of life major changes in brain function that support high-level social and communication skills take place and network malfunctions during these changes are the foundation of the difficulties associated with ASD. Some of these changes include losing the ability to perceive speech sounds from non-native languages and gaining the ability of perceiving others' intentional actions (Behne, Carpenter et al. 2005, Rivera-Gaxiola, Silva-Pereyra et al. 2005). These developmental changes should be taken into consideration when testing these variables.

Another limitation coming from the data used in this study is the medical comorbidity of the ASD patients in the Kenyan cohort. Out of the 11 ASD patients, six were also diagnosed with epilepsy. The interpretation and analysis of the EEG signal and the variables computed to characterise the signal may be complicated by the presence of epilepsy. Epilepsy is associated with abnormal EEG, which is the principal method to diagnose the condition as the signs are very clear in the signal. Therefore, this may complicate the separation of those effects by those caused by ASD. For example, measures such as entropy, laminarity and determinism are useful in delineating epilepsy patients from healthy controls. Therefore, the effects of epilepsy when investigating these variables in the context of ASD should be taken into consideration.

Lastly an important limitation of this study comes from the set of variables used. At present, none of the RQA variables have been associated with any cognitive or neural functions. Previous studies sought to measure their utility in diagnosis or classification, and only measured their accuracy of prediction. However, no study so far correlated these measures with any biological function. This limitation therefore makes it difficult to draw conclusions on which ASD symptoms or which cognitive aspect of ASD these variables could underlie.

5.1.2. Data analysis

Another set of limitations of this study comes from the data analysis methods used. PCA and logistic regression were the suitable tools to use in order to answer the questions asked in the hypotheses. However, further tests would have been appropriate in order to make this investigation even more accurate. In order to determine if the results, or lack of statistical significance in certain variables were due to the small sample size or the lack of utility of the variable in distinguishing the two groups, power tests would have been appropriate. These tests involve simulating new data based on the existing data to determine an appropriate sample size

when significance is reached. However, the high number of data points, 114 for each variable for each participant, made that an impossible task for this project.

Secondly, the accuracy of the classifications returned by the logistic regressions could have also been tested using machine learning algorithms such as a support vector machine. However using such methods involves using part of the data for training the algorithm, to then test it on the remaining data. The sample sizes of the two cohorts were insufficient for splitting the data this way.

5.2. Sample Entropy

5.2.1 Whole Brain Analysis

The findings of the analysis performed on sample entropy data at the whole brain level show significant promise for the sample entropy measure to be used to distinguish ASD from control individuals, confirming previous research. For both cohorts sample entropy showed a significant capacity to correctly classify individuals, with very high sensitivity, specificity and accuracy. The sensitivity, specificity and accuracy were lower in the NDAR cohort compared to the Kenyan cohort, which may be explained by the difference in ages between cohorts or comorbidities, as discussed in Limitations.

The results for the Kenyan cohort, do not indicate any statistically significant differences across the six frequency bands examined. However, sample entropy in the gamma band was very close to the traditional significance threshold ($p<0.05$). As the purpose of this study was to explore a large dataset and measuring the utility of these variables in separating ASD from non-ASD, this finding can be considered as suggestive evidence that sample entropy in the gamma band could potentially be used to delineate ASD patients from controls, when using whole brain measurements.

The findings in the NDAR cohort were clearer. They can be considered as strong evidence and a confirmation that sample entropy measurements are very useful in distinguishing ASD individuals from non-ASD individuals. Moreover, these findings show that alpha, beta and gamma are the frequency bands that most accurately classify ASD, indicating that ASD is associated with lower complexity measurements at the whole brain level in the alpha and gamma bands, as well as an increase in beta complexity in the beta band. The results in the gamma band are in concordance with previous findings by Bosl and colleagues who identified lower high frequency entropy associated with infants at risk of developing ASD (Bosl, Tierney et al. 2011). His findings were concentrated mostly in the frontal region of the brain. This study shows lower high frequency entropy across the whole brain could be characteristic to ASD patients. Previous research also found lower connectivity in the alpha band, corresponding to a decrease in long range connections in ASD (Murias, Webb et al. 2007, Gurau, Bosl et al. 2017). This finding may also be consistent with the under-connectivity theory developed by Just and colleagues (Just, Keller et al. 2012). The results of this analysis in the alpha band support these theories, showing lower alpha complexity, as complexity and connectivity are highly correlated (Sakkalis, Tsiaras et al. 2008).

5.2.2. Single Electrode Analysis

The findings of the analysis performed on sample entropy at all electrode locations reinforce the variable's utility in distinguishing ASD patients from neurotypical individuals. Testing the components that the PCAs identified in order to determine the ability to distinguish between the two groups, yielded significant results for both cohorts.

The Kenyan cohort could be clearly categorised in ASD and non-ASD using sample entropy measurements from all 19 scalp electrodes across all six frequency bands, with an 81% accuracy (81.8% sensitivity, 81.8% specificity). This finding supports the whole brain findings

in sample entropy. An in depth investigation of the scalp locations and frequency bands useful for this accurate classification revealed that the most prominent difference in sample entropy between the two groups was in the frontal region (Fp1, Fp2, F7, F3, F4, F8) in the theta band. Moreover, sample entropy in the delta band also played a significant role in the group delineation in the frontal areas (Fp1, Fp2). These findings in the low frequency bands are important because they may be consistent with findings of excessive short-range frontal connectivity from previous EEG, MEG and fMRI studies (Ghanbari, Bloy et al. 2015). These findings suggest increases in short-range association fibres (Herbert, Ziegler et al. 2004). In turn, these fibres could redirect cortical connections towards local, instead of global, long-range information processing (Courchesne, Karns et al. 2001, Casanova 2006). Furthermore, previous MRI studies consistently showed decreased volumes of the corpus callosum in ASD, further supporting the theory that cortical connections tend to form predominantly locally, rather than globally in ASD patients (Belmonte, Allen et al. 2004, Casanova 2006). Therefore, these findings could support the hypothesis that sample entropy is a measure of the brain's signal complexity, which underlies its adaptability and has been proved to intertwine with network connectivity. Additionally, theta differences were observed in the occipital (O1, O2) and right parietal regions (P4).

Sample entropy in the beta band also distinguishes the two groups in the Kenyan cohort, particularly in the central (Fz, Cz), parietal (P3, P4, P8) and frontal areas (F7). Beta brain oscillations have been associated with encoding of sensory information and sensory perception (Kopell, Ermentrout et al. 2000). Abnormal beta complexity in ASD, could then be hypothesized to underlie the malfunctions in the sensory information processing of the patients and could potentially explain the hypersensitivity observed in ASD. Lastly, sample entropy in the high gamma band in the frontal region (Fp1, Fp2) also played a role in distinguishing the two groups. Gamma oscillations have previously been associated with early states of sensory

perception, which could potentially link these complexity findings to sensory malfunctions in ASD (Pantev, Makeig et al. 1991).

The findings in the NDAR cohort did not fully replicate those in the Kenyan cohort, but some patterns were observed. One consistent result was the sample entropy in the theta band in the frontal areas of the brain (Fp1, Fp2). These findings provide evidence for the assumptions made above and may further support the over-connectivity theory. Moreover, sample entropy in the theta band in temporal (T7, T8) also played an important role in classifying the NDAR cohort. Murias and colleagues also found theta differences in functional connectivity in the frontal and temporal regions (Murias, Webb et al. 2007). These findings further emphasize the link between connectivity and complexity measures and emphasize the need for new research that combines both analysis methods. Other areas in which sample entropy in the theta band was useful for the delineation were the occipital (O1, O2) and parietal regions (P7, P8), similarly to the findings in the Kenyan cohort. Furthermore, sample entropy in the high gamma band in the frontal areas (Fp1, Fp2, F7) was also observed to play a role in the delineation of the NDAR cohort, reinforcing a connection between complexity findings and malfunctions in the sensory processing in ASD. Compared to the Kenyan cohort, no specific pattern was identified for the beta band for sample entropy, playing a role only in the right frontal (F8) and central regions (C3, C4, Pz).

Overall, entropy in the theta band in the frontal and occipital regions, as well as high gamma entropy in the prefrontal regions were the consistent findings in the two cohorts. Additionally, in the Kenyan cohort, sample entropy in the beta band in the central, parietal and frontal areas and in the delta band in the frontal areas were useful markers, which did not appear in the NDAR cohort. These findings stand as evidence that entropy is a brain measure that can be used to distinguish ASD patients from healthy controls. Adding to previous research that initially established the high utility of entropy in characterising ASD and its potential to

become a useful tool in ASD diagnosis, this study identified certain frequency bands and brain regions in which entropy measurements can be most relevant.

5.3. Determinism

5.3.1. Whole brain analysis

In this step of the analysis, determinism did not show any significant results either in the Kenyan cohort, or the NDAR cohort. That means that computing the determinism values of whole brain signals is not a useful method to distinguish ASD patients from neurotypical controls. The potential reasons for this results are discussed in the Limitations section.

5.3.2. Single electrode analysis

Determinism values measured across six frequency bands and 19 scalp locations in the Kenyan cohort did not yield any significant results. These measurements did not accurately classify the data in the two categories, meaning that, similarly to the whole brain analysis, none of the determinism values in any of the regions or frequency bands could be used to detect ASD in this cohort.

However, determinism showed potential in the NDAR cohort. These findings show that measures of determinism may be a useful invariant, with the most prominent findings found in the theta band, in which determinism appeared to distinguish between the two groups in every brain region. Similarly, determinism in the highest frequency bands, gamma and high gamma in all brain regions distinguished between the two groups. Determinism is a measure of predictability of the signal. In the lower frequencies, determinism in the delta band was relevant in the classification in the left frontal (F7, F3) and temporal (T7) regions. Lastly the variable measured in the alpha band showed utility in the left occipital (O1), parietal (P7, P3), temporal (T7) and central areas (C3, Cz, Pz). Since there was no available phenotypical data that

characterise either of the two cohorts, associations and correlations between this variable and specific behavioural, cognitive or neurological traits could not be inferred. Moreover, there is no previous research that interpreted determinism in the context of behaviour or cognition. Previous research did however identify a correlation between determinism and epilepsy, with lower determinism characterising the epileptic patients (Ngamga, Bialonski et al. 2016). Since ASD and epilepsy often occur together, conclusions on the correlation between determinism and ASD should take into consideration the patient's medical history. The conclusion supported by these findings is that signal predictability measured using determinism could potentially be used to characterise and identify ASD.

5.4. Laminarity

5.4.1. Whole brain analysis

In the whole brain analysis, laminarity did not show any significant results in either of the two cohorts. Thus measuring laminarity at the whole brain level is not a useful method to distinguish ASD patients from healthy controls. The potential reasons for this results are discussed in the Limitations section.

5.4.2 Single electrode analysis

Laminarity measured across all six frequency bands and 19 scalp locations in the Kenyan cohort did not show any significant results and thus was not useful in distinguishing between the groups.

In the NDAR cohort, laminarity was useful in distinguishing ASD individuals from healthy controls. The differences laminarity were particularly observed in the low frequency bands: in the theta band in the frontal (Fp1, F7, F8), temporal (T8) and parietal regions (P4), as well as in the delta band in the occipital (O1, O2), temporal (T7, T8) and parietal areas (P4). The

variable did now show classification accuracy in the high frequency bands (beta, gamma, high gamma).

Laminarity is a measure of the signal's smoothness. Therefore, a difference in the brain signal's smoothness in ASD might be inferred from these findings. As no phenotypical data for either of the two cohorts was available, associations and correlations between laminarity and behavioural, cognitive or neurological aspects could not be examined. However, previous research identified a correlation between laminarity and epilepsy, with lower laminarity values found in patients with epilepsy (Ngamga, Bialonski et al. 2016). Considering the comorbidity between ASD and epilepsy, conclusions on the correlation between determinism and ASD should take into consideration the patient's medical history. The conclusion supported by these findings is that signal smoothness quantified using laminarity could potentially be used to characterise and identify ASD.

5.5. L_entropy

5.5.1. Whole Brain Analysis

In the whole brain analysis, l_entropy measures did not show any significant results in either of the two cohorts. The variable was not accurate in classifying the individuals, and thus measuring l_entropy at the whole brain level is not a useful method to distinguish ASD patients from healthy controls. The potential reasons for this results are discussed in the Limitations section.

5.5.2 Single electrode analysis

L_entropy measured across all six frequency bands and 19 scalp locations in the Kenyan cohort did not show any significant results. These measurements did not accurately classify the data in the two categories, meaning that, similarly to the whole brain analysis, none of the l_entropy

values measured from any of the regions or frequency bands could be used to detect ASD in this cohort.

In the NDAR cohort, l_entropy distinguished the two groups. When measured in the theta band in the central (C3, C4), temporal (T8) and occipital regions (O1, O2), l_entropy showed particularly high utility. Sample entropy and l_entropy are both measures of entropy computed using different algorithms, although they both measure signal complexity. L_entropy was also significant in the delta band in the right frontal and central areas of the brain. The high frequency measurements of l_entropy did not help in classification. The consistent results found when investigating the two variables, are the findings in the theta band. The findings obtained using l_entropy in the theta band, however are not focused in the frontal region. Moreover, in a previous study, Bosl and colleagues showed that l_entropy values are useful in delineating ASD patients and usually lower when compared to controls' values. The conclusion supported by these findings is that signal complexity quantified using l_entropy be a tool to characterise and identify ASD.

5.6. L_max

5.6.1. Whole Brain Analysis

In this step of the analysis, l_max did not show any significant results both in the Kenyan cohort, or the NDAR cohort. That means that computing the l_max values of whole brain signals is not a useful method to distinguish ASD patients from neurotypical controls. The potential reasons for this results are discussed in the Limitations section.

5.6.2. Single electrode analysis

L_max values measured across six frequency bands and 19 scalp locations in the Kenyan cohort did not yield any significant results. These measurements did not accurately classify the

data in the two categories, meaning that, similarly to the whole brain analysis, none of the l_max values in any of the regions or frequency bands could be used to detect ASD in this cohort.

L_max showed potential utility in distinguishing the two groups in the NDAR cohort. The variable played an important role in the classification when measured in the theta band in the frontal (F7, F8) and central (Cz, C4) areas and in the alpha band in the parietal areas (P7, P4, P8). L_max is a measure of the signal's stability in a certain state. Therefore, a difference in the brain signal's stability in ASD might be inferred from these findings. As no phenotypical data for the two cohorts was available, correlations between l_max and behavioural, cognitive or neurological aspects could not be inferred. Previous research identified a correlation between l_max and ASD in the central parietal and occipital areas (Bosl, Loddenkemper et al. 2017). These findings take this investigation one step further and show that signal stability quantified using l_max could potentially be used to characterise and identify ASD, particularly when measured in the theta or alpha bands.

5.7. Trapping time

5.7.1. Whole Brain Analysis

The findings of the analysis performed on trapping time data at the whole brain level show potential utility for measure to be used to distinguish ASD from control individuals. In the Kenyan cohort trapping time showed a significant capacity to correctly classify individuals, with high sensitivity, specificity and accuracy. Moreover, these findings show that this invariant shows the most accurate classification in the gamma band, also indicating that ASD is associated with lower trapping time measurements at the whole brain level in the gamma band. Since no phenotypical data for either of the two cohorts was available, correlations between trapping time and behavioural, cognitive or neurological aspects could not be inferred.

However, previous research identified a correlation between trapping time and epilepsy (Bosl, Loddenkemper et al. 2017). Considering the comorbidity between ASD and epilepsy, conclusions on the correlation between determinism and ASD should take into consideration the patient's medical history. These finding were not replicated in the NDAR cohort. Lastly, trapping time was not found to play any significant role in the delineation of ASD at a single electrode level.

5.8. Recurrence Rate and L_mean

Recurrence rate and L_mean are the two variables computed in this study that did not appear significant in any of the analysis steps. These findings are also supported by previous research looking at associations between these variable and ASD. It can therefore be concluded that recurrence rate and l_mean are not useful in separating ASD patients from healthy controls and that in further investigations they could potentially be excluded from the analysis.

To summarize, the first hypothesis was confirmed, the results showing that complexity measured using sample entropy is useful in distinguishing the two categories, both at a whole brain level in the alpha, beta and gamma bands, and at a single electrode level, mainly in the theta band in the frontal, occipital and parietal electrodes and in the high gamma band in the frontal and prefrontal areas. Examination of the second hypothesis found the following: determinism can be used to delineate ASD in the theta, gamma and high gamma bands in all electrode locations, in the delta band mainly in the left frontal and temporal areas and in the alpha band mainly in the left hemisphere in the occipital, parietal, temporal and central electrodes; laminarity is useful in delineating ASD, particularly in the frontal, temporal and parietal regions in the theta band and the occipital, parietal and temporal regions in the delta band; another measure of complexity, l_entropy played a role in ASD delineation in the central, temporal and occipital areas in the theta frequency; and, lastly, l_max was another brain

invariant that accurately distinguished the two groups, mainly in the frontal and central areas in the theta band and in the parietal region in the alpha frequency.

5.9. Recommendations for Future Research

Most of the findings of this study are supported by previous evidence or could be associated or explained by previous studies or theories. However, certain results are not grounded in past evidence or cannot be correlated with other measures because the variables used in this study have not been tested before to identify their utility in ASD delineation in different frequency bands and scalp locations. Using this study as pilot evidence of potential high utility of these variables paired with specific electrodes and frequencies, further research should prioritise the search for neural correlates of these measures. Moreover, building on these findings, further research should use these measures on large samples in order to approach a generalisation and turn these findings into biomarkers of ASD. Not only should these variables be further tested, but also combinations of these variables should be investigated as pairs could yield higher accuracy in ASD delineation. Not understanding what these variables mean at a neurological, cognitive or behavioural level also implies that the way they interact or complement each other is unknown and should be explored. Additionally, based on the systematic review presented and certain evidence that supports the results, further research should attempt to combine several methods of EEG analysis, particularly functional connectivity and complexity measures, for a better characterisation of ASD and higher chances of identifying a biomarker. New, more advanced methods of analysis, such as the ones presented in the Limitations, should be used. Machine learning has become an invaluable tool in clinical research and the search for a new tool for ASD delineation could benefit from its power of classification. Lastly, several aspects have to be considered when designing new studies. These include the age of the participants, as the motivation of this field of research is to also lower the age of diagnosis, the medical history of the patients, as several conditions could interfere with the interpretation of

the EEG signals, and the sample size of the cohort, with larger sample sizes producing more reliable results.

6. Conclusion

The aim of this study was to use complexity measures and RQA to analyse EEG signals in order to identify quantifiable neural correlates associated with an ASD diagnosis, to distinguish ASD from non-ASD individuals. Both hypotheses investigated were confirmed. This study combined EEG measurements with sophisticated signal processing methods to identify non-linear measures that correlate with ASD and could be used for ASD identification. Building on these preliminary findings, using this technology could reveal evidence that can be used as a much sought after biomarker for early detection of ASD. An accurate biomarker that can lower the age of diagnosis will have tremendous impact on the practice of early screening and diagnosis.

7. References

Ahmadlou, M., H. Adeli and A. Adeli (2010). "Fractality and a wavelet-chaos-neural network methodology for EEG-based diagnosis of autistic spectrum disorder." Journal of Clinical Neurophysiology **27**(5): 328-333.

Ahmadlou, M., H. Adeli and A. Adeli (2012). "Fuzzy Synchronization Likelihood-wavelet methodology for diagnosis of autism spectrum disorder." Journal of Neuroscience Methods **211**(2): 203-209.

Al-Fahoum, A. S. and A. A. Al-Fraihat (2014). "Methods of EEG signal features extraction using linear analysis in frequency and time-frequency domains." ISRN neuroscience **2014**.

American Psychiatric Association (1994). Diagnostic and statistical manual of mental disorders : DSM-4. Washington, DC, American Psychiatric Publishing.

American Psychiatric Association (2013). Diagnostic and statistical manual of mental disorders : DSM-5. Washington, DC, American Psychiatric Publishing.

Asperger, H. (1944). "Die „Autistischen Psychopathen" im Kindesalter." Archiv für Psychiatrie und Nervenkrankheiten **117**(1): 76-136.

Assaf, M., K. Jagannathan, V. D. Calhoun, L. Miller, M. C. Stevens, R. Sahl, J. G. O'Boyle, R. T. Schultz and G. D. Pearlson (2010). "Abnormal functional connectivity of default mode sub-networks in autism spectrum disorder patients." NeuroImage **53**(1): 247-256.

Baio, J. (2012). "Prevalence of Autism Spectrum Disorders: Autism and Developmental Disabilities Monitoring Network, 14 Sites, United States, 2008. Morbidity and Mortality Weekly Report. Surveillance Summaries. Volume 61, Number 3." Centers for Disease Control and Prevention.

Baron-Cohen, S. (1997). Mindblindness: An essay on autism and theory of mind, MIT press.

Baron-Cohen, S. (2000). "Theory of mind and autism: A fifteen year review."

Baron-Cohen, S., A. M. Leslie and U. Frith (1985). "Does the autistic child have a "theory of mind" ?" Cognition **21**(1): 37-46.

Barttfeld, P., L. Amoruso, J. Ais, S. Cukier, L. Bavassi, A. Tomio, F. Manes, A. Ibanez and M. Sigman (2013). "Organization of brain networks governed by long-range connections index autistic traits in the general population." Journal of neurodevelopmental disorders **5**(1): 16.

Behne, T., M. Carpenter, J. Call and M. Tomasello (2005). "Unwilling versus unable: infants' understanding of intentional action." Developmental psychology **41**(2): 328.

Belmonte, M. K., G. Allen, A. Beckel-Mitchener, L. M. Boulanger, R. A. Carper and S. J. Webb (2004). "Autism and abnormal development of brain connectivity." J Neurosci **24**(42): 9228-9231.

Billeci, L., F. Sicca, K. Maharatna, F. Apicella, A. Narzisi, G. Campatelli, S. Calderoni, G. Pioggia and F. Muratori (2013). "On the application of quantitative EEG for characterizing autistic brain: a systematic review."

Binnie, C. D., A. J. Rowan and T. Gutter (1982). A manual of electroencephalographic technology, CUP Archive.

Boersma, M., C. Kemner, M. A. de Reus, G. Collin, T. M. Snijders, D. Hofman, J. K. Buitelaar, C. J. Stam and M. P. van den Heuvel (2013). "Disrupted functional brain networks in autistic toddlers." Brain connectivity **3**(1): 41-49.

Bosl, W. (2016). EEG-Derived Neurophenotypes. Neurophenotypes, Springer**:** 263-282.

Bosl, W., A. Tierney, H. Tager-Flusberg and C. Nelson (2011). "EEG complexity as a biomarker for autism spectrum disorder risk." BMC medicine **9**(1): 18.

Bosl, W. J., T. Loddenkemper and C. A. Nelson (2017). "Nonlinear EEG biomarker profiles for autism and absence epilepsy." Neuropsychiatric Electrophysiology **3**(1): 1.

Bosl, W. J., H. Tager-Flusberg and C. A. Nelson (2011). "EEG Complexity as a Biomarker for Autism Spectrum Disorder." BMC Medicine **9**(18).

Boutros, N. N., R. Lajiness-O'Neill, A. Zillgitt, A. E. Richard and S. M. Bowyer (2015). "EEG changes associated with autistic spectrum disorders." Neuropsychiatric Electrophysiology **1**(1): 3.

Buckley, A. W., R. Scott, A. Tyler, J. M. Mahoney, A. Thurm, C. Farmer, S. Swedo, S. A. Burroughs and G. L. Holmes (2015). "State-Dependent Differences in Functional Connectivity in Young Children With Autism Spectrum Disorder." EBioMedicine **2**(12): 1905-1915.
Cantor, D. S., R. W. Thatcher, M. Hrybyk and H. Kaye (1986). "Computerized EEG analyses of autistic children." Journal of autism and developmental disorders **16**(2): 169-187.
Carson, A. M., N. M. Salowitz, R. A. Scheidt, B. K. Dolan and A. V. Van Hecke (2014). "Electroencephalogram coherence in children with and without autism spectrum disorders: decreased interhemispheric connectivity in autism." Autism Research **7**(3): 334-343.
Casanova, M. F. (2006). "Neuropathological and genetic findings in autism: the significance of a putative minicolumnopathy." Neuroscientist **12**(5): 435-441.
Catarino, A., A. Andrade, O. Churches, A. P. Wagner, S. Baron-Cohen and H. Ring (2013). "Task-related functional connectivity in autism spectrum conditions: an EEG study using wavelet transform coherence." Molecular autism **4**(1): 1.
Catarino, A., O. Churches, S. Baron-Cohen, A. Andrade and H. Ring (2011). "Atypical EEG complexity in autism spectrum conditions: a multiscale entropy analysis." Clinical Neurophysiology **122**(12): 2375-2383.
Chan, A. S., Y. M. Han, S. L. Sze, M.-c. Cheung, W. W.-m. Leung, R. C. Chan and C. Y. To (2011). "Disordered connectivity associated with memory deficits in children with autism spectrum disorders." Research in Autism Spectrum Disorders **5**(1): 237-245.
Chan, A. S. and W. W. Leung (2006). "Differentiating autistic children with quantitative encephalography: A 3-month longitudinal study." Journal of child neurology **21**(5): 391-399.
Chan, A. S., S. L. Sze and M.-c. Cheung (2007). "Quantitative electroencephalographic profiles for children with autistic spectrum disorder." Neuropsychology **21**(1): 74.
Charman, T., E. Taylor, A. Drew, H. Cockerill, J.-A. Brown and G. Baird (2005). "Outcome at 7 years of children diagnosed with autism at age 2: predictive validity of assessments conducted at 2 and 3 years of age and pattern of symptom change over time." Journal of Child Psychology and Psychiatry **46**(5): 500-513.
Coben, R., A. R. Clarke, W. Hudspeth and R. J. Barry (2008). "EEG power and coherence in autistic spectrum disorder." Clinical Neurophysiology **119**(5): 1002-1009.
Coben, R. and T. E. Myers (2008). "Connectivity theory of autism: Use of connectivity measures in assessing and treating autistic disorders." Journal of Neurotherapy **12**(2-3): 161-179.
Collura, T. F. (1996). Neocortical Dynamics and Human EEG Rhythms, LWW.
Costa, M., A. Goldberger and C.-K. Peng (2002). Multiscale entropy to distinguish physiologic and synthetic RR time series. Computers in Cardiology, 2002, IEEE.
Costa, M., A. L. Goldberger and C.-K. Peng (2005). "Multiscale entropy analysis of biological signals." Physical review E **71**(2): 021906.
Courchesne, E., R. Carper and N. Akshoomoff (2003). "Evidence of brain overgrowth in the first year of life in autism." JAMA **290**(3): 337-344.
Courchesne, E., C. M. Karns, H. R. Davis, R. Ziccardi, R. A. Carper, Z. D. Tigue, H. J. Chisum, P. Moses, K. Pierce, C. Lord, A. J. Lincoln, S. Pizzo, L. Schreibman, R. H. Haas, N. A. Akshoomoff and R. Y. Courchesne (2001). "Unusual brain growth patterns in early life in patients with autistic disorder: an MRI study." Neurology **57**(2): 245-254.
Critchley, H. D., E. M. Daly, E. T. Bullmore, S. C. R. Williams, T. Van Amelsvoort, D. M. Robertson, A. Rowe, M. Phillips, G. McAlonan, P. Howlin and D. G. M. Murphy (2000). "The functional neuroanatomy of social behaviourChanges in cerebral blood flow when people with autistic disorder process facial expressions." Brain **123**(11): 2203-2212.
Daoust, A.-M., É. Limoges, C. Bolduc, L. Mottron and R. Godbout (2004). "EEG spectral analysis of wakefulness and REM sleep in high functioning autistic spectrum disorders." Clinical Neurophysiology **115**(6): 1368-1373.

Dawson, G., L. G. Klinger, H. Panagiotides, A. Lewy and P. Castelloe (1995). "Subgroups of autistic children based on social behavior display distinct patterns of brain activity." Journal of Abnormal Child Psychology **23**(5): 569-583.
Dawson, G., S. Rogers, J. Munson, M. Smith, J. Winter, J. Greenson, A. Donaldson and J. Varley (2010). "Randomized, Controlled Trial of an Intervention for Toddlers With Autism: The Early Start Denver Model." Pediatrics **125**(1): e17-e23.
Eckmann, J.-P., S. O. Kamphorst and D. Ruelle (1987). "Recurrence plots of dynamical systems." EPL (Europhysics Letters) **4**(9): 973.
Eldridge, J., A. E. Lane, M. Belkin and S. Dennis (2014). "Robust features for the automatic identification of autism spectrum disorder in children." Journal of neurodevelopmental disorders **6**(1): 12.
Elhabashy, H., O. Raafat, L. Afifi, H. Raafat and K. Abdullah (2015). "Quantitative EEG in autistic children." The Egyptian Journal of Neurology, Psychiatry and Neurosurgery **52**(3): 176.
Falkmer, T., K. Anderson, M. Falkmer and C. Horlin (2013). "Diagnostic procedures in autism spectrum disorders: a systematic literature review." European child & adolescent psychiatry **22**(6): 329-340.
Fletcher, R. J., E. Loschen and C. Stavrakaki (2007). A textbook of diagnosis of mental disorders in persons with intellectual disability, Kingston (New York): National Association for the Dually Diagnosed Press.
Frith, U. (1989). Autism: Explaining the enigma, Wiley Online Library.
Gasser, T., R. Verleger, P. Bächer and L. Sroka (1988). "Development of the EEG of school-age children and adolescents. I. Analysis of band power." Electroencephalography and clinical neurophysiology **69**(2): 91-99.
Ghanbari, Y., L. Bloy, J. C. Edgar, L. Blaskey, R. Verma and T. P. L. Roberts (2015). "Joint Analysis of Band-Specific Functional Connectivity and Signal Complexity in Autism." J Autism Dev Disord **45**(2): 444-460.
Gilchrist, A., J. Green, A. Cox, D. Burton, M. Rutter and A. L. Couteur (2001). "Development and Current Functioning in Adolescents with Asperger Syndrome: A Comparative Study." Journal of Child Psychology and Psychiatry **42**(2): 227-240.
Goldberger, A. L. (1997). "Fractal variability versus pathologic periodicity: complexity loss and stereotypy in disease." Perspect Biol Med **40**(4): 543-561.
Gomez, C. and R. Hornero (2010). "Entropy and Complexity Analyses in Alzheimer's Disease: An MEG Study." Open Biomed Eng J **4**: 223-235.
Gregory, M. D. and D. E. Mandelbaum (2012). "Evidence of a faster posterior dominant EEG rhythm in children with autism." Research in Autism Spectrum Disorders **6**(3): 1000-1003.
Gurau, O., W. J. Bosl and C. R. Newton (2017). "How Useful Is Electroencephalography in the Diagnosis of Autism Spectrum Disorders and the Delineation of Subtypes: A Systematic Review." Frontiers in Psychiatry **8**(121).
Herbert, M. R., D. A. Ziegler, N. Makris, P. A. Filipek, T. L. Kemper, J. J. Normandin, H. A. Sanders, D. N. Kennedy and V. S. Caviness (2004). "Localization of white matter volume increase in autism and developmental language disorder." Annals of neurology **55**(4): 530-540.
Hirata, Y. and K. Aihara (2011). "Statistical Tests for Serial Dependence and Laminarity on Recurrence Plots." International Journal of Bifurcation and Chaos: 1077-1084.
Jasper, H. (1958). "Report of the committee on methods of clinical examination in electroencephalography." Electroencephalogr Clin Neurophysiol **10**: 370-375.
Juarrero, A. (2012). Complex dynamical systems theory. The Cognitive Edge.
Juneja, M., D. Mishra, P. S. S. Russell, S. Gulati, V. Deshmukh, P. Tudu, R. Sagar, D. Silberberg, V. K. Bhutani, J. M. Pinto, M. Durkin, R. M. Pandey, M. Nair and N. K. Arora (2014). "INCLEN diagnostic tool for autism spectrum disorder (INDT-ASD): Development and validation." Indian Pediatrics **51**(5): 359-365.

Just, M. A., T. A. Keller, V. L. Malave, R. K. Kana and S. Varma (2012). "Autism as a neural systems disorder: a theory of frontal-posterior underconnectivity." Neuroscience & Biobehavioral Reviews **36**(4): 1292-1313.
Kandel, E. R., J. H. Schwartz, T. M. Jessell, S. A. Siegelbaum and A. J. Hudspeth (2000). Principles of neural science, McGraw-hill New York.
Kanner, L. (1943). "Autistic disturbances of affective contact. The Nervous Child, 2, 217–250." Google Scholar.
Kello, C. T., J. Rodny, A. S. Warlaumont and D. C. Noelle (2012). "Plasticity, learning, and complexity in spiking networks." Critical Reviews™ in Biomedical Engineering **40**(6).
Komalapriya, C., M. Thiel, M. Romano, N. Marwan, U. Schwarz and J. Kurths (2008). "Reconstruction of a system's dynamics from short trajectories." Physical Review E **78**(6): 066217.
Kopell, N., G. B. Ermentrout, M. A. Whittington and R. D. Traub (2000). "Gamma rhythms and beta rhythms have different synchronization properties." Proc Natl Acad Sci U S A **97**(4): 1867-1872.
Krumm, N., T. N. Turner, C. Baker, L. Vives, K. Mohajeri, K. Witherspoon, A. Raja, B. P. Coe, H. A. Stessman, Z.-X. He, S. M. Leal, R. Bernier and E. E. Eichler (2015). "Excess of rare, inherited truncating mutations in autism." Nat Genet **47**(6): 582-588.
Lazarev, V. V., A. Pontes and A. A. Mitrofanov (2015). "Reduced interhemispheric connectivity in childhood autism detected by electroencephalographic photic driving coherence." Journal of autism and developmental disorders **45**(2): 537-547.
Le Couteur, A. (2003). National Autism Plan for Children (NAPC): Plan for the Identification, Assessment, Diagnosis and Access to Early Interventions for Pre-school and Primary School Aged Children with Autsim Spectrum Disorders, National Autistic Society.
Léveillé, C., E. B. Barbeau, C. Bolduc, É. Limoges, C. Berthiaume, É. Chevrier, L. Mottron and R. Godbout (2010). "Enhanced connectivity between visual cortex and other regions of the brain in autism: a REM sleep EEG coherence study." Autism Research **3**(5): 280-285.
Lippé, S., N. Kovacevic and A. R. McIntosh (2009). "Differential maturation of brain signal complexity in the human auditory and visual system." Frontiers in Human Neuroscience **3**.
Lord, C., S. Risi, P. S. DiLavore, C. Shulman, A. Thurm and A. Pickles (2006). "Autism from 2 to 9 years of age." Archives of General Psychiatry **63**(6): 694-701.
Lotter, V. (1966). "Epidemiology of autistic conditions in young children." Social psychiatry **1**(3): 124-135.
Lushchekina, E., E. Podreznaya, V. Lushchekin, V. Y. Novototskii-Vlasov and V. Strelets (2014). "Comparative Studies of EEG Theta and Gamma Rhythms in Normal Children and Children with Early Childhood Autism." Neuroscience and Behavioral Physiology **44**(8): 902-908.
Lushchekina, E., E. Podreznaya, V. Lushchekin and V. Strelets (2012). "A comparative EEG study in normal and autistic children." Neuroscience and Behavioral Physiology **42**(3): 236-243.
Machado, C., M. Estévez, G. Leisman, R. Melillo, R. Rodríguez, P. DeFina, A. Hernández, J. Pérez-Nellar, R. Naranjo and M. Chinchilla (2015). "QEEG spectral and coherence assessment of autistic children in three different experimental conditions." Journal of autism and developmental disorders **45**(2): 406-424.
Marosi, E., T. Harmony, L. Sánchez, J. Becker, J. Bernal, A. Reyes, A. E. D. de León, M. Rodríguez and T. Fernández (1992). "Maturation of the coherence of EEG activity in normal and learning-disabled children." Electroencephalography and clinical Neurophysiology **83**(6): 350-357.
Marwan, N., M. C. Romano, M. Thiel and J. Kurths (2007). "Recurrence plots for the analysis of complex systems." Physics reports **438**(5): 237-329.
Mathewson, K. J., M. K. Jetha, I. E. Drmic, S. E. Bryson, J. O. Goldberg and L. A. Schmidt (2012). "Regional EEG alpha power, coherence, and behavioral symptomatology in autism spectrum disorder." Clinical Neurophysiology **123**(9): 1798-1809.
Matlis, S., K. Boric, C. J. Chu and M. A. Kramer (2015). "Robust disruptions in electroencephalogram cortical oscillations and large-scale functional networks in autism." BMC neurology **15**(1): 97.

Maxwell, C. R., M. E. Villalobos, R. T. Schultz, B. Herpertz-Dahlmann, K. Konrad and G. Kohls (2015). "Atypical laterality of resting gamma oscillations in autism spectrum disorders." Journal of Autism and Developmental Disorders **45**(2): 292-297.
Motter, A. E. and R. Albert (2012). "Networks in motion." Physics Today **65**(4): 43-48.
Murias, M., S. J. Webb, J. Greenson and G. Dawson (2007). "Resting state cortical connectivity reflected in EEG coherence in individuals with autism." Biological psychiatry **62**(3): 270-273.
Nelson, C. A. (2016). "Introduction to special issue on The Role of Connectivity in Developmental Disorders: Genetic and Neural Network Approaches." Developmental Science **19**(4): 523-523.
Ngamga, E. J., S. Bialonski, N. Marwan, J. Kurths, C. Geier and K. Lehnertz (2016). "Evaluation of selected recurrence measures in discriminating pre-ictal and inter-ictal periods from epileptic EEG data." Physics Letters A **380**(16): 1419-1425.
Noonan, S. K., F. Haist and R.-A. Müller (2009). "Aberrant functional connectivity in autism: evidence from low-frequency BOLD signal fluctuations." Brain research **1262**: 48-63.
Okazaki, R., T. Takahashi, K. Ueno, K. Takahashi, M. Ishitobi, M. Kikuchi, M. Higashima and Y. Wada (2015). "Changes in EEG complexity with electroconvulsive therapy in a patient with autism spectrum disorders: a multiscale entropy approach." Frontiers in human neuroscience **9**.
Orekhova, E. V., M. Elsabbagh, E. J. Jones, G. Dawson, T. Charman and M. H. Johnson (2014). "EEG hyper-connectivity in high-risk infants is associated with later autism." Journal of neurodevelopmental disorders **6**(1): 40.
Orekhova, E. V., T. A. Stroganova, G. Nygren, M. M. Tsetlin, I. N. Posikera, C. Gillberg and M. Elam (2007). "Excess of high frequency electroencephalogram oscillations in boys with autism." Biological psychiatry **62**(9): 1022-1029.
Pantev, C., S. Makeig, M. Hoke, R. Galambos, S. Hampson and C. Gallen (1991). "Human auditory evoked gamma-band magnetic fields." Proc Natl Acad Sci U S A **88**(20): 8996-9000.
Peng, C.-K., M. Costa and A. L. Goldberger (2009). "Adaptive Data Analysis of Complex Fluctuations in Physiologic Time Series." Advances in Adaptive Data Analysis **1**(1): 61-70.
Persico, A. M. and T. Bourgeron (2006). "Searching for ways out of the autism maze: genetic, epigenetic and environmental clues." Trends in Neurosciences **29**(7): 349-358.
Peter Szatmari, A. D. P., Lonnie Zwaigenbaum, Wendy Roberts et al. (2007). "Mapping autism risk loci using genetic linkage and chromosomal rearrangements." Nat Genet **39**(3): 319-328.
Pierce, K., R. A. Müller, J. Ambrose, G. Allen and E. Courchesne (2001). "Face processing occurs outside the fusiform `face area' in autism: evidence from functional MRI." Brain **124**(10): 2059-2073.
Pikovsky, A., M. Rosenblum and J. Kurths (2003). Synchronization: a universal concept in nonlinear sciences, Cambridge university press.
Rapp, P. E., D. O. Keyser, A. Albano, R. Hernandez, D. B. Gibson, R. A. Zambon, W. D. Hairston, J. D. Hughes, A. Krystal and A. S. Nichols (2015). "Traumatic brain injury detection using electrophysiological methods." Frontiers in human neuroscience **9**: 11.
Righi, G., A. L. Tierney, H. Tager-Flusberg and C. A. Nelson (2014). "Functional connectivity in the first year of life in infants at risk for autism spectrum disorder: An EEG study." PLoS ONE **9** (8).
Rigotti, M., O. Barak, M. R. Warden, X.-J. Wang, N. D. Daw, E. K. Miller and S. Fusi (2013). "The importance of mixed selectivity in complex cognitive tasks." Nature **497**(7451): 585-590.
Ritvo, E. R., L. B. Jorde, A. Mason-Brothers, B. Freeman and C. Pingree (1989). "The UCLA-University of Utah epidemiological survey of autism: Recurrence risk estimates and genetic counseling." The American journal of psychiatry **146**(8): 1032.
Rivera-Gaxiola, M., J. Silva-Pereyra and P. K. Kuhl (2005). "Brain potentials to native and non-native speech contrasts in 7-and 11-month-old American infants." Developmental science **8**(2): 162-172.
Rogers, S. J. (1996). "Brief report: Early intervention in autism." Journal of autism and developmental disorders **26**(2): 243-246.
Roth, I. and P. Rezaie (2011). Researching the autism spectrum : contemporary perspectives. Cambridge, Cambridge University Press.

Sakkalis, V., V. Tsiaras, K. Michalopoulos and M. Zervakis (2008). Assessment of neural dynamic coupling and causal interactions between independent EEG components from cognitive tasks using linear and nonlinear methods. Engineering in Medicine and Biology Society, 2008. EMBS 2008. 30th Annual International Conference of the IEEE, IEEE.
Santosh, P. J., W. P. L. Mandy, K. Puura, M. Kaartinen, R. Warrington and D. H. Skuse (2009). "The construction and validation of a short form of the developmental, diagnostic and dimensional interview." European Child & Adolescent Psychiatry **18**(8): 521-524.
Sato, J. R., M. Vidal, S. de Siqueira Santos, K. B. Massirer and A. Fujita (2015). "Complex network measures in Autism Spectrum Disorders." IEEE/ACM transactions on computational biology and bioinformatics.
Sato, J. R., M. Vidal, S. d. S. Santos, K. B. Massirer and A. Fujita (2017). "Complex network measures in Autism Spectrum Disorders." IEEE/ACM Transactions on Computational Biology and Bioinformatics **PP**(99): 1-1.
Schinkel, S., N. Marwan and J. Kurths (2007). "Order patterns recurrence plots in the analysis of ERP data." Cognitive neurodynamics **1**(4): 317-325.
Schinkel, S., N. Marwan and J. Kurths (2009). "Brain signal analysis based on recurrences." Journal of Physiology-Paris **103**(6): 315-323.
Schinkel, S., N. Marwan and J. Kurths (2009). "Brain signal analysis based on recurrences." J Physiol Paris **103**(6): 315-323.
Schultz, R. T., I. Gauthier, A. Klin and et al. (2000). "Abnormal ventral temporal cortical activity during face discrimination among individuals with autism and asperger syndrome." Archives of General Psychiatry **57**(4): 331-340.
Scope, A., O. Pascalis, D. Buckley and S. Makeig (2009). "Independent Component Analysis Reveals Atypical Electroencephalographic Activity During Visual Perception in Individuals with Autism." Biological Psychiatry **65**(1): 22-30.
Shafritz, K. M., G. S. Dichter, G. T. Baranek and A. Belger (2008). "The Neural Circuitry Mediating Shifts in Behavioral Response and Cognitive Set in Autism." Biological Psychiatry **63**(10): 974-980.
Shah, A. and U. Frith (1983). "An islet of ability in autistic children: A research note." Journal of child Psychology and Psychiatry **24**(4): 613-620.
Sheikhani, A., H. Behnam, M. Noroozian, M. R. Mohammadi and M. Mohammadi (2009). "Abnormalities of quantitative electroencephalography in children with Asperger disorder in various conditions." Research in Autism Spectrum Disorders **3**(2): 538-546.
Simonoff, E., A. Pickles, T. Charman, S. Chandler, T. Loucas and G. Baird "Psychiatric Disorders in Children With Autism Spectrum Disorders: Prevalence, Comorbidity, and Associated Factors in a Population-Derived Sample." Journal of the American Academy of Child & Adolescent Psychiatry **47**(8): 921-929.
Skuse, D., R. Warrington, D. Bishop, U. Chowdhury, J. Lau, W. Mandy and M. Place (2004). "The developmental, dimensional and diagnostic interview (3di): a novel computerized assessment for autism spectrum disorders." Journal of the American Academy of Child & Adolescent Psychiatry **43**(5): 548-558.
Slappendel, G., W. Mandy, J. van der Ende, F. C. Verhulst, A. van der Sijde, J. Duvekot, D. Skuse and K. Greaves-Lord (2016). "Utility of the 3Di short version for the diagnostic assessment of autism spectrum disorder and compatibility with DSM-5." Journal of autism and developmental disorders **46**(5): 1834-1846.
Srinivasan, R. (2005). "High-resolution EEG: theory and practice." Event-related potentials: A methods handbook: 167-188.
Stroganova, T. A., G. Nygren, M. M. Tsetlin, I. N. Posikera, C. Gillberg, M. Elam and E. V. Orekhova (2007). "Abnormal EEG lateralization in boys with autism." Clinical Neurophysiology **118**(8): 1842-1854.
Struzik, Z. R. and A. Siebes (1999). The Haar Wavelet Transform in the Time Series Similarity Paradigm. Principles of Data Mining and Knowledge Discovery: Third European Conference, PKDD'99, Prague,

Czech Republic, September 15-18, 1999. Proceedings. J. M. Żytkow and J. Rauch. Berlin, Heidelberg, Springer Berlin Heidelberg**:** 12-22.
Tager-Flusberg, H. (2007). "Evaluating the theory-of-mind hypothesis of autism." Current directions in psychological science **16**(6): 311-315.
Takahashi, T. (2013). "Complexity of spontaneous brain activity in mental disorders." Progress in Neuro-Psychopharmacology and Biological Psychiatry **45**: 258-266.
Tani, P., N. Lindberg, T. Nieminen-von Wendt, L. von Wendt, J. Virkkala, B. Appelberg, o. rn and T. Porkka-Heiskanen (2004). "Sleep in young adults with Asperger syndrome." Neuropsychobiology **50**(2): 147-152.
Tuchman, R. and I. Rapin (2002). "Epilepsy in autism." The Lancet Neurology **1**(6): 352-358.
Turner, L. M., W. L. Stone, S. L. Pozdol and E. E. Coonrod (2006). "Follow-up of children with autism spectrum disorders from age 2 to age 9." Autism **10**(3): 243-265.
van Diessen, E., J. Senders, F. E. Jansen, M. Boersma and H. Bruining (2015). "Increased power of resting-state gamma oscillations in autism spectrum disorder detected by routine electroencephalography." European archives of psychiatry and clinical neuroscience **265**(6): 537-540.
Webber Jr, C. L. and N. Marwan (2015). Mathematical and computational foundations of recurrence quantifications. Recurrence Quantification Analysis, Springer**:** 3-43.
Webber Jr, C. L. and J. P. Zbilut (2005). "Recurrence quantification analysis of nonlinear dynamical systems." Tutorials in contemporary nonlinear methods for the behavioral sciences: 26-94.
Wen, D., Y. Zhou and X. Li (2015). "A critical review: coupling and synchronization analysis methods of EEG signal with mild cognitive impairment." Frontiers in aging neuroscience **7**: 54.
Wing, L. and J. Gould (1979). "Severe impairments of social interaction and associated abnormalities in children: Epidemiology and classification." Journal of autism and developmental disorders **9**(1): 11-29.
Yang, H. H., A. N. Savostyanov, A. C. Tsai and M. Liou (2011). "Face recognition in Asperger syndrome: a study on EEG spectral power changes." Neuroscience letters **492**(2): 84-88.
Zbilut, J. P., N. Thomasson and C. L. Webber (2002). "Recurrence quantification analysis as a tool for nonlinear exploration of nonstationary cardiac signals." Medical engineering & physics **24**(1): 53-60.

8. Appendix

Table A: Results for recurrence rate of binary logistic regression with a dichotomous outcome and six predictor variables for: Kenyan cohort: overall model fit: chi^2= 8.390, p=0.211; additional fit statistics: Cox&Snell R^2=0.317, Nagelkerke R^2=0.423; linearity fit: R^2 p=0.632 (Hosmer-Lemeshow); classification sensitivity=81.8%, specificity=72.7%, accuracy=77.3%; NDAR cohort: overall model fit: chi^2= 6.315 p=0.389; additional fit statistics: Cox&Snell R^2=0.121, Nagelkerke R^2=0.161; Linearity fit: R^2 p=0.070 (Hosmer-Lemeshow); classification sensitivity=47.8%, specificity=69.2%, accuracy=59.2%.

Variable	Cohort	Frequency	b	Wald statistic	p-value (df=1)	95% CI for Odds ratio		
						Lower	Odds ratio(ExpB)	Upper
Recurrence rate	**Kenyan**	Delta	457.678	0.306	0.580	0.000	5.847e+198	
		Theta	-183.432	0.082	0.775	0.000	2.1703e-80	
		Alpha	-59.540	0.443	0.506	9.8324e-103	1.3867e-26	1.956e+50
		Beta	-4.329	1.034	0.309	0.000003	0.013	55.345
		Gamma	-0.641	0.004	0.948	1.9747e-9	0.527	140407644.342
		High gamma	-25.335	0.330	0.566	2.852e-49	9.9306e-12	3.458e+26
	NDAR	Delta	-39.966	0.598	0.439	4.4068e-62	4.3951e-18	4.383e+26
		Theta	4.836	0.498	0.480	0.000186	126.020	85569253.759
		Alpha	0.453	0.019	0.891	0.002	1.573	1041.257
		Beta	3.317	1.301	0.254	0.092	27.568	8227.499
		Gamma	-4.136	1.383	0.240	0.000016	0.016	15.745
		High gamma	0.309	0.014	0.906	0.008	1.361	231.531

Table B: Results for determinism of binary logistic regression with a dichotomous outcome and six predictor variables for: Kenyan cohort: overall model fit: chi^2=4.485, p=0.611; additional fit statistics: Cox&Snell R^2=0.184, Nagelkerke R^2=0.246; linearity fit: R^2 p=0.229 (Hosmer-Lemeshow); classification sensitivity=63.3%, specificity=63.3%, accuracy=63.3%; NDAR cohort: overall model fit: chi^2=7.212 p=0.302; additional fit statistics: Cox&Snell R^2=0.137, Nagelkerke R^2=0.183; Linearity fit: R^2 p=0.632 (Hosmer-Lemeshow); classification sensitivity=56.5%, specificity=76.9%, accuracy=67.3%.

Variable	Cohort	Frequency	b	Wald statistic	p-value (df=1)	95% CI for Odds ratio		
						Lower	Odds ratio(ExpB)	Upper
Determinism	**Kenyan**	Delta	1.446	0.004	0.947	1.2105e-18	4.245	1.488e+19
		Theta	-12.563	0.549	0.459	1.2877e-20	0.000003	950294822.184
		Alpha	7.850	0.717	0.397	0.000033	2566.213	1.994e+11
		Beta	-2.933	0.569	0.451	0.000026	0.053	108.465
		Gamma	-3.795	0.265	0.607	1.1823e-8	0.022	42776.493
		High gamma	-14.524	0.022	0.882	5.0021e-90	4.9258e-7	4.851e+76
	NDAR	Delta	2.389	0.629	0.428	0.030	10.901	3983.967
		Theta	-0.363	0.003	0.956	0.000002	0.695	318530.563
		Alpha	2.438	0.292	0.589	0.002	11.452	79576.529
		Beta	0.734	0.035	0.852	0.001	2.084	4557.661
		Gamma	-2.712	0.402	0.526	0.000015	0.066	290.491
		High gamma	-4.215	1.139	0.286	0.000006	0.015	33.969

Table C: Results for laminarity of binary logistic regression with a dichotomous outcome and six predictor variables for: Kenyan cohort: overall model fit: chi^2=8.779, p=0.186; additional fit statistics: Cox&Snell R^2=0.329, Nagelkerke R^2=0.439; linearity fit: R^2 p=0.432 (Hosmer-Lemeshow); classification sensitivity=72.7%, specificity=81.8%, accuracy=77.3%; NDAR cohort: overall model fit: chi^2=3.934 p=0.686; additional fit statistics: Cox&Snell R^2=0.077, Nagelkerke R^2=0.103; Linearity fit: R^2 p=0.258 (Hosmer-Lemeshow); classification sensitivity=30.4%, specificity=76.9%, accuracy=55.1%.

Variable	Cohort	Frequency	b	Wald statistic	p-value (df=1)	95% CI for Odds ratio		
						Lower	Odds ratio(ExpB)	Upper
Laminarity	**Kenyan**	Delta	8.898	0.127	0.722	3.7098e-18	7317.654	1.443e+25
		Theta	-26.438	1.882	0.170	1.3013e-28	3.2978e-12	83573.772
		Alpha	12.366	1.893	0.169	0.005	234769.455	1.051e+13
		Beta	-3.103	0.448	0.503	0.000005	0.045	398.257
		Gamma	-3.429	0.194	0.659	7.7776e-9	0.032	135067.503
		High gamma	-52.189	1.237	0.266	2.4625e-63	2.1605e-23	1.895e+17
	NDAR	Delta	-0.189	0.003	0.960	0.001	0.827	1341.407
		Theta	3.876	0.305	0.581	0.000051	48.245	45485204.434
		Alpha	2.755	0.491	0.484	0.007	15.728	35080.531
		Beta	-2.291	0.692	0.405	0.000459	0.101	22.319
		Gamma	1.362	0.552	0.458	0.107	3.904	142.019
		High gamma	-1.640	0.825	0.364	0.006	0.194	6.684

Table D: Results for l_max of binary logistic regression with a dichotomous outcome and six predictor variables for: Kenyan cohort: overall model fit: chi^2=6.136, p=0.408; additional fit statistics: Cox&Snell R^2=0.243, Nagelkerke R^2=0.325; linearity fit: R^2 p=0.649 (Hosmer-Lemeshow); classification sensitivity=63.6%, specificity=72.7%, accuracy=68.2%; NDAR cohort: overall model fit: chi^2=5.088 p=0.533; additional fit statistics: Cox&Snell R^2=0.099, Nagelkerke R^2=0.132; Linearity fit: R^2 p=0.685 (Hosmer-Lemeshow); classification sensitivity=52.2%, specificity=69.2%, accuracy=61.2%.

Variable	Cohort	Frequency	b	Wald statistic	p-value (df=1)	95% CI for Odds ratio		
						Lower	Odds ratio(ExpB)	Upper
L_max	**Kenyan**	Delta	5.751	0.272	0.602	1.3189e-7	314.427	7.496e+11
		Theta	-2.645	0.547	0.459	0.000064	0.071	78.443
		Alpha	0.246	0.025	0.874	0.061	1.278	26.671
		Beta	0.176	0.012	0.911	0.054	1.193	26.549
		Gamma	-1.423	1.631	0.202	0.027	0.241	2.139
		High gamma	0.362	0.103	0.748	0.158	1.437	13.091
	NDAR	Delta	0.020	0.083	0.773	0.892	1.020	1.165
		Theta	0.003	0.006	0.940	0.934	1.003	1.077
		Alpha	0.006	0.262	0.609	0.982	1.006	1.031
		Beta	0.001	0.045	0.832	0.990	1.001	1.013
		Gamma	-0.002	0.123	0.726	0.990	0.998	1.007
		High gamma	-0.001	0.272	0.602	0.997	0.999	1.002

Table E: Results for l_mean of binary logistic regression with a dichotomous outcome and six predictor variables for: Kenyan cohort: overall model fit: chi^2=8.874, p=0.181; additional fit statistics: Cox&Snell R^2=0.332, Nagelkerke R^2=0.443; linearity fit: R^2 p=0.241 (Hosmer-Lemeshow); classification sensitivity=72.7%, specificity=72.7%, accuracy=72.7%; NDAR cohort: overall model fit: chi^2=4.305 p=0.636; additional fit statistics: Cox&Snell R^2=0.084, Nagelkerke R^2=0.112; Linearity fit: R^2 p=0.073 (Hosmer-Lemeshow); classification sensitivity=47.8%, specificity=50.0%, accuracy=49.0%.

Variable	Cohort	Frequency	b	Wald statistic	p-value (df=1)	95% CI for Odds ratio		
						Lower	Odds ratio(ExpB)	Upper
L_mean	**Kenyan**	Delta	1.003	1.445	0.229	0.531	2.726	13.990
		Theta	-0.705	1.034	0.309	0.127	0.494	1.924
		Alpha	0.023	0.033	0.856	0.795	1.024	1.317
		Beta	0.002	0.038	0.846	0.982	1.002	1.023
		Gamma	-0.005	1.537	0.215	0.988	0.995	1.003
		High gamma	-0.002	0.227	0.634	0.989	0.998	1.007
	NDAR	Delta	0.094	0.455	0.500	0.836	1.099	1.444
		Theta	-0.066	0.384	0.535	0.761	0.936	1.153
		Alpha	0.022	0.556	0.456	0.965	1.022	1.083
		Beta	0.001	0.020	0.887	0.982	1.001	1.022
		Gamma	-0.004	0.620	0.431	0.985	0.996	1.006
		High gamma	0.000301	0.041	0.839	0.997	1.000	1.003

Table F: Results for l_ent of binary logistic regression with a dichotomous outcome and six predictor variables for: Kenyan cohort: overall model fit: chi^2=10.509, p=0.105; additional fit statistics: Cox&Snell R^2=0.380, Nagelkerke R^2=0.506; linearity fit: R^2 p=0.666 (Hosmer-Lemeshow); classification sensitivity=81.8%, specificity=81.8%, accuracy=81.8%; NDAR cohort: overall model fit: chi^2=6.563 p=0.363; additional fit statistics: Cox&Snell R^2=0.125, Nagelkerke R^2=0.167; Linearity fit: R^2 p=0.346 (Hosmer-Lemeshow); classification sensitivity=56.5%, specificity=69.2%, accuracy=63.3%.

Variable	Cohort	Frequency	b	Wald statistic	p-value (df=1)	95% CI for Odds ratio		
						Lower	Odds ratio(ExpB)	Upper
L_ent	**Kenyan**	Delta	-1.954	0.475	0.491	0.001	0.142	36.637
		Theta	-1.239	1.031	0.310	0.026	0.290	3.167
		Alpha	0.671	1.946	0.163	0.762	1.955	5.016
		Beta	-0.018	0.014	0.905	0.734	0.982	1.315
		Gamma	-0.020	3.193	0.074	0.958	0.980	1.002
		High gamma	0.006	2.010	0.156	0.998	1.007	1.016
	NDAR	Delta	0.513	0.653	0.419	0.481	1.670	5.790
		Theta	-0.316	0.068	0.794	0.068	0.729	7.806
		Alpha	0.433	0.272	0.602	0.303	1.542	7.850
		Beta	0.494	0.395	0.530	0.351	1.639	7.661
		Gamma	-1.215	1.902	0.168	0.053	0.297	1.668
		High gamma	0.244	0.298	0.585	0.531	1.277	3.066

Table G: Results for l_max binary logistic regression with a dichotomous outcome and the PCA regression scores of factors 1-9 as predictors for the Kenyan cohort: overall model fit: $chi^2=11.775$, $p=0.226$; additional fit statistics: Cox&Snell $R^2=0.414$, Nagelkerke $R^2=0.553$; linearity fit: R^2 p=0.126 (Hosmer-Lemeshow); classification sensitivity=72.7%, specificity=72.7%, accuracy=72.7%.

Variable	Cohort	Component	b	Wald statistic	p-value (df=1)	95% CI for Odds ratio		
						Lower	Odds ratio(ExpB)	Upper
L_max	**Kenyan**	1	-1.432	1.965	0.161	0.032	0.239	1.769
		2	-1.906	1.617	0.204	0.008	0.149	2.807
		3	-0.212	0.105	0.746	0.224	0.809	2.924
		4	-1.186	1.388	0.239	0.042	0.305	2.197
		5	0.660	0.907	0.341	0.498	1.934	7.519
		6	-1.072	1.180	0.277	0.049	0.342	2.368
		7	0.681	1.308	0.253	0.615	1.977	6.354
		8	-1.333	2.966	0.085	0.058	0.264	1.202
		9	0.283	0.093	0.760	0.216	1.327	8.167

Table H: Results for recurrence rate binary logistic regression with a dichotomous outcome and the PCA regression scores of factors 1-6 as predictors for the Kenyan cohort: overall model fit: $chi^2=12.371$, $p=0.054$; additional fit statistics: Cox&Snell $R^2=0.430$, Nagelkerke $R^2=0.573$; linearity fit: R^2 p=0.122 (Hosmer-Lemeshow); classification sensitivity=72.7%, specificity=81.8%, accuracy=77.3%.

Variable	Cohort	Component	b	Wald statistic	p-value (df=1)	95% CI for Odds ratio		
						Lower	Odds ratio(ExpB)	Upper
Recurrence rate	**Kenyan**	1	-0.969	0.958	0.328	0.055	0.380	2.640
		2	-5.754	1.306	0.253	1.6401e-7	0.003	61.239
		3	-3.785	1.487	0.223	0.000052	0.023	9.960
		4	-0.885	1.487	0.223	0.099	0.413	1.712
		5	0.062	0.004	0.952	0.144	1.064	7.886
		6	0.380	0.301	0.583	0.376	1.462	5.681

Table I: Results for recurrence rate binary logistic regression with a dichotomous outcome and the PCA regression scores of factors 1-10 as predictors for the NDAR cohort: overall model fit: $chi^2=14.614$, $p=0.147$; additional fit statistics: Cox&Snell $R^2=0.258$, Nagelkerke $R^2=0.344$; linearity fit: R^2 p=0.618 (Hosmer-Lemeshow); classification sensitivity=60.9%, specificity=69.2%, accuracy=65.3%.

Variable	Cohort	Component	b	Wald statistic	p-value (df=1)	95% CI for Odds ratio		
						Lower	Odds ratio(ExpB)	Upper
Recurrence rate	**NDAR**	1	-0.559	2.400	0.121	0.282	0.572	1.160
		2	-0.207	0.345	0.557	0.408	0.813	1.621
		3	-0.416	0.981	0.322	0.289	0.660	1.503
		4	0.253	0.536	0.464	0.655	1.287	2.531
		5	0.055	0.027	0.870	0.548	1.056	2.035
		6	0.594	2.196	0.138	0.826	1.811	3.971
		7	0.078	0.052	0.820	0.553	1.081	2.111
		8	-0.576	1.366	0.243	0.214	0.562	1.477
		9	0.036	0.010	0.920	0.518	1.036	2.073
		10	0.852	4.466	0.035	1.064	2.343	5.163

Table J: Results for l_mean binary logistic regression with a dichotomous outcome and the PCA regression scores of factors 1-3 as predictors for the Kenyan cohort: overall model fit: chi^2=6.090, p=0.107; additional fit statistics: Cox&Snell R^2=0.242, Nagelkerke R^2=0.322; linearity fit: R^2 p=0.454 (Hosmer-Lemeshow); classification sensitivity=63.6%, specificity=72.7%, accuracy=68.2%.

Variable	Cohort	Component	b	Wald statistic	p-value (df=1)	95% CI for Odds ratio		
						Lower	Odds ratio(ExpB)	Upper
L_mean	**Kenyan**	1	-0.718	1.589	0.207	0.160	0.488	1.490
		2	-1.499	2.774	0.096	0.038	0.223	1.303
		3	-0.334	0.444	0.505	0.268	0.716	1.912

Table K: Results for l_mean binary logistic regression with a dichotomous outcome and the PCA regression scores of factors 1-11 as predictors for the NDAR: overall model fit: chi^2=17.247, p=0.101; additional fit statistics: Cox&Snell R^2=0.297, Nagelkerke R^2=0.396; linearity fit: R^2 p=0.712 (Hosmer-Lemeshow); classification sensitivity=69.6%, specificity=73.1%, accuracy=71.4%.

Variable	Cohort	Component	b	Wald statistic	p-value (df=1)	95% CI for Odds ratio		
						Lower	Odds ratio(ExpB)	Upper
L_mean	**NDAR**	1	-0.712	0.373	3.648	0.236	0.491	1.019
		2	0.498	0.374	1.771	0.790	1.645	3.423
		3	-0.521	0.446	1.365	0.248	0.594	1.423
		4	1.957	0.905	4.673	1.200	7.078	41.727
		5	0.470	0.486	0.936	0.617	1.600	4.149
		6	0.136	0.368	0.137	0.557	1.146	2.356
		7	-0.370	0.591	0.392	0.217	0.691	2.200
		8	0.083	0.335	0.062	0.563	1.087	2.097
		9	-0.679	0.416	2.668	0.225	0.507	1.145
		10	0.223	0.351	0.402	0.628	1.249	2.485
		11	-0.123	0.371	0.109	0.427	0.885	1.831

Table L: Results for trapping time binary logistic regression with a dichotomous outcome and the PCA regression scores of factors 1-10 as predictors for the Kenyan: overall model fit: chi^2=15.752, p=0.107; additional fit statistics: Cox&Snell R^2=0.511, Nagelkerke R^2=0.682; linearity fit: R^2 p=0.474 (Hosmer-Lemeshow); classification sensitivity=90.9%, specificity=81.8%, accuracy=86.4%.

Variable	Cohort	Component	b	Wald statistic	p-value (df=1)	95% CI for Odds ratio		
						Lower	Odds ratio(ExpB)	Upper
Trapping time	**Kenyan**	1	-0.736	1.581	0.217	0.022	0.479	10.615
		2	-1.230	0.979	1.578	0.043	0.292	1.991
		3	-7.743	5.449	2.019	0.000	0.000	18.846
		4	1.319	1.564	0.712	0.174	3.741	80.209
		5	-1.257	1.102	1.302	0.033	0.284	2.465
		6	-2.065	1.343	2.365	0.009	0.127	1.763
		7	-5.907	3.513	2.827	0.000	0.003	2.661
		8	0.226	1.066	0.045	0.155	1.254	10.127
		9	-2.664	1.869	2.031	0.002	0.070	2.717
		10	-0.831	0.700	1.407	0.110	0.436	1.719

Table M: Results for trapping time binary logistic regression with a dichotomous outcome and the PCA regression scores of factors 1-13 as predictors for the NDAR: overall model fit: $chi^2=21.265$, $p=0.068$; additional fit statistics: Cox&Snell $R^2=0.352$, Nagelkerke $R^2=0.470$; linearity fit: R^2 p=0.004 (Hosmer-Lemeshow); classification sensitivity=82.6%, specificity=84.6%, accuracy=83.7%.

Variable	Cohort	Component	b	Wald statistic	p-value (df=1)	95% CI for Odds ratio		
						Lower	Odds ratio(ExpB)	Upper
Trapping time	**NDAR**	1	-0.722	3.645	0.056	0.231	0.486	1.019
		2	-0.647	0.961	0.327	0.144	0.524	1.909
		3	0.294	0.319	0.572	0.483	1.342	3.727
		4	1.711	2.982	0.084	0.794	5.533	38.568
		5	-0.501	0.430	0.512	0.135	0.606	2.710
		6	0.006	0.000	0.990	0.435	1.006	2.326
		7	0.351	0.637	0.425	0.600	1.420	3.361
		8	-0.319	0.572	0.449	0.318	0.727	1.660
		9	0.543	1.207	0.272	0.653	1.721	4.536
		10	0.256	0.293	0.589	0.510	1.292	3.270
		11	-0.588	1.089	0.297	0.184	0.556	1.675
		12	0.338	0.784	0.376	0.664	1.402	2.962
		13	0.591	1.224	0.268	0.634	1.806	5.146

frontiers in Psychiatry

REVIEW
published: 12 July 2017
doi: 10.3389/fpsyt.2017.00121

How Useful Is Electroencephalography in the Diagnosis of Autism Spectrum Disorders and the Delineation of Subtypes: A Systematic Review

Oana Gurau[1], William J. Bosl[2,3] and Charles R. Newton[1,4]*

[1] Department of Psychiatry, University of Oxford, Oxford, United Kingdom, [2] School of Nursing and Health Professions, University of San Francisco, San Francisco, CA, United States, [3] Benioff UCSF Children's Hospital Oakland Research Institute, Oakland, CA, United States, [4] KEMRI-Wellcome Trust Research Program, Centre for Geographic Medicine Research (Coast), Kilifi, Kenya

Autism spectrum disorders (ASD) are thought to be associated with abnormal neural connectivity. Presently, neural connectivity is a theoretical construct that cannot be easily measured. Research in network science and time series analysis suggests that neural network structure, a marker of neural activity, can be measured with electroencephalography (EEG). EEG can be quantified by different methods of analysis to potentially detect brain abnormalities. The aim of this review is to examine evidence for the utility of three methods of EEG signal analysis in the ASD diagnosis and subtype delineation. We conducted a review of literature in which 40 studies were identified and classified according to the principal method of EEG analysis in three categories: functional connectivity analysis, spectral power analysis, and information dynamics. All studies identified significant differences between ASD patients and non-ASD subjects. However, due to high heterogeneity in the results, generalizations could not be inferred and none of the methods alone are currently useful as a new diagnostic tool. The lack of studies prevented the analysis of these methods as tools for ASD subtypes delineation. These results confirm EEG abnormalities in ASD, but as yet not sufficient to help in the diagnosis. Future research with larger samples and more robust study designs could allow for higher sensitivity and consistency in characterizing ASD, paving the way for developing new means of diagnosis.

Keywords: autism spectrum disorders, autism, electroencephalography, functional connectivity, spectral analysis, information dynamics

OPEN ACCESS

Edited by:
Ashok Mysore,
St. John's Medical College Hospital, India

Reviewed by:
Nishant Goyal,
Central Institute of Psychiatry, India
Hanna E. Stevens,
University of Iowa, United States

****Correspondence:***
Oana Gurau
oana.gurau@some.ox.ac.uk

Specialty section:
This article was submitted to Child and Adolescent Psychiatry, a section of the journal Frontiers in Psychiatry

Received: *02 February 2017*
Accepted: *23 June 2017*
Published: *12 July 2017*

Citation:
Gurau O, Bosl WJ and Newton CR (2017) How Useful Is Electroencephalography in the Diagnosis of Autism Spectrum Disorders and the Delineation of Subtypes: A Systematic Review. Front. Psychiatry 8:121. doi: 10.3389/fpsyt.2017.00121

INTRODUCTION

History and Definition of Autism Spectrum Disorders (ASD) and Its Subtypes

Autism spectrum disorders are a group of lifelong neurodevelopmental disorders. Recent epidemiological research estimates the prevalence of ASD at around 1 in 100 children in the UK (1) and 1 in 68 children in the USA (2). ASD include the following subtypes: autistic disorder, Asperger syndrome, childhood disintegrative disorder, and pervasive developmental disorder-not otherwise

specified (PDD-NOS) (3). In a more recent classification in the Diagnostic and Statistical Manual of Mental Disorders, Fifth Edition, all these subcategories are subsumed under "Autism Spectrum Disorder" (4).

Autism spectrum disorder was first described by Kanner in 1943 who identified the triad of core characteristics: impaired social interaction and communication involving reduced eye contact, facial expression, and body gestures, a restricted range of interests and repetitive behavior (5). Research indicates that ASD are on a broad continuum of severity and differences in symptoms can be detected, with the clinical symptoms becoming evident from the second year of life. These features are thought to be the result of atypical neural connections within the brain (6–11). Electroencephalography (EEG) can measure neural activity and may provide a useful tool to detect children at risk of developing ASD and, thus, provide an opportunity for early intervention. In addition, it may help delineate between the subtypes.

Autism may be described as a dynamical disorder and analyzed from the perspective of complex dynamical systems (10, 12–15). Measureable changes in cortical excitability may contribute to, or be a manifestation of, connectivity abnormalities (16). The two concepts, neural connectivity and neural dynamics, are related. For example, studies of complex networks reveal that they can exhibit a kind of "spatial chaos" in which network properties can change drastically with small changes to key network connections, analogous to the sensitive dependence of chaotic time series on initial conditions (17). Therefore, computing of dynamical system features of the brain from EEG time series may be used to infer atypical neural connectivity that is associated with autism. Although neural connectivity can be measured directly using diffusion tensor imaging, non-linear time series analysis methods have begun to provide a tool for detecting differences in neural connectivity measured with EEG devices on multiple smaller scales through quantitative analysis of signal complexity (12, 18–21).

The interpretation of the EEG may be complicated by the presence of epilepsy, which develops in adolescence in one-third of the patients. Subtypes of ASD include Asperger syndrome, which involves social symptoms, with typical language development and non-verbal intelligence. PDD-NOS differs from autistic disorder by lacking repetitive behaviors or evident social deficits. Disintegrative Disorder is a severe form of autism acquired after normal development until 2–10 years of age. This phenotypic diversity in ASD also involves a varying degree of impairment in each symptom category between individuals (22). These are not the only subtypes of ASD. But these are the most encountered ones in research papers, particularly the ones selected for this review.

The implication for neural connectivity disorders such as autism is that EEG analysis may reveal neural network abnormalities that are related to functional and behavioral symptoms associated with the disorder. Reliable and relatively low cost, simple EEG measurements may provide important clinical biomarkers for early risk assessment and for monitoring the condition's progression. The aim of this review is to evaluate evidence for the utility of EEG in identifying such abnormal activity for the diagnosis of ASD and for the delineation of its subtypes.

Electroencephalography (EEG) and Quantitative EEG (qEEG)

Scalp EEG sensors measure the summed potentials of several millions of neurons. The physiological interpretations of the recorded signal describe both intrinsic properties of the neurons such as their ionic conductance, as well as connectivity characteristics and neural networks interactions (23). These characteristics are typically classified in five "classic" frequency bands: delta (0–4 Hz), theta (4–8 Hz), alpha (8–12 Hz), beta (12–30 Hz), and gamma (30–100 Hz), but the definitions of these bands may vary between studies. These frequencies characterize different states of the brain, each with a specific function, physiology, and cortical topography. However, newer methods of EEG analysis, such as using multiscale entropy (12, 13, 24), measure "scales" rather than the traditional frequency bands.

Evaluation of the power of EEG signals in various frequency bands and the nature of connectivity between brain regions using correlation analysis is commonly performed using qEEG: a collection of computerized tools and algorithms to analyze the EEG signal (25). The qEEG encompasses methods of EEG analysis, such as spectral analysis, functional connectivity analysis, and, recently, information dynamics, and is used in the search for quantitative features associated with altered behaviors in ASD. The values computed using various methods of qEEG analysis may be collectively referred to as EEG signal features.

The specific questions that we set out to address in this review were as follows: (i) can analysis of EEG be used to detect subjects with ASD, in particular is it useful in the diagnosis and (ii) can EEG features identify subtypes of ASD?

METHODS

Search and Selection Strategy

The literature search was conducted in three peer-reviewed databases: PubMed, Embase, and PsycInfo. Keyword searches were performed in order to identify the most suitable studies for this review. The key terms used were "ASD," "Asperger," "autism," "EEG," "encephalography," "spectral analysis," "functional connectivity," and "information dynamics". On each database, the searches consisted of each of the three key terms describing the disorder and subtypes plus each of the terms describing the methods (**Table 1**).

In addition, to select the studies to be reviewed, the following inclusion criteria were used:

1. The studies were performed on humans, either children or adults;
2. A comparison was performed between either: (i) ASD patients and healthy controls or (ii) ASD patient with different subtypes;
3. The studies' outcome consisted of specific EEG features of ASD, not its comorbidities;
4. The studies included patients diagnosed according to the clinical criteria from DSM III onward;
5. The studies were published between 1980 and May 2016;

TABLE 1 | Description of the search strategy.

Search element	PubMed	Embase	PsycInfo
Disorder	Autism spectrum disorders (ASD)	ASD	ASD
	Autism	Autism	Autism
	Asperger	Asperger	Asperger
Method	Electroencephalography (EEG)	EEG	EEG
	Encephalography	Encephalography	Encephalography
	Spectral analysis	Spectral analysis	Spectral analysis
	Functional connectivity	Functional connectivity	Functional connectivity
	Information dynamics	Information dynamics	Information dynamics

TABLE 2 | Total number of papers identified from each database before and after the exclusion of duplicates.

Database	Total number of titles	Total number of titles-duplicates
PubMed	2,155	1,523
Embase	2,095	1,467
PsycInfo	964	649

6. The studies were performed using EEG and the signal was analyzed using spectral analysis, functional connectivity measures, or information dynamics methods.

In order to filter the initial number of titles obtained (**Table 2**), according to the six eligibility criteria, a three-step strategy was followed (**Figure 1**). First, the titles of each of the papers yielded by the initial search were examined for relevance to the topic. The absence of any of the key words from the titles led to the exclusion of the studies. Second, the abstracts were scanned for relevance, as they briefly indicate the methods used in the study and their results. Animal studies, review papers, or studies combining different methods of analysis were excluded. The review papers were used as sources for relevant papers to be examined. Lastly, a full text analysis was performed, allowing a closer examination of diagnostic criteria of the patients and the quality of their results. This process yielded the final collection of studies used for data extraction in the review (**Figure 1**).

Following the selection stage, the relevant data were extracted from each paper. For this purpose, in consistency with the PRISMA 2009 checklist (http://www.prisma-statement.org/), a template with a number of descriptive variables for each study such as its authors and publishing year; a detailed section describing the methods used in the study, including description of the patient and the control groups, the task performed, methods of EEG analysis as well as statistical tests; and a summary of the results was used. For consistency, all data were extracted from the studies using this template.

Inspection of the literature selected for data extraction revealed three types of EEG signal analysis used for detection of ASD: (i) spectral analysis; (ii) functional connectivity and coherence analysis; and (iii) a larger category, information dynamics, including several methods based on dynamical systems theory and mathematical concepts.

The Methods Categories

Functional connectivity evaluates the relationship between the signals recorded at different brain regions simultaneously. Usually these relationships are quantified in terms of some measure of synchronization between two signals. Synchronization may be defined in several different ways (26, 27). Variations of this analysis include coherence, phase locking index, phase synchronization, phase lag index, and synchronization index. Functional connectivity analysis also involves measures of embedded data, such as cross recurrence diagrams and synchronization likelihood. Often signals are decomposed into standard frequency bands.

Spectral analysis is the most common quantitative method used for EEG signal analysis and interpretation. It breaks the continuous range of frequencies into defined bands and evaluates the signal distribution over several frequency bands, usually as the five divisions described above. The spectral power may be computed for each frequency band at each sensor (28). Sometimes the total power in each frequency band is summed over all sensors, giving a single power value over the entire scalp for each frequency band. For example, a power value for the alpha band over the entire scalp may be reported. Or, power in the alpha band at each sensor location may be reported. Group differences between populations with autism and typically developing controls were assessed. Results were presented either as absolute power or relative power (the ratio of band power to total power over bands).

Information dynamics methods make use of non-linear analysis methods. These include various measures of entropy, or other dynamical concepts such as Lyapunov exponents or recurrence plot analysis, among others. The meaning of these concepts has been derived from physical systems, but it is not clear how they related to neural systems. Thus, significant correlations between non-linear features and neural or behavioral observations are sought using machine learning algorithms and mathematical classifiers based on neural networks, graph theory, fractals, or Bayesian methods. Machine learning algorithms and classifiers use a set of rules characterizing members of one or more categories and then apply these rules to a dataset for classification. The most commonly used non-linear feature used in neuroscience has been multiscale entropy, a measure of signal complexity. The original EEG signal is used to create a sequence of coarse-grained time series. Each scale of entropy is obtained as follows: scale 2 is calculated by averaging every two values, scale 3 time series is obtained by averaging every three values, etc. The sample entropy is then computed for each time series to produce entropy as a function of time. This coarse graining procedure was first introduced to signal analysis by Costa et al. (29). Although this procedure is commonly used, it has only recently been noted that for powers of 2 (1, 2, 4, 8, …) the coarse graining procedure is mathematically identical to the Haar wavelet transform (30). Much is known about wavelet transforms and their relationship

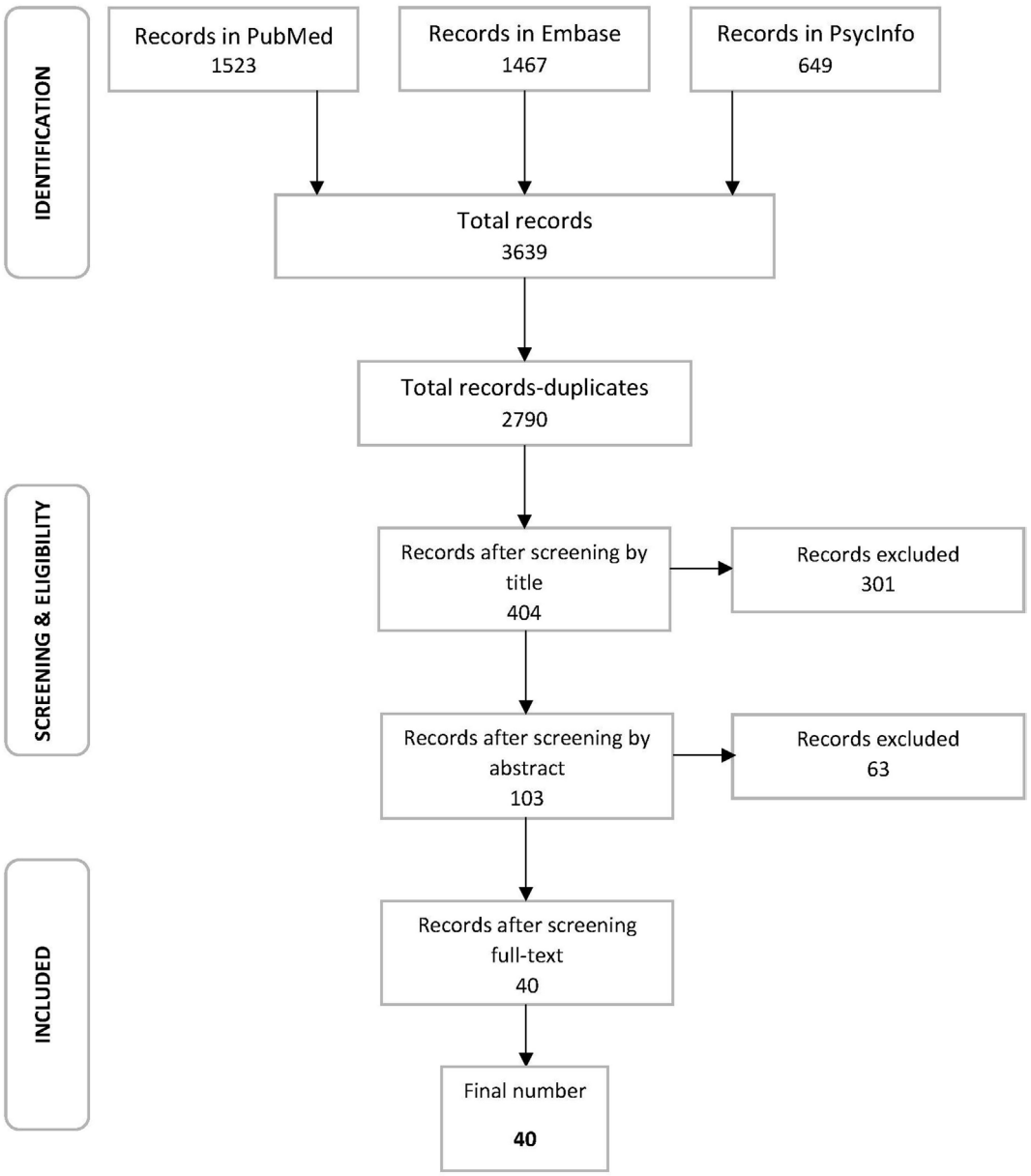

FIGURE 1 | Flow diagram presenting the process of study selection, including the three-step strategy used to reach the final collection of studies and number of records in every step.

to frequency decomposition (31). Multiscale entropy is, thus, a computation of sample entropy on each of the wavelet transform scales.

According to the PRISMA 2009 checklist, the analysis of the utility of each of these methods includes a general description, a critical evaluation of statistically significant evidence to differentiate between ASD patients and non-ASD subjects, or different ASD subtypes extracted from the literature, advantages the technique holds over others, as well as gaps and future lines of improvement followed by a conclusion summarizing the overall prospects of using it as a tool in ASD detection.

RESULTS

An evaluation of the selected literature led to the presentation of the papers in three EEG signal analysis methods used to characterize ASD described above.

Functional Connectivity

Of the 40 studies selected for review, 12 studies compared functional connectivity between ASD patients and non-ASD subjects. All studies reported at least one statistically significant difference in ASD connectivity in at least one frequency band. Of the 12

studies employing this method of analysis, 10 use coherence as a measure of connectivity, 1 calculated the phase lag index of the time series, and 1 calculated clustering to determine the level of synchronization. EEG recordings were performed under relaxed, no task conditions, with eyes either open or closed, during sleep or during an object recognition, audio or video task. The overall patterns in results are presented in **Table 3** together with the condition of the EEG recording and the principal measure of each study.

Although the results are variable, some generalizations can be inferred. Thus, ASD is usually associated with reduced long-range connections in the alpha band between the frontal lobe and other brain regions. This finding supports the under-connectivity theory of ASD, which is supported by fMRI studies (47). Seven out of 11 studies performed coherence analyses in the alpha band, of which 4 supported the presence of under connectivity. For instance, Murias et al. studied coherence in ASD in a relaxed eyes closed condition, using a high-density EEG montage (124

TABLE 3 | Studies using functional connectivity.

Paper	Patients characteristics	Controls characteristics	Condition	Measure	Changes in ASD
Orekhova et al. (32, 33)	n = 28; mean age = 14.4 months; sex = 18 F, 10 M; HR	n = 10; mean age = 38 months; sex = 3 F, 7 M; High-risk ASD (HR-ASD)	3 video stimuli	De-biased weighted phase lag index	HR-ASD: hyper-connectivity in alpha band in frontal and central areas ($p < 0.05$)
	n = 26; mean age = 14.7 months; sex = 14 F, 12 M; Low-risk (LR)	n = 18; mean age = 38 months; sex = 15 F, 3 M; High-risk non-ASD			The degree of hyper-connectivity correlated with the severity of ASD symptoms in later diagnosed
Righi et al. (34)	n = not specified; adults HR of ASD Had an older sibling with ASD	n = not specified; adults LR of ASD	Speech sounds	Coherence	Infants at risk: reduced connectivity ($p < 0.005$) Connectivity: HR-ASD < HR-NASD < LR
Barttfeld et al. (35)	n = 10; mean age = 23.8 years; sex = 1 F, 9 M; subtypes = autism, Asperger syndrome	n = 10; mean age = 25.3 years; sex = 1 F, 9 M	Relaxed eyes closed	Coherence (synchronization likelihood)	Delta band: decreased long-range connectivity (fronto-occipital) and increased short-range connectivity (frontal lateral) in ASD ($p < 0.05$)
Murias et al. (36)	n = 18; adults sex = 18 M diagnosis = ASD; Some were taking medication	n = 18; age-matched sex = 18 M	Relaxed eyes closed	Coherence	Theta: increased connectivity in frontal and temporal left hemisphere ($p < 0.025$) Alpha: decreased long-range connections of the frontal area ($p < 0.025$)
Leveille et al. (37)	n = 9; mean age = 21.1 years; diagnosis = ASD	n = 13; mean age = 21.5 years	Rapid eye movement (REM) sleep	Coherence	Theta and delta: increased long-range coherence between the occipital region and the rest of the brain and decreased the frontal area ($p < 0.05$)
Boersma et al. (38)	n = 12; mean age = 3.5 years; sex = 2 F, 10 M; subtypes = autism (2), Asperger syndrome (1), PDD-NOS (9); average IQ = 85	n = 19; mean age = 3.5 years; sex = 19 M; average IQ = 108	Pictures of cars	Clustering	Overall whole brain under-connectivity in beta, theta, and alpha bands ($p < 0.01$)
Catarino et al. (13, 39)	n = 15; mean age = 31 months; diagnosis = ASD	n = 15; mean age = 29 months	Object recognition	Coherence	Decreased coherence for both tasks in alpha and theta bands ($p < 0.05$)
Carson et al. (40)	n = 19; mean age = 9.9 years; sex = 1 F, 19 M; diagnosis = ASD	n = 13; mean age = 10 years; sex = 4 F, 9 M	Videos of someone reading a story	Coherence	Decreased coherence in alpha band in frontal and temporal lobes at baseline ($p < 0.05$)
Cantor et al. (41)	n = 11; age range = 4–12 years; sex = 2 F, 9 M; subtypes = autism	n = 119; classification = normal children (n = 88, age range = 5–15 years), a matched group of intellectually disabled children (n = 18, age range = 5–15 years) and a group of mentally age-matched normal toddlers (n = 13, age range = 16 months to 5 years)	Relaxed eyes open	Coherence	Higher coherence between and within hemispheres in delta and alpha bands ($p < 0.05$)
Chan et al. (42, 43)	n = 21; mean age = 10.27 years; sex = 2 F, 19 M	n = 21; mean age = 9.85 years; sex = 7 F, 14 M	Object recognition	Coherence	Increased frontal coherence in left hemisphere in theta bands ($p < 0.05$)

(*Continued*)

TABLE 3 | Continued

Paper	Patients characteristics	Controls characteristics	Condition	Measure	Changes in ASD
Coben et al. (44)	*n* = 20; mean age = 6–11 years; sex = 6 F, 14 M	*n* = 20; mean age = 6–11 years; sex = 6 F, 14 M	Relaxed eyes close	Coherence	Decreased coherence in theta and delta bands in frontal region ($p < 0.005$), delta, theta, and alpha in temporal region ($p < 0.05$) and delta, theta, and beta in parietal and occipital regions ($p < 0.05$)
Buckley et al. (45)	*n* = 87; age range = 2–6 years; diagnostic = ASD *n* = 21; age range = 2–6 years; diagnosis = developmental delay without ASD (DD)	*n* = 29; age range = 2–6 years (TYP)	Awake, slow-wave sleep, and REM sleep	Coherence, phase lag	Increased coherence observed in ASD compared to TYP, almost exclusively during slow-wave sleep, in the frontal–parietal areas, in long-distance pairs
Lazarev et al. (46)	*n* = 14; age range = 6–14 years; sex = 14 M; diagnosis = ASD	*n* = 19; age range = 6–14 years; sex = 19 M	Intermittent photic stimulation	Coherence	Significantly lower coherence in ASD than the control group in the beta frequencies

n, number of subjects; F, female; M, male; PDD-NOS, pervasive developmental disorder-not otherwise specified; REM, rapid eye movement; ASD, autism spectrum disorders; HR-ASD, High-risk ASD; HR, high-risk.

electrodes) in male adults and found significant differences in the alpha band between patients and controls, with reduced long-range connections particularly from the frontal areas. Some of the patients were taking medication, which may have influenced the results (36). Catarino et al. also identified an overall decrease in brain connectivity in the alpha band, in subjects with ASD performing two object recognition tasks (39). In a more recent study, Carson et al. performed a study on a younger pool of participants that replicated the decrease in the long-range connectivity in the alpha band, while they were attending to a video of either a familiar or unfamiliar person readying a story (40). The fourth study to support this theory calculates clustering as a measure of brain connectivity. Boersma et al. used graph analytical tools to demonstrate reduced whole brain connectivity in toddlers, particularly in the alpha band (38). However, three of the six studies show contradictory results. Orekhova et al. performed a longitudinal study, testing participants at high risk (HR) and low risk (LR) of developing ASD at 14 months and at 38 months, after part of the HR participants were diagnosed with ASD. The study showed significant differences between the children diagnosed with ASD and the other participants, with hyper-connectivity in the alpha band between the frontal and central areas in those at risk of developing autism (33). Testing participants in a relaxed eyes open condition, Cantor et al. supports the decrease in alpha connectivity, this time within and between hemispheres (41). Buckley et al. tested participants aged 2–6 years old during three sleep state conditions and found an increase in coherence in ASD patients compared to neurotypical subjects, particularly in long-range connections in the frontal–parietal areas (45).

Anatomical and functional studies have also demonstrated short-range, local over connectivity, reflected in increases of short-range association fibers (48). Moreover, it is known that theta oscillations underlie locally dominant processes (49). Six out of 11 studies investigated connectivity differences in this frequency band: 3 of the studies supporting previous fMRI findings (36, 37, 43) and 3 not finding any evidence of over connectivity (38, 39, 44). Murias et al. identified significant over connectivity in the theta band in the frontal and temporal areas of the left hemisphere (36). Leville et al. studied participants during rapid eye movement sleep and identified increased long-range connectivity between the visual area V1 in the occipital lobe and other parts of the brain (37). During an object recognition task, Chan found increased frontal coherence in the theta band, confirming fMRI findings (43); but three studies found whole brain under connectivity in the theta band, the first two employing object recognition tasks (38, 39), while Coben et al. demonstrated under connectivity in the frontal, temporal, and parietal regions (44).

The delta and beta bands yielded significant results in 6 of the 11 functional connectivity studies, but lacked consistency. Barttfeld et al. showed ambivalent results in the delta band, with decreased long-range delta connectivity between the frontal and occipital areas and increased short-range delta connectivity in the frontal region (35). In a sleep study, Leville et al. had contradictory results, showing increased long-range delta connectivity between the occipital area and the rest of the brain (37). Coben also shows decreased frontal and temporal coherence in the theta band (44). Decreases in connectivity were detected by Boersma et al. (38), Coben et al. (44), and Lazarev et al. (46) in the analysis of the beta band. Despite these results, it is notable that 9 of the 11 papers did not find any significant difference in the beta band. Generalization, in this case, could not be inferred because of the different conditions of the EEG recordings and the age differences between the participants of each study.

Spectral Analysis

Twenty-one of the selected studies used spectral analysis to characterize ASD. All studies recorded statistically significant variants in spectral power in ASD patients compared to non-ASD subjects in at least one frequency band. The studies measured differences in relative or absolute spectral power across frequency band, power spectrum density, or spectral properties such as amplitude. The signal was recorded during relaxed conditions with eyes either open or closed, during sleep, cognitive tasks, or while attending to video or audio stimuli. The overall trend of results can be visualized in **Table 4**, along with participants' characteristics, recording condition and the main measure of the study.

TABLE 4 | Studies using spectral analysis.

Paper	Patients characteristics	Controls characteristics	Condition	Measure	Changes in ASD
Matlis et al. (50)	n = 27; mean age = 4–8 years; sex = 2 F, 25 M; subtypes = autism	n = 55; mean age = 4–8 years; sex = 26 F, 29 M	Relaxed eyes open	Spectral properties	Reduced posterior/anterior power ratio in the alpha frequency range (8–14 Hz) ($p \leq 0.0025$)
Sheikhani et al. (51)	n = 15; age range = 6–11 years; sex = 5 F, 10 M; subtypes = Asperger syndrome; verbal IQ > 85; handedness = 1 LH, 14RH	n = 11; age range = 6–11 years; sex = 4 F, 7 M; handedness = 1LH, 1AD, 9RH	Eyes closed, relaxed eyes opened, looking at 3 puzzle shapes, looking at mother's and stranger's pictures upright and inverted	Spectral power	Higher power in gamma band while resting with eyes open ($p < 0.05$)
Cantor et al. (41)	n = 11; age range = 4–12 years; sex = 2 F, 9 M; mean IQ = 37.5; subtypes = autism	n = 119; classification = normal children (n = 88, age range = 5–15 years), age-matched group of mentally disabled children (n = 18, age range = 5–15 years) and a group of mentally age-matched normal toddlers (n = 13, age range = 16 months to 5 years)	Relaxed eyes opened	1. relative power 2. total power	ANCOVAs and t-tests: Lower alpha power in all regions in ASD subjects compared to age-matched normal and age-matched mentally disabled children ($p < 0.001$) Higher power than the normal or mentally handicapped children in the bilateral fronto-temporal and left temporal regions ($p < 0.005$). Lower power in the bilateral occipital regions normal ($p < 0.05$). Lower power than toddlers in the left central, midline central, and left fronto-temporal regions ($p < 0.05$)
Chan et al. (42, 43)	n = 17; mean age = 7.1 years; sex = 3 F, 14 M	n = 105; mean age = 7.7 years; sex = 61 F, 44 M	Relaxed eyes opened	Spectral profiles: absolute delta, theta, alpha, sensorimotor rhythm, beta; relative delta, theta, alpha, sensorimotor rhythm, beta bands	Absolute amplitudes: higher amplitudes in all five frequency bands ($p < 0.005$)
Chan et al. (42, 43)	n = 66; age range = 5–18 years; sex = 6 F, 60 M	n = 90; age range = 6–12 years; sex = 42 F, 48 M	Relaxed eyes opened	Mean absolute and relative power of typically developing children and children with ASD	ASD less relative alpha (91% sensitivity, 73% specificity) and more relative delta (76% sensitivity, 78% specificity)
Daoust et al. (52)	n = 9; age range = 12–53 years; sex = 1 F, 8 M; diagnosis = ASD; subtypes = autism, Asperger syndrome	n = 8; age range = 8–56 years; sex = 1 F, 7 M	Relaxed, eyes closed morning and evening and sleep	1. Awake absolute spectral power 2. REM sleep spectral amplitude	Higher absolute theta over the left frontal pole region during evening wakefulness, but not during morning wakefulness Lower absolute beta spectral amplitude over the primary ($p < 0.05$) and associative ($p < 0.03$) visual areas
van Diessen et al. (53)	n = 19; mean age = 10.6 years; sex = 3 F, 16 M	n = 19; mean age = 10.1 years; sex = 3 F, 16 M; 7 taking medication	Relaxed, eyes closed	Spectral power	Higher relative gamma power in frontal, parietal, and temporal regions ($p = 0.002$)
Mathewson et al. (54)	n = 15; mean age = 18–51 years; sex = 3 F, 12 M; subtypes = autism, Asperger syndrome, PDD-NOS; medication = 8; handedness = 13RH, 2LH	n = 16; mean age = 22–47 years; sex = 4 F, 12 M; handedness = 14RH, 2LH	Relaxed eyes opened and eyes closed	Differences in alpha power	Alpha power in each region greater in ASD than in control in the eyes open condition ($p < 0.05$)

(*Continued*)

TABLE 4 | Continued

Paper	Patients characteristics	Controls characteristics	Condition	Measure	Changes in ASD
Dawson et al. (55)	*n* = 28; mean age = 11 years; sex = 5 F, 23 M; diagnosis = ASD; subtypes = autism, PDD-NOS; peabody picture vocabulary test-revised scores = 39–108; verbal age average = 5.8	1. *n* = 28; mean age = 11 years; sex = 5 F, 23 M; verbal age average = 16 2. *n* = 24; mean age = 4.6 years; sex = 2 F, 22 M; verbal age average = 5.7	Relaxed eyes opened	Chronological-age-matched power spectra group comparison	Delta: ASD reduced power in the frontal and temporal regions ($p < 0.1$) Theta: ASD reduced power in all three brain regions ($p < 0.05$). Alpha: ASD reduced power in the frontal and temporal regions ($p < 0.05$) Beta: no significant differences
Machado et al. (56)	*n* = 11; mean age = 70.3 months; sex = 4 F, 7 M; diagnosis = ASD; subtypes = autism	*n* = 14; mean age = 66.7 months; sex = 5 F, 9 M	Control: relaxed eyes opened; watching a popular cartoon; watching the cartoon without audio	PSD	Decreased PSD in the central region for delta and theta, and in the posterior region for sigma and beta bands, lateralized to the right hemisphere ($p < 0.05$)
Maxwell et al. (57)	*n* = 15; mean age = 15.1 years; sex = 15 M; diagnosis = ASD; subtypes = 14 Asperger syndrome, 1 autism	*n* = 18; mean age = 14.2 years; sex = 18 M	Relaxed eyes opened	Resting gamma power	Decreased gamma power at the right lateral electrodes ($p = 0.04$)
Scope et al. (58)	*n* = 20; mean age = 12 years; sex = 2 F, 18 M; subtypes = 9 autism, 8 Asperger syndrome, 3 PDD-NOS	*n* = 20; mean age = 13 years; sex = 2 F, 18 M	Looking at Gabor patches of different frequencies	Differences in changes in alpha and gamma frequencies of independent components	Induced alpha power of components that were in or near the cingulate gyrus was increased in ASD ($p < 0.05$)
Stroganova et al. (59)	*n* = 40; age range = 3–8 years; sex = 40 M; subtypes = 38 autism, 2 PDD = NOS	*n* = 40; age range = 3–8 years; sex = 40 M	Sustained visual attention	Spectral power	Increase of gamma at the electrode locations distant from the sources of myogenic artifacts ($p < 0.05$)
Stroganova et al. (59)	*n* = 44; age range = 3–8 years; sex = 44 M; diagnosis = ASD; subtypes = 42 autism, 2 PDD-NOS	*n* = 44; age range = 3–8 years; sex = 44 M	Sustained visual attention	Spectral power	Higher amount of prefrontal delta in autism ($p < 0.05$)
Tani et al. (60)	*n* = 20; mean age = 27.2 years; subtype = Asperger syndrome; diagnosis = ASD	*n* = 10; mean age = 26.5 years	Asleep	Spectral power	Non-significant trend toward decreased relative delta power and increased theta power in slow-wave sleep was found in the AS group
Yang et al. (61)	*n* = 5; age range = 16–22 years; sex = 1 F, 4 M; subtype = Asperger syndrome	*n* = 7; age matched	Looking at photographs of familiar faces	Spectral power	Decrease following the stimulus onset in two time-frequency intervals—(1) 150–300 ms in the 1–16 Hz frequency range and (2) 300–650 ms in the 1–8 Hz range ($p < 0.01$)
Tierney et al. (62)	*n* = 168l; diagnosis = ASD	Longitudinal studies: same patients at 6, 9,12, 18,24 months	Resting state	Change over time in spectral power	Across all bands, spectral power was lower in high-risk infants as compared to low-risk infants at 6 months of age ($p < 0.01$)
Sheikhani et al. (51)	*n* = 17; age range = 6–11 years; sex = 4 F, 13 M; diagnosis = ASD; handedness = 1LH, 1 AD, 15 RH	*n* = 11; age range = 6–11 years; sex = 4 F, 7 M	Relaxed eyes opened	Accuracy in differentiating ASD using spectrogram criteria	Alpha frequency band had the best distinction level of 96.4% in relaxed eye-opened condition using spectrogram criteria. ASD had significant lower spectrogram criteria values in left hemisphere ($p < 0.01$), at F3, T3, FP1, F7, C3, Cz, and T5 electrodes ($p < 0.05$)

(*Continued*)

TABLE 4 | Continued

Paper	Patients characteristics	Controls characteristics	Condition	Measure	Changes in ASD
Lushchekina et al. (63, 64)	n = 27; mean age = 5.8 years; diagnosis = ASD; subtypes = autism	n = 24; mean age = 6.1 years	Relaxed eyes closed, mental loading (counting, adding and subtracting numbers)	Spectral power in theta and gamma bands	ASD-lower theta spectral power in baseline (p = 0.001) and higher gamma spectral power in baseline (p = 0.005); cognitive loading presented no changes from baseline in either bands
Lushchekina et al. (63, 64)	n = 27; age range = 5–7 years; sex = 27 M diagnosis = ASD; subtypes = autism	n = 19; age range = 5–7 years; sex = 19 M	Relaxed eyes closed, mental loading (counting, adding and subtracting numbers)	Spectral power in alpha, beta, and gamma bands	The cognitive task led to increases in spectral power in alpha1 and alpha 3 but no changes in alpha 2 ASD-gamma spectral power higher than control and did not change during the task (p < 0.05)
Elhabashy et al. (65)	n = 21; age range = 4–12 years; diagnosis = ASD	n = 21; age range = 4–12 years	Relaxed eyes open	Absolute and relative spectral power	Increased absolute delta and theta power in ASD especially at the frontal region

n, number of subjects; F, female; M, male; LH, left-handed; RH, right-handed; AD, ambidextrous; PDD-NOS, pervasive developmental disorder-not otherwise specified; PSD, power spectral density; ASD, autism spectrum disorders.

Inconsistencies are observed in the spectral band findings, although some generalizations can be inferred. First, significant differences in the alpha band were shown by five studies with relaxed eyes open condition (41, 42, 50, 54, 55). While four studies show a decrease in absolute spectral power in ASD in children of similar ages (41, 42, 50, 55), another showed elevated absolute alpha power in adults (54). The inconsistencies might be attributed to the age differences between participants and differing developmental trajectories in children with ASD. Yang et al. tested participants while they were performing a cognitive task and showed an increase in alpha power compared to non-ASD controls, but insufficient studies calculated similar measures under the same conditions to make robust conclusions (61).

Calculating spectral amplitudes in all frequency bands, Chan et al. also found significantly increased amplitudes in the ASD population. Moreover, using discriminant function analyses, the study finds that beta amplitudes had high specificity (98.1%) and sensitivity (77.8%) in differentiating ASD from non-ASD subjects (70). The most consistent result that could lead to a generalization is an increase in absolute gamma power in ASD compared to non-ASD subjects. Sheikhani et al. tested their participants in a variety of conditions and found statistically significant elevated gamma power, particularly in the relaxed eyes open condition (51). van Diessen et al. confirms the increase in gamma power, particularly in the frontal, parietal, and temporal regions in the relaxed eyes open condition (53). Stroganova et al. replicate this finding, using a visual attention task (59), while Lushchekina et al. supports these findings in two studies involving a cognitive task (64).

As for the theta band, none of the results could be validated due to inconsistencies. While Daoust et al., Tani et al., Elhabashy et al., and Yang et al. show increased power in the theta band in two studies performed during sleep, one during a relaxed eyes open and one involving a cognitive task (52, 60, 61, 65); three studies show a reduction in theta power in relaxed eyes open conditions and during a cognitive task (55, 56, 64). Variations in the participants' age, as well as small sample sizes might lead to the lack of consistency in these results.

Information Dynamics

Information dynamics comprises a collection of new methods derived (28) from analysis of non-linear physical systems using new computational methods from the mathematics of complex dynamical systems (71, 72). Of the all studies representing the final literature pool considered in this review, six studies used these interdisciplinary methods to compare ASD patients and non-ASD subjects. These studies may use machine learning algorithms, neural networks, graph theory, or Bayesian methods to find group differences from features computed with non-linear algorithms, such as multiscale entropy or fractal analysis. The challenge with these methods is to determine neurophysiological meaning associated with the measures. All studies reported at least one statistically significant difference in at least one variable measured and very high classification capabilities based on those variables. Of the six studies employing such methods of analysis, only two have a common measure.

The other four studies use distinct variables and concepts with the same goal. EEG recordings were performed under relaxed, no task conditions, with eyes either open or closed, or during an object recognition or audio task. The overall patterns in results are presented in **Table 5**, which show the condition of the EEG recording and the main measure of each study or means of classification.

Multiscale entropy measurements were employed by Catarino et al. and Bosl et al. to measure brain signal complexity in children with autism, infants at HR of developing ASD and non-ASD subjects during a relaxed eyes open condition and an object detection task, respectively. Catarino et al. found significantly decreased multiscale entropy in ASD-diagnosed participants compared to controls, predominantly in temporo–parietal and occipital areas of the brain (13). Bosl et al. found the same results in multiscale entropy, averaged over the entire scalp. The latter found that the greatest differences are observed between 9 and 12 months of age, as multiscale entropy shows an overall different developmental trajectory for infants at HR of developing ASD compared to LR infants. Bosl et al. used classification algorithms to show that children with a HR of developing autism based on family history could be detected with high accuracy at 9–12 months of age, leading to the more important question of whether an autistic neuroelectrophysical phenotype could be detected early in infancy. This supervised learning experiment yielded a sensitivity value of over 80% at 9 months of age, remaining very high (70–90%) until 12 months of age (12).

Elridge et al. used Bayesian methods to perform a similar classification between ASD and typically developing children, between 6 and 10 years old. This study extracted robust features such as variance in time, entropy, or sum of signed differences from the EEG signal and then used logistic regression and a native Bayes classifier to divide the two groups with a 79% accuracy (66). Ahmadlou et al. used a different method of classification based

TABLE 5 | Studies using information dynamics.

Paper	Patients characteristics	Controls characteristics	Condition	Measure	Changes in ASD
Bosl et al. (12, 30)	$n = 46$; age range = 6–24 months; diagnosis = HRA	$n = 33$; age range = 6–24 months	Infants' attention was engaged by the researcher blowing bubbles	1. mMSE 2. Machine learning classification accuracy	1. HRA lower mean complexity over all channels; most prominent differences between groups was the change in mMSE between 9 and 12 months 2. Machine learning techniques threshold $p = 0.05$: HRA and control groups classified at age 9 months for boys and girls together and for boys separately with accuracies of 80% and well over 90%, respectively
Eldridge et al. (66)	$n = 19$; age range = 6–10 years; diagnosis = ASD	$n = 30$; age range = 6–10 years	Auditory paradigm (oddball paradigm)	1. Classification accuracy using robust features, a support vectormachine, logistic regression, and a naive Bayes classifier	1. Bayesian classification: sensitivity of 79% was achieved for classifying ASD and non-ASD subjects
Gregory and Mandelbaum (67)	$n = 56$; age range = 2–22 years; diagnosis = ASD	$n = 56$; age range = 2–22 years	Relaxed eyes open	Differences in posterior dominant EEG rhythm (PDR) between groups	1. 2-sampled t-tests: across the entire pool of participants: significantly different PDR between ASD and non-ASD subjects ($p = 0.014$) ages 2. 2–5.9 years ($n = 22$): significantly different PDR between ASD and non-ASD subjects ($p = 0.047$).ages 6–22 years ($n = 34$): no significant differences in PDR between ASD and non-ASD subjects ($p > 0.05$)
Ahmadlou et al. (68, 69)	$n = 9$; age range = 7–13 years; subtypes = autism	$n = 9$; age range = 7–13 years	Resting state, eyes closed	1. Discriminative capacity of functional connectivity within and between regions 2. Accuracy of EPNN classification of ASD and non-ASD	1. One way ANOVAs: Theta band right-temporal-right-temporal; Occipital-Frontal; Parietal-Right-temporal; Occipital-Central ($p < 0.0005$) 2. 95.5% sensitivity with 1.2% variance of classification of ASD and non-ASD subjects
Ahmadlou et al. (69)	$n = 9$; age range = 6–13 years; sex = 2 F, 7 M	$n = 8$; age range = 7–13 years; sex = 2 F, 6 M	Resting state, eyes closed	1. Discriminative capacity of Fractal Dimensions (FD) in 5 sub-bands 2. Accuracy of Radial Basis Function Neural Network classification of ASD and non-ASD	1. One way ANOVAsSignificant differences using Katz's Fractal Dimension: gamma in temporal regions, delta in frontal and central regions ($p < 0.001$) 2. 90% accuracy in the 3 parameter feature space with 0.15% variance
Catarino et al. (13, 39)	$n = 15$; mean age = 31.4 years; diagnosis = ASD	$n = 15$; mean age = 29.4 years	Face and chair detection task	Signal complexity (multiscale entropy)	1. ASD decreased multiscale entropy over temporo-parietal and occipital regions ($p = 0.036$)

n, number of subjects; F, female; M, male; HRA, high risk for autism; mMSE, modified multiscale entropy; ANOVAs, analyses of variance; ASD, autism spectrum disorders.

on complexity and chaos theory. Two types of fractal dimensions were used to assess dynamical changes in the brains of ASD children and non-ASD subjects in all frequency sub-bands: Higuchi's Fractal Dimension and Katz's Fractal Dimension, which indicate non-integers or fractional dimensions of time series, based on regularity or self-similarity of a time series. After computation of fractal dimensions, the most significant characteristics were extracted using analysis of variance. Finally, a Radial Basis Function Neural Network classifier was used to separate ASD from non-ASD subjects. The accuracy of this classification was 90 % (68).

DISCUSSION

The aim of this review is to determine the utility of EEG in identifying abnormal activity in brain signal to help in the diagnosis of ASD and for the delineation of its three main subtypes; autism, Asperger syndrome, and PDD-NOS.

Most of the reviewed studies identify differences between ASD and non-ASD subjects regardless of the recording conditions or analysis. However, there is no sufficient evidence to support any of these methods in the diagnosis of ASD. Sources of heterogeneity such as gaps in study designs were identified and recommendation for future research is given.

Functional Connectivity—Utility, Research Gaps, and Future Directions

Functional connectivity studies showed consistent decreased long-range connectivity in the alpha band and short-range connectivity in the theta band in ASD. However generalizations cannot be inferred yet due to either contradictory results of some studies, or differences in study design. These results only indicate potential reasonable utility of using functional connectivity measures for ASD detection. Methodological challenges involve interpretation of functional connectivity between surface or scalp regions. More than six different methods can be found to define synchronization between time series alone (73). Coherence, correlation, and synchronization can then be used in different ways to determine the strength of connectivity between sensor locations.

It should be noted that EEG recordings usually involve more complex electrode montages and advanced computational capacity for this method of data analysis. These requirements may not necessarily involve the simple, lightweight devices, with high portability that could be operated by non-specialized staff. In addition, the computational challenges required by this type of analysis should not be underestimated. Moreover, since there is little homogeneity in the results obtained using this method, future studies should take into consideration current limitations. Numerous concerns of study design suggest that future research must ensure robust experimental designs and limited reliance on patients with comorbidities, such as epilepsy or subjects taking medication. Epilepsy, one of the most common comorbidities of ASD, is associated with abnormal EEGs and this may complicate the separation of those effects by those caused by ASD (22). Moreover, different types of medication have varied effects on the EEG signal and could be a source of heterogeneity in the results (74). The different means of computing coherence should also be investigated, since different studies yielded contradicting results depending on the analysis method.

In the context of ASD, functional connectivity has not been studied as extensively as spectral analysis. The number of studies identified indicates that coherence may have high utility as a means of accurately detecting ASD. However, the heterogeneity of the coherence results comes partly from a disregard of developmental trajectories of this variable. Previous studies showed that coherence is elevated with age in the high-frequency bands. Children with ASD undergo a slower maturation process and they show generally greater long-range coherence than typical developing children. As coherence increases with age, the values become comparable in adulthood between ASD and non-ASD subjects (75). Thus, age and developmental trajectories must be included in any studies that examine differences between children with ASD and typically developing children.

Spectral Analysis—Utility, Research Gaps, and Future Directions

Spectral analysis was the most common method of EEG signal interpretation for the detection of ASD identified in this review. The most consistent finding was an increase in absolute gamma power in ASD compared to non-ASD controls. However, inconsistencies between the studies appear due to differences in experimental designs. These may be related to differences in the age of the population studied and failure to fully account for developmental changes.

A major feature of spectral analysis that reinforces its utility for ASD detection is the fact that it does not require elaborate electrode montages, as the analysis can be performed on signals extracted from one single electrode. It is also simple to compute and interpret. However, it is highly reliant on the study condition given that, in essence, it gives a description of the signal in terms of its frequencies, which are dependent on the task performed. For example, greater alpha amplitudes may reflect inhibition of unnecessary activity and better performance on the task, in accordance with the neural efficiency hypothesis (76, 77). Therefore, generalization can only be drawn from studies testing their participants in very similar experimental conditions. Future studies might consider examination of lower frequency bands, such as every 2 or 5 Hz.

Spectral analysis measurements are also dependant on brain maturation and developmental trajectories. For instance, in typically developing children, power distribution tends to shift to higher frequencies with age, with lower frequencies decreasing in relative power (78). Therefore, the age is critical in the interpretation of the results and has to be taken into consideration when comparisons are drawn.

Another important aspect that requires consideration in future studies is whether patients are taking medication. Different types of medicine could influence the EEG signal. For example, many ASD patients receive antiepileptic medication,

which shows abnormal brain topography particularly in the gamma band (74).

Information Dynamics—Utility, Research Gaps, and Future Directions

Information dynamics was used in a limited number of studies in this review. This is due in part to the fact that these methods have been more recently developed in the mathematical community, and are less well known in general as signal analysis tools. Information dynamics computations are also more difficult to perform and fewer ready-to-use software packages are available. The preliminary results, thus, far indicate potential for accurately classifying ASD and non-ASD subjects. However, the limited number of studies must be replicated more widely and with much larger sample sizes before their clinical usefulness can be determined. Conclusions and generalizations on the utility of information dynamics methods cannot yet be drawn as a number of technical difficulties, such as appropriate sample sizes, have to be overcome. A much higher number of studies are required in order to assess and compare these methods with more common spectral power methods used in the field. Further research using measurements such as entropy is encouraged as they interpret the EEG recording as a non-linear signal and bring new perspectives to the field.

EEG—General Utility

Besides the direct relation between EEG and the neurophysiological features described above, EEG provides a much lower cost, ease of use, as it is portable and can be applied by someone with minimal training, compared to neuroimaging methods. Moreover, EEG data have excellent temporal resolution and measures brain activity directly. This facilitates research as it allows for numerous analyses revolving around direct responses to stimuli, inter-regional connectivity, or topography of brain oscillations. The low cost and ease of use also means that EEG findings have potential clinical application in primary care settings. Therefore, an understanding of qEEG methods and an evaluation of their utility is very important for future research and for the prospective use of EEG in a clinical context. Furthermore, as discussed, developmental trajectories may be more important than single measurements in time for determining functional brain development patterns. The low cost and ease of use of EEG devices is a prerequisite for a brain-based measurement that can be used routinely to monitor brain development.

Delineation of Subtypes

The second goal of this review was to identify the utility of EEG in the delineation of ASD subtypes. Out of 40 papers, only seven stated the subtype of the ASD group tested. However, testing was not done in comparison between subtypes, which would help delineate them according to one or more characteristics. In addition, none of the studies explores the genetic aspect of neurophysiological subtypes in ASD. Subtypes may be associated with a candidate gene, or complex gene profiles, and, therefore, future studies should consider association between genetic underpinnings and abnormal neurophysiological activity. ASD subtypes also have differences both in their neurological and behavioral manifestations. Moreover, different subtypes may have different developmental trajectories (62). Together, these become sources of heterogeneity in the results. This lack of evidence to help a distinction between different subtypes on the spectrum, represents nothing but strong motivation for further research, with experimental designs that would differentiate, classify, and compare their populations.

Lastly, it is notable that the brain's electrical activity and indeed overall function necessarily exhibits individual characteristics that vary from subject to subject. Taking this into consideration has a substantial impact on establishing a baseline before any analysis is performed. Even within the broad autism phenotype, there is wide variation in intelligence, social skills, language ability, and other specialized abilities in music, visual arts, and motor development. Deciphering the characteristics that are essential to the autism phenotype within the background of widely varying cofounding functional brain characteristics is a major challenge.

Conclusion and Recommendations

Overall current EEG signal analysis is not able to identify children with ASD with sufficient sensitivity or specificity to be clinically useful at this time. However, these methods of analysis and their results to date suggest high utility in characterizing the disorder and may be a vital complement to other existing technologies. The use of EEG as a brain development measure may eventually become useful as an indicator that a child requires further evaluation. The current literature supports further research, suggesting different electrophysiological features of high importance and major gaps that can be filled. Bearing in mind that ASD is a neurodevelopmental disorder, diagnosed in childhood, age should be considered when designing the experiment. Moreover, longitudinal studies could reinforce important findings and also delineate developmental stages of ASD. New, advanced methods of analysis should be considered and combined with already established ones in order to fulfill the final goal: early detection of emerging autism, which may open a window for early intervention and prevention.

AUTHOR CONTRIBUTIONS

OG developed the protocol, she then followed to perform the literature search, followed by a three-step selection that led to the final pool of articles to review. She performed the data extraction and analysis and wrote the review accordingly. CN and WB supervised the entire process closely, playing a role in the selection of the final literature pool and in the editing of the paper.

FUNDING

This study was supported by the Wellcome Trust, through a senior research fellowship (083744) to Professor Charles Newton.

REFERENCES

1. Baird G, Simonoff E, Pickles A, Chandler S, Loucas T, Meldrum D, et al. Prevalence of disorders of the autism spectrum in a population cohort of children in South Thames: the special needs and autism project (SNAP). *Lancet* (2006) 368(9531):210–5. doi:10.1016/S0140-6736(06)69041-7
2. Centers for Disease Control and Prevention. Prevalence of autism spectrum disorders autism and developmental disabilities monitoring network, 14 sites, United States, 2008. *MMWR Surveill Summ* (2012) 61(3):1–19.
3. American Psychiatric Association. *Autism Spectrum Disorder. Diagnostic and Statistical Manual of Mental Disorders*. Washington, DC: American Psychiatric Association (1994).
4. American Psychiatric Association. *Autism Spectrum Disorder. Diagnostic and Statistical Manual of Mental Disorders*. Washington, DC: American Psychiatric Association (2013).
5. Kanner L. Autistic disturbances of affective contact. *Acta Paedopsychiatrica* (1968) 35(4):100–36.
6. Wang J, Barstein J, Ethridge LE, Mosconi MW, Takarae Y, Sweeney JA. Resting state EEG abnormalities in autism spectrum disorders. *J Neurodev Disord* (2013) 5(1):1–14. doi:10.1186/1866-1955-5-24
7. Belmonte MK, Allen G, Beckel-Mitchener A, Boulanger LM, Carper RA, Webb SJ. Autism and abnormal development of brain connectivity. *J Neurosci* (2004) 24(42):9228–31. doi:10.1523/JNEUROSCI.3340-04.2004
8. Assaf M, Jagannathan K, Calhoun VD, Miller L, Stevens MC, Sahl R, et al. Abnormal functional connectivity of default mode sub-networks in autism spectrum disorder patients. *Neuroimage* (2010) 53(1):247–56. doi:10.1016/j.neuroimage.2010.05.067
9. Minshew NJ, Keller TA. The nature of brain dysfunction in autism: functional brain imaging studies. *Curr Opin Neurol* (2010) 23(2):124–30. doi:10.1097/WCO.0b013e32833782d4
10. Sato JR, Vidal M, de Siqueira Santos S, Massirer KB, Fujita A. Complex network measures in autism spectrum disorders. *IEEE/ACM Trans Comput Biol Bioinform* (2015). doi:10.1109/TCBB.2015.2476787
11. Nelson CA III. Introduction to special issue on the role of connectivity in developmental disorders: genetic and neural network approaches. *Dev Sci* (2016) 19(4):523. doi:10.1111/desc.12477
12. Bosl WJ, Tierney A, Tager-Flusberg H, Nelson CA. EEG complexity as a biomarker for autism spectrum disorder. *BMC Med* (2011) 9(18). doi:10.1186/1741-7015-9-18
13. Catarino A, Churches O, Baron-Cohen S, Andrade A, Ring H. Atypical EEG complexity in autism spectrum conditions: a multiscale entropy analysis. *Neurophysiol Clin* (2011) 122(12):2375–83. doi:10.1016/j.clinph.2011.05.004
14. Perez Velazquez JL, Galan RF. Information gain in the brain's resting state: a new perspective on autism. *Front Neuroinformatics* (2013) 7:37. doi:10.3389/fninf.2013.00037
15. Megremi A. Autism spectrum disorders through the lens of complex-dynamic systems theory. *Open Access Autism* (2014) 22(2):1–10.
16. Boutros NN, Lajiness-O'Neill R, Zillgitt A, Richard AE, Bowyer SM. EEG changes associated with autistic spectrum disorders. *Neuropsychiatr Electrophysiol* (2015) 1(1):1–20. doi:10.1186/s40810-014-0001-5
17. Motter A, Albert R. Networks in motion. *Phys Today* (2012) 65(4):43–8. doi:10.1063/PT.3.1518
18. Janjarasjitt S, Scher MS, Loparo KA. Nonlinear dynamical analysis of the neonatal EEG time series: the relationship between neurodevelopment and complexity. *Neurophysiol Clin* (2008) 119(4):822–36. doi:10.1016/j.clinph.2008.03.024
19. Lippe S, Kovacevic N, McIntosh AR. Differential maturation of brain signal complexity in the human auditory and visual system. *Front Hum Neurosci* (2009) 3:48. doi:10.3389/neuro.09.048.2009
20. Takahashi T, Cho RY, Mizuno T, Kikuchi M, Murata T, Takahashi K, et al. Antipsychotics reverse abnormal EEG complexity in drug-naive schizophrenia: a multiscale entropy analysis. *Neuroimage* (2010) 51(1):173–82. doi:10.1016/j.neuroimage.2010.02.009
21. Takahashi T. Complexity of spontaneous brain activity in mental disorders. *Prog Neuropsychopharmacol Biol Psychiatry* (2013) 45:258–66. doi:10.1016/j.pnpbp.2012.05.001
22. Tuchman R, Rapin I. Epilepsy in autism. *Lancet Neurol* (2002) 1(6):352–8. doi:10.1016/S1474-4422(02)00160-6
23. Coben R, Myers TE. Connectivity theory of autism: use of connectivity measures in assessing and treating autistic disorders. *J Neurotherapy* (2008) 12(2–3):161–79. doi:10.1080/10874200802398824
24. Okazaki R, Takahashi T, Ueno K, Takahashi K, Ishitobi M, Kikuchi M, et al. Changes in EEG complexity with electroconvulsive therapy in a patient with autism spectrum disorders: a multiscale entropy approach. *Front Hum Neurosci* (2015) 9:106. doi:10.3389/fnhum.2015.00106
25. Billeci L, Sicca F, Maharatna K, Apicella F, Narzisi A, Campatelli G, et al. On the application of quantitative EEG for characterizing autistic brain: a systematic review. *Front Hum Neurosci* (2013) 7:442. doi:10.3389/fnhum.2013.00442
26. Pikovsky A, Rosenblum M, Kurths J. *Synchronization: A Universal Concept in Nonlinear Sciences*. Cambridge: Cambridge University Press (2001).
27. Wen D, Zhou Y, Li X. A critical review: coupling and synchronization analysis methods of EEG signal with mild cognitive impairment. *Front Aging Neurosci* (2015) 7:54. doi:10.3389/fnagi.2015.00054
28. Rapp PE, Keyser DO, Albano A, Hernandez R, Gibson DB, Zambon RA, et al. Traumatic brain injury detection using electrophysiological methods. *Front Hum Neurosci* (2015) 9:11. doi:10.3389/fnhum.2015.00011
29. Costa M, Goldberger AL, Peng CK. Multiscale entropy analysis of biological signals. *Phys Rev E Stat Nonlin Soft Matter Phys* (2005) 71(2 Pt 1):021906. doi:10.1103/PhysRevE.71.021906
30. Bosl WJ, Tager-Flusberg H, Nelson CA. EEG complexity for early detection of autism spectrum disorder and the broader autism phenotype. (in preparation).
31. Al-Fahoum AS, Al-Fraihat AA. Methods of EEG signal features extraction using linear analysis in frequency and time-frequency domains. *ISRN Neurosci* (2014) 2014:730218. doi:10.1155/2014/730218
32. Orekhova EV, Stroganova TA, Nygren G, Tsetlin MM, Posikera IN, Gillberg C, et al. Excess of high frequency electroencephalogram oscillations in boys with autism. *Biol Psychiatry* (2007) 62(9):1022–9. doi:10.1016/j.biopsych.2006.12.029
33. Orekhova EV, Elsabbagh M, Jones EJH, Dawson G, Charman T, Johnson MH, et al. EEG hyper-connectivity in high-risk infants is associated with later autism. *J Neurodev Disord* (2014) 6(1):1–11. doi:10.1186/1866-1955-6-40
34. Righi G, Tierney AL, Tager-Flusberg H, Nelson CA. Functional connectivity in the first year of life in infants at risk for autism spectrum disorder: an EEG study. *PLoS One* (2014) 9(8):e105176. doi:10.1371/journal.pone.0105176
35. Barttfeld P, Amoruso L, Ais J, Cukier S, Bavassi L, Tomio A, et al. Organization of brain networks governed by long-range connections index autistic traits in the general population. *J Neurodev Disord* (2013) 5(1):1–9. doi:10.1186/1866-1955-5-16
36. Murias M, Webb SJ, Greenson J, Dawson G. Resting state cortical connectivity reflected in EEG coherence in individuals with autism. *Biol Psychiatry* (2007) 62(3):270–3. doi:10.1016/j.biopsych.2006.11.012
37. Leveille C, Barbeau EB, Bolduc C, Limoges E, Berthiaume C, Chevrier E, et al. Enhanced connectivity between visual cortex and other regions of the brain in autism: a REM sleep EEG coherence study. *Autism Res* (2010) 3(5):280–5. doi:10.1002/aur.155
38. Boersma M, Kemner C, De Reus MA, Collin G, Snijders TM, Hofman D, et al. Disrupted functional brain networks in autistic toddlers. *Brain Connect* (2013) 3(1):41–9. doi:10.1089/brain.2012.0127
39. Catarino A, Andrade A, Churches O, Wagner AP, Baron-Cohen S, Ring H. Task-related functional connectivity in autism spectrum conditions: an EEG study using wavelet transform coherence. *Mol Autism* (2013) 4(1):1. doi:10.1186/2040-2392-4-1
40. Carson AM, Salowitz NM, Scheidt RA, Dolan BK, Van Hecke AV. Electroencephalogram coherence in children with and without autism spectrum disorders: decreased interhemispheric connectivity in autism. *Autism Res* (2014) 7(3):334–43. doi:10.1002/aur.1367
41. Cantor DS, Thatcher RW, Hrybyk M, Kaye H. Computerized EEG analyses of autistic children. *J Autism Dev Disord* (1986) 16(2):169–87. doi:10.1007/BF01531728
42. Chan AS, Sze SL, Cheung MC. Quantitative electroencephalographic profiles for children with autistic spectrum disorder. *Neuropsychology* (2007) 21(1):74–81. doi:10.1037/0894-4105.21.1.74
43. Chan AS, Han YM, Sze SL, Cheung M-C, Leung WW-M, Chan RC, et al. Disordered connectivity associated with memory deficits in children with autism spectrum disorders. *Res Autism Spectr Disord* (2011) 5(1):237–45. doi:10.1016/j.rasd.2010.04.005

44. Coben R, Clarke AR, Hudspeth W, Barry RJ. EEG power and coherence in autistic spectrum disorder. *Neurophysiol Clin* (2008) 119(5):1002–9. doi:10.1016/j.clinph.2008.01.013
45. Buckley AW, Scott R, Tyler A, Mahoney JM, Thurm A, Farmer C, et al. State-dependent differences in functional connectivity in young children with autism spectrum disorder. *EBioMedicine* (2015) 2(12):1905–15. doi:10.1016/j.ebiom.2015.11.004
46. Lazarev VV, Pontes A, Mitrofanov AA, deAzevedo LC. Reduced interhemispheric connectivity in childhood autism detected by electroencephalographic photic driving coherence. *J Autism Dev Disord* (2015) 45(2):537–47. doi:10.1007/s10803-013-1959-8
47. Just MA, Keller TA, Malave VL, Kana RK, Varma S. Autism as a neural systems disorder: a theory of frontal-posterior underconnectivity. *Neurosci Biobehav Rev* (2012) 36(4):1292–313. doi:10.1016/j.neubiorev.2012.02.007
48. Herbert MR, Ziegler DA, Makris N, Filipek PA, Kemper TL, Normandin JJ, et al. Localization of white matter volume increase in autism and developmental language disorder. *Ann Neurol* (2004) 55(4):530–40. doi:10.1002/ana.20032
49. Collura TF. Neocortical dynamics and human EEG rhythms. *J Clin Neurophysiol* (1996) 13(2):177–8. doi:10.1097/00004691-199603000-00010
50. Matlis S, Boric K, Chu CJ, Kramer MA. Robust disruptions in electroencephalogram cortical oscillations and large-scale functional networks in autism. *BMC Neurol* (2015) 15:97. doi:10.1186/s12883-015-0391-4
51. Sheikhani A, Behnam H, Noroozian M, Mohammadi MR, Mohammadi M. Abnormalities of quantitative electroencephalography in children with Asperger disorder in various conditions. *Res Autism Spectr Disord* (2009) 3(2):538–46. doi:10.1016/j.rasd.2008.11.002
52. Daoust A-M, Limoges E, Bolduc C, Mottron L, Godbout R. EEG spectral analysis of wakefulness and REM sleep in high functioning autistic spectrum disorders. *Neurophysiol Clin* (2004) 115(6):1368–73. doi:10.1016/j.clinph.2004.01.011
53. van Diessen E, Senders J, Jansen FE, Boersma M, Bruining H. Increased power of resting-state gamma oscillations in autism spectrum disorder detected by routine electroencephalography. *Eur Arch Psychiatry Clin Neurosci* (2015) 265(6):537–40. doi:10.1007/s00406-014-0527-3
54. Mathewson KJ, Jetha MK, Drmic IE, Bryson SE, Goldberg JO, Schmidt LA. Regional EEG alpha power, coherence, and behavioral symptomatology in autism spectrum disorder. *Clin Neurophysiol* (2012) 123(9):1798–809. doi:10.1016/j.clinph.2012.02.061
55. Dawson G, Klinger LG, Panagiotides H, Lewy A, Castelloe P. Subgroups of autistic children based on social behavior display distinct patterns of brain activity. *J Abnorm Child Psychol* (1995) 23(5):569–83. doi:10.1007/BF01447662
56. Machado C, Estevez M, Leisman G, Melillo R, Rodriguez R, DeFina P, et al. QEEG spectral and coherence assessment of autistic children in three different experimental conditions. *J Autism Dev Disord* (2015) 45(2):406–24. doi:10.1007/s10803-013-1909-5
57. Maxwell CR, Villalobos ME, Schultz RT, Herpertz-Dahlmann B, Konrad K, Kohls G. Atypical laterality of resting gamma oscillations in autism spectrum disorders. *J Autism Dev Disord* (2015) 45(2):292–7. doi:10.1007/s10803-013-1842-7
58. Scope A, Pascalis O, Buckley D, Makeig S. Independent component analysis reveals atypical electroencephalographic activity during visual perception in individuals with autism. *Biol Psychiatry* (2009) 65(1):22–30. doi:10.1016/j.biopsych.2008.07.017
59. Stroganova TA, Nygren G, Tsetlin MM, Posikera IN, Gillberg C, Elam M, et al. Abnormal EEG lateralization in boys with autism. *Neurophysiol Clin* (2007) 118(8):1842–54. doi:10.1016/j.clinph.2007.05.005
60. Tani P, Lindberg N, Nieminen-von Wendt T, von Wendt L, Virkkala J, Appelberg B, et al. Sleep in young adults with Asperger syndrome. *Neuropsychobiology* (2004) 50(2):147–52. doi:10.1159/000079106
61. Yang HH, Savostyanov AN, Tsai AC, Liou M. Face recognition in Asperger syndrome: a study on EEG spectral power changes. *Neurosci Lett* (2011) 492(2):84–8. doi:10.1016/j.neulet.2011.01.061
62. Tierney AL, Gabard-Durnam L, Vogel-Farley V, Tager-Flusberg H, Nelson CA.Developmental trajectories of resting EEG power: an endophenotype of autism spectrum disorder. *PLoS One* (2012) 7(6):e39127. doi:10.1371/journal.pone.0039127
63. Lushchekina E, Podreznaya E, Lushchekin V, Strelets V. A comparative EEG study in normal and autistic children. *Neurosci Behav Physiol* (2012) 42(3):236–43. doi:10.1007/s11055-012-9558-2
64. Lushchekina E, Podreznaya E, Lushchekin V, Novototskii-Vlasov V, Strelets V. Comparative studies of EEG theta and gamma rhythms in normal children and children with early childhood autism. *Neurosci Behav Physiol* (2014) 44(8):902–8. doi:10.1007/s11055-014-9999-x
65. Elhabashy H, Raafat O, Afifi L, Raafat H, Abdullah K. Quantitative EEG in autistic children. *Egypt J Neurol Psychiatry Neurosurg* (2015) 52(3):176. doi:10.4103/1110-1083.162031
66. Eldridge J, Lane AE, Belkin M, Dennis S. Robust features for the automatic identification of autism spectrum disorder in children. *J Neurodev Disord* (2014) 6(1):12. doi:10.1186/1866-1955-6-12
67. Gregory MD, Mandelbaum DE. Evidence of a faster posterior dominant EEG rhythm in children with autism. *Res Autism Spectr Disord* (2012) 6(3):1000–3. doi:10.1016/j.rasd.2012.01.001
68. Ahmadlou M, Adeli H, Adeli A. Fractality and a wavelet-chaos-neural network methodology for EEG-based diagnosis of autistic spectrum disorder. *J Clin Neurophysiol* (2010) 27(5):328–33. doi:10.1097/WNP.0b013e3181f40dc8
69. Ahmadlou M, Adeli H, Adeli A. Fuzzy synchronization likelihood-wavelet methodology for diagnosis of autism spectrum disorder. *J Neurosci Methods* (2012) 211(2):203–9. doi:10.1016/j.jneumeth.2012.08.020
70. Chan AS, Leung WW. Differentiating autistic children with quantitative encephalography: a 3-month longitudinal study. *J Child Neurol* (2006) 21(5):391–9. doi:10.1177/08830738060210050501
71. Marwan N, Romano MC, Thiel M, Kurths J. Recurrence plots for the analysis of complex systems. *Phys Rep* (2007) 438:237–329. doi:10.1016/j.physrep.2006.11.001
72. Webber CL, Marwan N, editors. *Recurrence Quantification Analysis. Understanding Complex Systems*. New York: Springer (2015).
73. Sakkalis V, Doru Giurc Neanu C, Xanthopoulos P, Zervakis ME, Tsiaras V, Yang Y, et al. Assessment of linear and nonlinear synchronization measures for analyzing EEG in a mild epileptic paradigm. *IEEE Trans Inf Technol Biomed* (2009) 13(4):433–41. doi:10.1109/TITB.2008.923141
74. Arzy S, Allali G, Brunet D, Michel CM, Kaplan PW, Seeck M. Antiepileptic drugs modify power of high EEG frequencies and their neural generators. *Eur J Neurol* (2010) 17(10):1308–12. doi:10.1111/j.1468-1331.2010.03018.x
75. Marosi E, Harmony T, Sánchez L, Becker J, Bernal J, Reyes A, et al. Maturation of the coherence of EEG activity in normal and learning-disabled children. *Electroencephalogr Clin Neurophysiol* (1992) 83(6):350–7. doi:10.1016/0013-4694(92)90070-X
76. Doppelmayr MM, Klimesch W, Pachinger T, Ripper B. The functional significance of absolute power with respect to event-related desynchronization. *Brain Topogr* (1998) 11(2):133–40. doi:10.1023/A:1022206622348
77. Klimesch W, Doppelmayr M, Russegger H, Pachinger T, Schwaiger J. Induced alpha band power changes in the human EEG and attention. *Neurosci Lett* (1998) 244(2):73–6. doi:10.1016/S0304-3940(98)00122-0
78. Gasser T, Verleger R, Bächer P, Sroka L. Development of the EEG of school-age children and adolescents. I. Analysis of band power. *Electroencephalogr Clin Neurophysiol* (1988) 69(2):91–9. doi:10.1016/0013-4694(88)90205-2

Conflict of Interest Statement: The authors declare that the research was conducted in the absence of any commercial or financial relationships that could be construed as a potential conflict of interest.